Prifysgol Cymru • University of Wales
BANGOR

Ysgol Peirianneg Electronig a Systemau Cyfrifiadurol
Prifysgol Cymru, Bangor,
Stryd y Deon,
Bangor, Gwynedd LL57 1UT.
Ffôn: Bangor (01248) 382686
Ffacs: (01248) 361429

School of Electronic Engineering and Computer Systems
University of Wales, Bangor,
Dean Street,
Bangor, Gwynedd LL57 1UT.
Tel: Bangor (01248) 382686
Fax: (01248) 361429

Ferroelectric Ceramic/Polymer Bimorph Sensor for Strain Measurement in Laminates

ERO Contract No. N68171-95-C-9111
(UWB Ref. No. R24-815)
R&D 7594-EE-01

FINAL REPORT

Principal Investigator: **D.K. Das-Gupta**
School of Electronic Engineering
and Computer Systems
University of Wales
Dean Street
Bangor
Gwynedd, LL57 1UT
UK

Tel. No: 01248 382696
Fax No: 01248 361429
E-Mail: dilip@sees.bangor.ac.uk (D.K. Das-Gupta)

Date: February 1998

The following notice applies to any unclassified (including originally classified and now declassified) technical reports released to "qualified U.S. contractors" under the provisions of DoD Directive 5230.25, Withholding of Unclassified Technical Data From Public Disclosure.

NOTICE TO ACCOMPANY THE DISSEMINATION OF EXPORT-CONTROLLED TECHNICAL DATA

1. Export of information contained herein, which includes, in some circumstances, release to foreign nationals within the United States, without first obtaining approval or license from the Department of State for items controlled by the International Traffic in Arms Regulations (ITAR), or the Department of Commerce for items controlled by the Export Administration Regulations (EAR), may constitute a violation of law.

2. Under 22 U.S.C. 2778 the penalty for unlawful export of items or information controlled under the ITAR is up to two years imprisonment, or a fine of $100,000, or both. Under 50 U.S.C., Appendix 2410, the penalty for unlawful export of items or information controlled under the EAR is a fine of up to $1,000,000, or five times the value of the exports, whichever is greater; or for an individual, imprisonment of up to 10 years, or a fine of up to $250,000, or both.

3. In accordance with your certification that establishes you as a "qualified U.S. Contractor", unauthorized dissemination of this information is prohibited and may result in disqualification as a qualified U.S. contractor, and may be considered in determining your eligibility for future contracts with the Department of Defense.

4. The U.S. Government assumes no liability for direct patent infringement, or contributory patent infringement or misuse of technical data.

5. The U.S. Government does not warrant the adequacy, accuracy, currency, or completeness of the technical data.

6. The U.S. Government assumes no liability for loss, damage, or injury resulting from manufacture or use for any purpose of any product, article, system, or material involving reliance upon any or all technical data furnished in response to the request for technical data.

7. If the technical data furnished by the Government will be used for commercial manufacturing or other profit potential, a license for such use may be necessary. Any payments made in support of the request for data do not include or involve any license rights.

8. A copy of this notice shall be provided with any partial or complete reproduction of these data that are provided to qualified U.S. contractors.

D E S T R U C T I O N N O T I C E

For classified documents, follow the procedures in DoD 5200.22-M, Industrial Security Manual, Section II-19 or DoD 5200.1-R, Information Security Program Regulation, Chapter IX. For unclassified, limited documents, destroy by any method that will prevent disclosure of contents or reconstruction of the document.

Abstract

In-situ acoustic emission (AE) sensors have been developed from an initial concept through to their application in detecting Lamb waves in laminate plates. Composite piezoelectric sensors have been fabricated from Calcium modified lead titanate (PTCa) and two polymer matrices (i.e., polar polyvinylidenefluoride-trifluoro-ethylene P(VDF-TrFE) and a nonpolar epoxy with a mixed 0-3 and 1-3 connectivity. Their dielectric and electroactive (i.e., piezoelectric) and other acoustic properties have been characterized. The applicability of these materials for use in surface mounted AE sensors has been investigated and their performance has been found to be compatible with those of a commercially available electroceramic sensor. Sensors of monomorph and bimorph design were embedded in unidirectional glass fibre reinforced epoxy plates and were seen to be capable of detecting and distinguishing between the extensional and flexural plate-wave modes of propagation.

Modelling of ultrasonic sensors, using ABCD matrices, based on the analysis of lossy transducers proved successful for the composite materials by accurately simulating high frequency acoustic pulses. An attempt has also been made to develop a finite element method for the modelling of composite piezoelectric sensors.

FINAL REPORT

1. Introduction

Ferroelectric ceramic and polymer composite films have been fabricated by dispersing electro-ceramic powder, calcium modified lead titanate (PTCa) with a composition of $Pb_{0.76}Ca_{0.24}$ $[(Co_{0.5}W_{0.5})_{0.04}To_{0.96}]0_3$ + $Mn0_2$ into two different polymer matrices, including a polar thermoplastic copolymer, polyvinylidene fluoride and trifluoroethylene, P(VDF-TrFE) and a nonpolar thermosetting epoxy (Epikote 828, shell resins). PTCa ceramic powder of ~ 10 μm grain size was obtained from GEC-Marconi Materials Research Laboratory at Caswell, UK. This particular ceramic powder was chosen for its appropriate dielectric constant and piezoelectric properties with its high electrochemical anisotropy. The polar P(VDF-TrFE) with a nominal 24% by weight of TrFE was supplied in fine powder form by Piezotech S.A., Saint-Louis, France. The epoxy resin Epikote 828 is a medium viscosity liquid epoxide, produced from bisphenolA and epichloro-hydrin with the curing agent, K61B, and was supplied by the Anchor chemicals, UK.

Composite films of PTCa/P(VDF-TrFE) of 50/50, 60/40 and 65/35 vol% compositions and PTCa/epoxy of 50/50, 55/45 and 60/40 vol% compositions of 0-3 and 1-3 mixed connectivity were fabricated and polarized with an externally impressed electric field of appropriate magnitude by methods described elsewhere [1-5] and will not be repeated here. The thickness of the composite films was in the range of 40-100 μm with approximately 10% thickness variation over a $10cm^2$ area. In a 0-3 connectivity, the first digit represents the ceramic phase in which the ceramic grains have no intra-connectivity throughout the composite in the x, y and z-directions whereas the second digit, which represents the polymer phase which possesses the full intra-connectivity in these directions. With 1-3 connectivity the ceramic particles are self-connected in 1 direction only. For thin composite films, where the ceramic grains size is comparable to the film thickness and for high ceramic volume content, the composite tends to have a mixed 0-3 and 1-3 connectivities. Piezoelectric sensors were produced with these composite films and their dielectric, piezoelectric and other relevant transducer

properties were measured [1-8] and are given in this report from which it may be observed that PTCa/epoxy sensors appear to be superior to PTCa/P(VDF-TrFE) by exhibiting a higher value of dg-product where d and g represent the piezoelectric strain and stress coefficients respectively (see the Third Interim Report).

Unfortunately, it was not possible to fabricate composite sensors with PTCa/Polyether-ether Ketone (PEEK) due to practical difficulties including sensitive thermal behaviour of this high temperature polymer.

Surface mounted acoustic emission (AE), based on conventional ultrasonic transducer design, were constructed and their frequency response characterized using a face to face method [9] and a pulse-echo method, commonly used in the evaluation of hydrophone performance [5]. The nature of broad bandwidth, extending above 20 MHz and the relative sensitivity of these transducers were established. Furthermore, simulation of the response of the composite transducers in the frequency and time domain was successfully accomplished by considering the transducer as a one-dimensional acoustic transmission line using parameter values obtained from near resonance measurements of free resonators in air [5, 8, see also 6th and 7th Interim Report].

Composite sensors embedded in fibre reinforced polymer (FRP) laminate showed that they are capable of detecting simulated AE source Lamb waves [see 5th and 6th Interim Reports and ref. 8]. In addition, bimorphs, constructed of two monomorphs, exhibiting a dual mode of operation, have been employed to distinguish between different modes of propagation of Lamb waves within the FRP laminate plates [2nd Interim Report and ref. 8].

An attempt has been made to use the Finite Element Method (FEM) in the modelling of piezoelectric polymer sensors, particularly in the calculation of natural frequencies and the results are included in this report (see Appendix 1).

Finally, the above work has culminated in the PhD degree of Dr. M.P. Wenger with his thesis, entitled "Ferroelectric Ceramic/Polymer Composite Sensors for In-Situ Acoustic Emission Detection". A copy of this thesis has been sent to Dr. P. Blanas, of the US Army Weapons and Materials Research Directorate, Aberdeen Proving Ground, MD21005-5069. Additional copies of this thesis are not submitted with this report for cost considerations and brevity. However, additional copies of this thesis can be supplied on request.

What follows is a brief summary of the seven interim reports together with a discourse on our programme with the Finite Element Modelling of embedded sensors (see Appendix 1). Also included in this report are copies of publications arising from the present work (see Appendix 2).

2. Characteristic Properties of Composite Sensors Fabricated in the Present Work and their Comparison with those of PTCa and P(VDF-TrFE)

The dielectric permittivity ε, and the piezoelectric strain coefficient d_{ij} were measured for the composite sensors in this work. The first suffix i represents the direction in which charge is generated and the second suffix j, indicates the direction of the applied stress. The piezoelectric stress coefficient g_{ij} coefficient is related to the dij coefficient thus [see 4th Interim Report].

$$\frac{d_{ij}}{j_{ij}} = \left[\varepsilon_0 \varepsilon_{ii}\right]_T \qquad \ldots(1)$$

i.e.

$$\frac{d_{31}}{g_{31}} = \left[\varepsilon_0 \varepsilon_{33}\right]_T \qquad \ldots(2)$$

where ε_0 is the permittivity of free space and T the stress. Similarly, for the converse effect, the piezoelectric strain coefficient e_{ij} and the stress coefficient h_{ij} are also related thus,

$$\frac{e_{ij}}{h_{ij}} = \left[\varepsilon_0 \varepsilon_{ii}\right]_s \qquad \ldots(3)$$

where s is the strain. Furthermore, we also have

$$\frac{e_{ij}}{d_{ij}} = \left[Y_{jj}\right]_E \qquad \ldots(4)$$

and

$$\frac{h_{ij}}{g_{ij}} = \left[Y_{jj}\right]_D \qquad \ldots(5)$$

where E is the electric field, D the electric displacement and Y the modulus of elasticity. As these coefficients are not independent of each other, once the values of d_{ij} and h_{ij} along with ε have been measured, the other piezoelectric coefficients (i.e. e- and g- coefficients) and the modulus of elasticity Y, at a constant D or E can be determined. It may also be noted that the dielectric permittivity ε_{ij} and the electromechanical coupling coefficient k_{ij} are related thus,

$$\left[\varepsilon_{33}\right]_s = \left[\varepsilon_{33}\right]_T \left(1 - k_{33}^2\right) \qquad \ldots(6)$$

The hydrostatic d_h and g_h coefficients are related thus,

$$d_h = d_{33} + 2d_{31} \qquad \ldots(7)$$

and

$$g_h = g_{33} + 2g_{31} \qquad \ldots(8)$$

In the present work the piezoelectric d_{33}-, g_{31}- and h_{31}-coefficients, the dielectric permittivity ε_{33} (at 1kHz) and the electromechanical coupling coefficient k_t (in the thickness) were measured. The details of the measurements are given in the interim reports and will not be repeated here. From data on the k_t measurement, the

mechanical quality factor Qm and the magnitude of acoustic impedance z_w were determined.

Table 1 gives the values of ε' and $\tan\delta_t$ at ~25°C and 1kHz for poled samples of PTCa, P(VDF-TrFE), Epoxy together with the composites of varying ceramic volume fractions. It may be observed that from these figures that the permittivity (ε') increases with the increasing volume fraction of the ceramic. PTCa/Epoxy composite exhibit lower permittivities than PTC/P(VDF-TrFE) for the same ceramic volume fraction.

A composite with mixed connectivity can be represented by a cube model where the ceramic is represented by a cube dimension m, in series with a polymer together with a parallelepiped of base dimension of a fraction n of the ceramic cube, extending between both surfaces of the unit cube (see figure 1), in the three direction [1, 5, 10]. In this mixed connectivity model [1] of the composite, the value of n determines the degree of 1-3 connectivity and the volume fractions are given by,

$$\phi^c = m^3 + (nm^2)(1-m) \qquad ...(9)$$

$$\phi^c_{ser} = m \qquad ...(10)$$

$$\phi^c_{par} = n^2m^2 \qquad ...(11)$$

$$\phi^{ser} = m^2(1 - n^2) \qquad ...(12)$$

where ϕ^c is the total volume fraction of the ceramic, ϕ^c_{series} the volume fraction of the ceramic in the series branch, ϕ^c_{par} the volume fraction of ceramic with parallel connectivity and ϕ^{ser} the volume fraction of the series branch in relation to the volume of the whole cube. In this model the dielectric and the piezoelectric properties of the composite cube as a whole are found from calculating the properties of the series branch alone, thus, knowing the series branch properties, the properties of the series branch in parallel with the polymer is calculated. We have two degrees of freedom [1, 10] in this model, i.e. m and n, and the composite properties are related to these two

parameters. Thus the properties can be represented by the contour plots in the m-n planes. Here, n = 1 represents a purely 1-3 connectivity for each value of m and n = 0 provides 1-3 connectivity. Figure 2 shows the permittivity contour plots in the m-n plane [5] of the mixed connectivity model for PTCa/P(VDF-TrFE) and PTCa/Epoxy composites. Figure 2 shows that the value of n increases with volume fraction of the ceramic (dashed-lines), the calculated permittivity contours being given by the solid lines. In this figure the measured data are represented by the dark circles. The average thickness of the PTCa/Epoxy composites was generally larger than that of PTCa/P(VDF-TrFE) composites. Thus the increase in the n- parameter value in the former composite can be explained as an increase in the ceramic connectivity throughout the thickness of the composite as the ceramic volume increases [5].

Table 2 shows the values of d_{33}- and g_{33}-coefficients and those of their constituent phases. It may be observed that the d_{33} values of the composites are lower than that of the ceramic alone, whereas the g- coefficients are larger for the composites due to the relatively lower permittivities of the composites with respect to the ceramic. The piezoelectric figure of merit (FOM) d_{33} g_{33} appears to increase steadily for PTCa/P(VDF-TrFE) with increasing volume fraction of the ceramic content, and it reaches a maximum for the PTCa/Epoxy composite with 55 vol% of ceramic loading. The decrease in this FOM value as the ceramic volume increases from 55 to 60% is thought to arise from limitations of the fabrication method including the higher viscosity in the precured state. It may also be observed that the PTCa/Epoxy composite exhibits a larger value of d_{33} g_{31} product than the PTCa/P(VDF-TrFE) composite for identical loading of the ceramic volume fraction which is due to the lower ε- value of epoxy than that of the polar copolymer.

Figure 3 shows [5] the d_{33} contour plots in the m-n plane of the mixed connectivity cube model [1] for PTCa/Epoxy composites. These contour plots were determined by considering the d- coefficient of the polymer as zero, which is a valid assumption as epoxy plays no role in the electroactivity of this composite. For the PTCa/P(VDF-TrFE) the corresponding d_{33} contour plot in the m-n plane show also good agreement with experimentally determined values and those calculated from mixed connectivity

mode by assigning reduced values due to the presence of polar copolymer [5]. An important conclusion arising from the above observation is that within the composite system the polar copolymer plays an active role in the electroactivity, as opposed to behaving as a passive compliant component as was previously thought [1].

Table 3 shows the values of d_{31}- and g_{31}-coefficients together with the $d_{31}g_{31}$ product values. The hydrostatic d_h and g_h values and the d_hg_h product are given in Table 4 for the composites and those the electroceramic, polar and nonpolar polymer constituents. It may be observed from Table 3 that the d_{31} values for the composites are relatively constant with ceramic volume fractions for each of the two composite systems, depending mostly on the d_{31}- value of the ceramic and little on the polymer. Other workers [11] have reported similar values to those given in Table 3 for a similar composite systems. A plot of d_{31} contours on the m-n plane show once again a good agreement with the experimentally determined d_{31}- values with the corresponding theoretical values [1] determined from the mixed connectivity model [5]. However, appropriate corrections have to be incorporated for the polar copolymer composites, as stated earlier [5].

From Table 4 it may be seen that the PTCa/Epoxy, with 55 vol% of ceramic, shows the largest d_hg_h value, although this value is lower than those of PTCa and P(VDF-TrFE) respectively. In the hydrostatic mode of operation the advantage of composites over either the ceramics or the polymers are the large anisotropy associated with the ceramic and the formability and flexibility of the polymers. The d_h coefficients of the composites are larger than that of the polymer and the g_h coefficients larger than that of the ceramic.

The typical electro-mechanical coupling coefficient, k_t- values along with other properties, i.e. mechanical quality factor Qm, acoustic impedance Z_a, acoustic velocity V_s, elastic constant C_{33}, converse piezoelectric stress coefficient h_{33} and density ρ, of the composites, PTCa, P(VDF-TrFE) and epoxy (density only) are given in Table 5. The values of k_t, Z_a, V_s, Qm and C_{33}^D were obtained from impedance measurement [5]. The composites exhibit a lower k_t- value than those of the copolymer and the ceramic.

The k_t- value of the PTCa/Epoxy (55/45 vol%) is comparable with that PTCa/P(VDF-TrFE), 65/35 vol%).

For the PTCa/Epoxy composites the, Qm- value increases with increasing ceramic volume fraction. As Qm is related to the frequency response of a transducer, it is of advantage to have low Qm- values which provide a wide bandwidth response. It may be observed from Table 5 that the Qm values of this composite are lower than those of PTCa/P(VDF-TrFE) which make the former composite more attractive for wide band transducer materials.

The acoustic impedance Z_a of PTCa/Epoxy appears to be independent of the ceramic volume fraction. Although the density of the composite increases with increasing ceramic volume fraction, the measured acoustic velocity Vs, decreases, thus resulting in a stable Z_a- value (=V_sP). The h_{33}-coefficient of this composite is also relatively constant and the same is also true for the elastic coefficient C_{33}^D over the range of ceramic volume fraction employed in the present work.

From the above observations it may be argued that PTCa/P(VDF-TrFE) composite system is suitable as an actuator whereas PTCa/Epoxy system would prove a good piezoelectric sensor. Comparing the dg- product of the two composite systems investigated in this work, it appears that PTCa/Epoxy system ($d_{33}g_{33}$ = 305 Tpa^{-1}; $d_{31}g_{31}$ = 52 x 10^{-3} Tpa^{-1}; d_ng_h = 1.7 Tpa^{-1}) is superior to the PTCa/P(VDF-TrFE) system ($d_{33}g_{33}$ = 2.41 Tpa^{-1}; $d_{31}g_{31}$ = 26.1 x 10^{-3} Tpa^{-1}; d_hg_h = 1.5 Tpa^{-1}) for transmitter/receiver material.

3. Surface Mounted Acoustic Sensors

The design of our AE Sensor is shown schematically in figure 4[5]. The transducer consists of a grounded stainless steel case, cylindrical in shape containing a backing material consisting of epoxy and tungsten composite materials. An electrical feed-through is incorporated into the side of the case enabling connection to the back face

of the electro-active composite transducer film which is fixed to the backing material using a very thin epoxy layer. Electrical connection is made to the electrode using a conductive epoxy applied to the central portion of the backing. The outer electrode is connected to the electrical ground of the metal case by evaporating gold or aluminium over the top surface of the transducer. The role of the backing materials is to reduce the magnitude of the acoustic ringing [12].

Experimental evaluation of three PTCa/P(VDF-TrFE) with 65/35 vol% and two PTCa/Epoxy with 55/45 vol% and 58/42 vol%, having thicknesses of active elements 138μm and 146μm respectively was carried out to investigate their frequency responses. The performance of these composite transducers were observed to be comparable with that of commercially available piezo-ceramic AE transducer (Parametric V109) in the frequency range 500kHz to 2MHz. In this work the composite transducers have been modelled to determine their response to a mechanical input, viz., the elastic response of a laminated plate. The transducer has been considered as a 'black box' containing the equivalent circuit of ABCD representation a linear three-part network [1, 5, 13, 14], i.e., two mechanical ports and one electrical port, where the voltage and current of the electrical port are related to the forces and velocities of the mechanical ports. A detailed analysis has been given in the 6th and 7th Interim Report and will not be repeated here.

The surface mounted composite transducers were applied to the detection of waves generated by simulated acoustic emissions in thin plates. The simulated acoustic emission source was a pencil lead break on the surface of the plate. The transducers were located on the surface of thin plates of aluminium and glass fibre reinforced plates. Acoustic coupling was achieved using a very thin layer of silicone grease applied to the transducer face prior to contact with the plate face. Figure 5 gives the transfer function of the PTCa/P(VDF-TrFE) and PTCa/Epoxy transducers. The output response of the transducer was calculated from the convolution of the frequency response of the plate, to a simulated lead break, with the transfer function of the transducer. Since both of these are in the frequency domain, the convolution is obtained by a simple multiplication of the vector elements. The time response of the

transducer is then obtained by an inverse fast Fourier transform. Figure 6 shows typical results, i.e., transducer AE detected response to a lead break on the surface of an orthotropic fibre reinforced plate (FRP) with the PTCa/Epoxy, 55/45 vol% transducer. Similar results were also obtained with the PTCa/P(VDF-TrFE), 65/35 vol% transducers. Throughout the simulation of the transducer responses, parameter values have been obtained from experimental measurements on the transducer materials and from the properties of the plates, published in literature.

The experimental results show that the surface mounted composite transducers are well suited for the use of AE sensors for the detection of acoustic waves in thin plates. Furthermore, the modelling of surface mounted transducers via a one dimensional analysis, implementing the use of well established electrical network theory in the form of ABCD matrices has proved to be suitable for predicting the response of these transducers.

4. Bimorph Sensors

Piezoelectric composite films can be used as monomorph or bimorph transducers. Bimorphs have been studied in the present work with respect to their enhanced sensing and actuating properties over monomorphs. A bimorph transducer can be configured from two monomorphs in four different ways, depending on the monomorph polarization direction and electrode configuration (see figure 7 and 2nd and 4th Interim Reports). The first two configurations of figure 7 are for a bimorph constructed from two monomorphs with polarization opposing each other, their equivalent configurations being shown to the right of the figure. Configurations 3 and 4 are for a bimorph constructed from two monomorphs whose directions of polarization are the same. To investigate their properties, monomorphs and series and parallel configured bimorphs were constructed from the PTCa/P(VDF-TrFE) and PTCa/Epoxy composites.

When a bimorph acts as a sensor there are essentially two modes in which it can sense. These modes are termed here as the thickness and bending modes respectively. In configuration 1 of figure 7, an application of stress normal to the film, i.e., on the thickness of the bimorph, will result in a cancellation of the signals from the two monomorphs arising from the piezoelectric g_{33} coefficients as the signals will be opposite signs due to the opposite polarizations of the bimorphs.

An application of a bending moment will result in the signals from the two monomorphs, arising from the respective g_{31} coefficients, complimenting each other. When the bimorph is bent, the monomorph making up the top half of the bimorph will be under extension (or compression) while the other monomorph, making up the lower half of the bimorph will be under compression (or extension). Thus the signals will be of the same polarity due to the applied stresses being of opposite sign. Hence, in this configuration 1 the bimorph will only be sensing in the bending mode as the thickness mode will produce a zero response.

With configuration 2, where the outer two electrodes of bimorphs are connected together and the signal is sensed between the inner electrode and the outer electrodes, it can be seen that the opposite is true. With this configuration the bimorph will be working in the thickness mode only as the bending mode will produce the null result. Thus a bimorph has a dual mode of operation and the sensing mode will be dependent on the electrode arrangement. The properties of configuration 1 is equivalent to the configuration 4 while configurations 2 and 3 are equivalent in figure 7.

If we consider configuration 2, for example, it may be assumed that there will be an amplification of the signal due to the fact that we are using a bimorph instead of a monomorph. This is, of course, incorrect, as an application of a normal stress will produce a charge displacement in both monomorphs, resulting in doubling the charge on the central electrode, but the voltage will be the same because the capacitance of the system has also doubled. There will, however, be an amplification of current in the external circuit as the total resistance will have been halved. For an actuator it is possible to produce twice the displacement or force, in a bimorph as opposed to a

monomorph with the same amount of voltage, although with a corresponding cost in current.

The 2nd Interim Report has provided the theory of monomorphs and bimorphs for two applications, i.e., operations in a cantilever mode (i.e., clamped at one end) and clamped at both ends respectively and will not be discussed in detail again here. The results of these measurements show that the signal to noise ratio of monomorphs appear to be greater than that of the bimorphs. The values of h_{31} calculated from the measurements of monomorphs agree well with the values calculated from results of the measurements on the bimorphs. A typical h_{31} value at 7Hz for a bimorph is 1.31 Mvm^{-1} for an output voltage of 24.80 mV and the corresponding figures for a monomorph are 0.74 Mvm^{-1} and 60.65 mV respectively [5].

5. Embedded Sensors

Many recent studies have been undertaken on embedded sensors in laminate structures using embedded piezo-ceramics in laminate structure [15] and using modal analysis to detect any damage which has occurred within the laminate [16], or have concentrated on active vibration control by embedded piezo-ceramic [17]. Some researchers have embedded optical fibres for use on vibration sensors and have looked at propagating Lamb waves generated from surface mounted ultrasonic transducers [18] and simulated AE source [19]. To the author's knowledge, prior to the present study, the use of embedded electro-ceramic polymer composite sensors for the detection of AE signals, has not been previously undertaken by other workers.

In this section the performance of composite film sensors embedded in glass fibre reinforced polymer laminates for the detection of simulated acoustic emission sources will be discussed briefly. A comparison between the performances of embedded monomorphs and bimorphs and their relevant advantages will also be addressed.

The laminate material, often called pre-preg, consists of parallel glass fibres in an epoxy matrix. The orientation of each ply can take on any number of directions with respect to each other. A typical laminate structure would have a thickness of approximately 20 - 30 plies with relative orientations of 0, ±45, ±60 or 90°. The relative orientation of the plies is not critical, but they should be such that the laminate structure is symmetrical about the neutral axis plane to avoid distortion during the curing process. The composite sensor film must be placed between two plies of the same orientation to avoid damage to the film due to local distortions of the laminate structure during curing. Figure 8 shows an exploded view of a laminate structure containing an embedded transducer [5].

Bimorphs and monomorphs were constructed with circular electrodes, 1 cm in diameter and these were embedded in the laminates for us by Dr. P. Blanas at the US Army Laboratory. The characterization of the embedded sensors was, however, made in our laboratories. Preliminary investigations were performed on a small 30cm x 30cm plate constructed from E-glass FRP composite with 16 plies containing two embedded sensors, a PTCa/Epoxy 60/40 vol% and a PTCa/P(VDF-TrFE) 65/35 vol% monomorphs, located at the centre of the plate, 5cm away from each other. Both transducers were located between the second and third ply with 0-0 orientations. Measurements were made using these transducers to detect lead breaks on the laminate surface 10cm away from the embedded sensors in direction 0° and 90°to the fibre axis. As can be seen from figures 9 and 10[5], both embedded sensors were able to detect the plate waves without any need for amplification. However, it was necessary to provide electrical screening of the circuit to enhance the signal/noise ratio. The signal produced by PTCa/Epoxy sensor (figure 10) was able to detect and distinguish both the extensional and flexural modes of a plate wave travelling in the 0° direction, whereas the corresponding signal for the extensional mode in the 90° direction is less discernible than that in the 0°- direction. It may also be observed from figure 9[5] that the response of the PTCa/P(VDF-TrFE) embedded sensor has a small magnitude, although discernible for the extensional mode for both 0° and 90° degree orientations. Now a signal produced by surface mounted AE sensors is a direct response of the d_{33}-coefficient in contrast to that generated by an embedded sensor whose response will be

affected by both the d_{33}- and d_{31}-coefficients. The effect of the latter coefficient will be to reduce the amplitude of the signal, since the value of d_{31}-coefficient of PTCa/Epoxy is less than that of PTCa/(P(VDF-TrFE), then the contribution to the signal due to the stresses in the 1-direction will be less for the former composite than for the latter one. The embedded PTCa/Epoxy sensor produces a signal comparable to that of a surface mounted transducer where stresses normal to the film surface is dominant. From a frequency analysis of the signals from the embedded transducers it was observed that in the 0°-direction, the extensional modes were centred at 200kHz and 260kHz for the PTCa/P(VDF-TrFE) and PTCa/Epoxy sensors respectively. The flexural mode frequencies were predominantly lower than 30kHz for both sensors.

It is to be noted that the same theoretically derived wave, used for the surface mounted case, was employed for the comparison of the results of both the embedded transducers. It can be seen that the experimentally observed waveforms (see figure 11) agree well with each other as far as time of arrival and peak positions are concerned; however, their fast Fourier transform (FFT) spectra show slight differences in the locations of peak frequencies. The high frequency components observed at the leading edge of the experimental waveform are attributed to the detection of the extensional modes of propagation. The experimentally derived waveforms differ from the theoretically derived waveform in appearance with regard to peak positions. However, the frequency spectra in (d) and (f) resemble closely that of (b) in figure 11[5]. The difference in appearance between the theoretical and experimental results may be explained by the choice of material parameters of the plate used within the algorithm. However, the limitations of the classical plate theory, by neglecting the effects due to rotational inertia and transverse shear are most probably the cause of the discrepancies. Furthermore, the material parameters for the plates were taken from the manufacturer's literature on the pre-preg material used in its construction. The characteristics of the cured plates would be different significantly depending on cure cycle, length of time of pre-preg storage before use, and minor variations in resin chemistry and fibre volume content.

Further results were obtained from two composite plate specimens with embedded monomorph and bimorph sensors. The plates were fabricated from prepeg materials of s-glass continuous reinforcing fibres in an epoxy (NCT-301) matrix. The laminate plates were fabricated, both containing four embedded sensors and consisting of 25 plies with a unidirectional stacking of (0°) and a normal thickness of approximately 0.3cm. The in-plane dimensions of the two unidirectional laminates were 56 x 56 cm and 70 x 70cm respectively. Once again the fabrication of the laminate plates and the embedding of the four sensors, supplied by us, were made by Dr. P. Blanas and his group at the US Army Laboratory. Figure 12[5] shows schematically the embedded monomorphs and bimorph sensor locations in the two laminate plates.

The response of the embedded bimorph PTCa/Epoxy sensor with configuration 2 of figure 7 is shown in figure 13[5], in which the two plate-wave modes of propagation is clearly seen. Fast Fourier transform (FFT) analysis, performed on the signal with a Hanning window gives the spectrum shown in figure 14[5].

In figure 15 the response of the same bimorph, with electrode configuration 1 of figure 7, is shown along with its FFT frequency spectrum given in figure 16[5]. The immediate noticeable difference between the two configurations is the greatly attenuated signal in the second case (i.e., bimorph electrodes with configuration 1 of figure 7), in which the flexural modes have been attenuated more than the extensional modes by a factor of 18dBV as opposed to 8dBV. A slight shift in peak frequencies was also observed between the two responses, but this is believed to be due to the resolution of the FFT.

The extensional modes, which are sometimes termed "stress waves" [20], cause particle motion within the middle or neutral plane of the plate, performing purely longitudinal oscillations. In the case of flexural modes, which are termed "bending waves" [20], the particle motions of the neutral plane are purely transverse oscillations. Particles away from the neutral plane oscillate in an elliptical manner for both modes of oscillations. The embedded bimorph sensors are able to differentiate between the two modes of propagation by sensing the longitudinal and bending stresses within the

laminate plates with monitoring signals obtained with different configurations of monomorph polarities and electrodes together with sensor dimensions. The dimension of the sensor compared to the wavelength of the flexural mode ultimately decides the type of stress the sensor will experience. If the sensor dimensions are comparable to half the wavelength of the flexural waves, it will experience a bending stress resulting in an output due to the bending piezoelectricity of the bimorph. If, however, the sensor dimensions are much smaller than the wavelength of the flexural waves, the stresses experienced by the sensors will predominantly be transverse in nature, resulting in an output from thickness mode piezoelectricity of the bimorph [5].

Similar responses were also obtained for an embedded PTCa/P(VDF-TrFE) sensor which again identified the two propagation modes for both 1 and 2 electrode configurations of figure 7. Again, the flexural mode signal was attenuated by 27dBV in comparison with 18dBV for the case of PTCa/Epoxy , whereas the attenuation of the flexural mode was comparable for the two cases. The difference in signal attenuation between these two types of bimorphs can be understood by considering their electroactive and dielectric properties. The measured piezoelectric d_{31}-coefficients are 4.5 and 0.4 pCN^{-1} and the dielectric permittivities are 45 and 26 for the PTCa/P(VDF-TrFE) and PTCa/Epoxy sensors respectively. These figures would indicate an appropriate 20dBv difference in a signal arising from the g_{31} coefficients (see equation 1) as would be the case for the bimorph sensing in its bending mode.

The approximate wavelengths found for the extensional and flexural modes are 1.4 and 11.0 cm respectively for a plate wave travelling along the direction of the fibres in a unidirectional composite plate. It may be noted that the dimensions of the bimorph transducers are comparable to those of the extensional modes. With configuration 1 (figure 7) of the bimorph electrodes, the bimorph device will be sensing in its bending mode as stresses experienced on the thickness of the bimorph will cancel. It is suggested that as the extensional modes of the plate wave are sensed by the bimorph, a sufficient bending moment is applied to it giving rise to the signal, whereas the bending moment applied to the bimorph by the flexural mode is somewhat reduced due to the greater wavelength involved, and thus the signal being produced is greatly attenuated.

Measurements were conducted with simulated AE sources at varying distances from the embedded sensors. Figure 17[5] shows a plot of signal amplitude as a function of source to detector distance measured with an embedded PTCa/Epoxy sensor. The attenuation coefficients of -6.03 and -8.77m^{-1} were found for the flexural and extension modes respectively. The difference in attenuation coefficients reflects the frequency dependence of the elastic wave attenuation.

The embedded sensors constructed with PTCa/Epoxy show higher amplitudes, by a factor of approximately 5 (i.e., 14dBV) than those with PTCa/P(VDF-TrFE). Although this is expected because the g-coefficient of the former sensor is greater than that of the latter one, however, a superiority of 14dBV would indicate other factors affecting the response, viz., a close match of acoustic properties of the plate and the PTCa/Epoxy sensor.

The results given above have shown that the embedded composite sensors are capable of detecting plate waves in laminate structure. Their broad bandwidth nature has allowed them to detect and distinguish between both the low frequency flexural modes and the higher frequency extensional modes associated with Lamb waves and the dispersive nature of the waves has been identified.

6. The Modelling of Composite Piezoelectric Sensors Using a Finite Element Method.

The finite element method for an approximate solving of differential equations has been applied to many areas of engineering. The freedom it allows in defining the geometry, material properties and boundary condition within the region of space of interest, makes it a valuable analytical tool.

Within the last fifteen years this method has been applied to the modelling of two phase (i.e., ceramic and polymer) composite piezoelectric transducers. The amount

and manner in which the phases of such composites are connected has a significant effect on the performance of the transducer. Particular interest has been given to composites having 0-3 connectivity, where one phase is connected to itself in one dimension throughout the material, while the other is connected to itself in three dimensions.

In the present work, the concepts of finite element method are applied to simulate the response of a ceramic and polymer composite piezoelectric transducer under different loading conditions. The thickness mode and hydrostatic mode of operation have been considered in order to emulate a surface mounted or an embedded transducer respectively. Composites having different connectivity patterns have also been considered and results are given. A computer algorithm has been written following existing finite element libraries to solve mechanical stress/strain problems with adaptation to the solution of a coupled electromechanical problem. The response of the open circuit sensor against frequency has been calculated for difference connectivity patterns and results are given and compared.

The details of the modelling have been included in Appendix 1.

Conclusion

Ultrasonic piezoelectric sensors were produced with PTCa/P(VDF-TrFE) and PTCa/Epoxy materials. The PTCa/P(VDF-TrFE) sensor shows a wider bandwidth response, approximately 50% fractional bandwidth than PTCa/Epoxy sensor with a fractional bandwidth of approximately 20%. This reflects the higher value of the mechanical quality factor Qm for the former composite than that of the latter one.

The work presented in this Contract has shown that embedded film sensors are capable of detecting and distinguishing the extensional and flexural modes of propagating plate waves. Embedded monomorph PTCa/Epoxy sensors appear to be superior to PTCa/P(VDF-TrFE) sensor. Embedded bimorph sensors are able to sense both

bending mode and thickness mode. Bimorphs operate in a similar manner to monomorphs in the thickness mode.

The benefits of using bimorphs as embedded sensors is in their dual mode of operation, enabling the determination of the extensional and flexural modes of plate wave propagation.

PTCa/P(VDF-TrFE) composites appear to be more efficient as actuators than PTCa/Epoxy composites which is a good receiver. A comparison of the monomorph signals to bimorph signals, where the monomorph is essentially operating in a hydrostatic mode and differentiation between the plate wave propagation modes could be made by signal processing, the bimorphs would appear to be the more cost effective way of detection due to their inherent nature of operation which reduces the need for post processing of signals.

Acknowledgements

The financial support of the European Research Office (ERO) of the US Army in London is gratefully acknowledged. It is also a pleasure to thank Dr. P. Blanas of the US Army Research Laboratory, Materials Division, APG, MD, for his invaluable assistance in constructing the laminate plates with embedded sensors, and for sharing his wide knowledge with us on structural composite materials. It is also a pleasure to thank Dr. J.L. Illinger of ERO, London and Dr. R.J. Shuford of the US Army Laboratory, Polymer Division, APG, MD, for their continued encouragement and help during the progress of this work.

References

1. C.J. Dias and D.K. Das-Gupta,
IEEE Trans. on Dielectrics and Electrical Insulation, 3, 706, (1996)

2. M.P. Wenger, P. Blanas, C.J. Dias, R.J. Shuford and D.K. Das-Gupta,
Ferroelectrics, 187, 75 (1996)

3. C.J. Dias and D.K. Das-Gupta,
Ferroelectrics, 157, 405 (1994)

4. P. Blanas, M. Wenger, R.J. Shuford and D.K. Das-Gupta,
Proc. Fourth International Symposium on Composite Materials, Corfu, Greece, 18-22 September (1995), p468

5. M.P. Wenger,
PhD Thesis, University of Wales, UK (1997)

6. C.J. Dias, M.P. Wenger, P. Blanas, R.J. Shuford and D.K. Das-Gupta,
Proc. IEEE Second International Conference on Intelligent Materials, Williamsberg, VA, USA, 5 - 8 June (1994), p437

7. C.J. Dias, M.P. Wenger, Y. Kaminorz, U. Hopfner and D.K. Das-Gupta,
Proc. Eighth International Symposium on Electrets (ISE8), Paris, France, 7-9 September (1994), p589

8. M.P. Wenger, P. Blanas, R.J. Shuford and D.K. Das-Gupta,
Polym. Eng. Sci. (PES), 36, 294 (1996)

9. W.H. Prossor,
NASA Report No. 104187 (1991)

10. H. Banno and S. Saito,
Jap. J. Appl. Phys., 22, 67 (1983)

11. H. Banno and P.K. Ogura,
Proc. Eighth IEEE Symp. on Appl. Ferroelectrics, P266 (1992)

12. M.G. Silk,
"Ultrasonic Transducers for Non-destructive Testing", Adam Hilgeo, UK (1984)

13. W.P. Mason,
"Electromechanical Transducers and Wave Filters", Van Nostrand, USA (1961)

14. G.R. Lockwood and S.F. Foster,
Ultrasonics, Ferroelectrics and Frequency Control, 41, 225 (1994)

15. S.P. Joshi and W.S. Chan,
Active Materials and Adaptive Structure, SPIE (1992)

16. A.S. Islam and K.C. Craig,
Smart Materials and Structure, 3, 318 (1994)

17. S.M. Yang and J.J. Bian,
Smart Materials and Structure, 5, 501 (1996)

18. W.J. Staszewski, S.G, Pierce, K. Worden, W.R. Philp, Tomlinson and B. Cutshaw,
Optical Engng., 36, 1877 (1997)

19. J.F. Dorighi, S. Krishnaswami and J.D, Achenbach,
Trans. IEEE on Ultrasonics, Ferroelectrics & Frequency Control, 42, 820 (1995)

TABLES AND FIGURES

	ε' (1 kHz)	$\tan\delta_e$ (1 kHz)
PTCa	209	0.012
P(VDF-TrFE)	8.1	0.019
Epikote 828	3.9	0.003
PTCa/P(VDF-TrFE) 50/50vol%	36	0.013
PTCa/P(VDF-TrFE) 60/40vol%	44	0.014
PTCa/P(VDF-TrFE) 65/35vol%	51	0.011
PTCa/Epikote 828 50/50vol%	17	0.008
PTCa/Epikote 828 55/45vol%	25	0.009
PTCa/Epikote 828 60/40vol%	36	0.008

Table 1 Permittivities and dielectric loss tangents for the constituent materials and composites taken at 1 kHz and at room temperature.

	ε_{33}	d_{33} [pC/N]	g_{33} [mV m/N]	$d_{33}g_{33}$ [p(Pa)$^{-1}$]
PTCa	209	68	36	2.40
Epikote 828	3.9	-	-	-
P(VDF-TrFE)	8.1	-34	-474	10.88
PTCa/P(VDF-TrFE) 50/50vol%	40	27	76	2.05
PTCa/P(VDF-TrFE) 60/40vol%	49	31	71	2.20
PTCa/P(VDF-TrFE) 65/35vol%	51	33	73	2.41
PTCa/Epikote 828 50/50vol%	17	19	126	2.40
PTCa/Epikote 828 55/45vol%	25	26	117	3.05
PTCa/Epikote 828 60/40vol%	36	30	94	2.82

Table 2 Piezoelectric d_{33} and g_{33} properties of composite systems and their constituent phases.

	ε_{33}	d_{31} [pC/N]	g_{31} [mV m/N]	$d_{31}g_{31}$ [f(Pa)$^{-1}$]
PTCa	209	-3.1	-1.21	3.75
Epikote 828	3.9	-	-	-
P(VDF-TrFE)	8.1	10.7	149	1590
PTCa/P(VDF-TrFE) 50/50vol%	40	-3.60	-10.2	36.7
PTCa/P(VDF-TrFE) 60/40vol%	49	-3.57	-8.23	29.4
PTCa/P(VDF-TrFE) 65/35vol%	51	-3.43	-7.60	26.1
PTCa/Epikote 828 50/50vol%	17	-2.74	-18.2	49.9
PTCa/Epikote 828 55/45vol%	25	-3.38	-15.3	51.7
PTCa/Epikote 828 60/40vol%	36	-3.59	-11.3	40.6

Table 3 Piezoelectric d_{31}, g_{31} and $d_{31}g_{31}$ properties of composite systems and their constituent phases.

	ε'	d_h [pC/N]	g_h [mV m/N]	$d_h g_h$ [p(Pa)$^{-1}$]
PTCa	205	61.8	33.6	2.1
Epikote 828	3.9	-	-	
P(VDF-TrFE)	8.1	-12.6	-176	2.2
PTCa/P(VDF-TrFE) 50/50vol%	40	19.8	55.6	1.1
PTCa/P(VDF-TrFE) 60/40vol%	49	24.0	54.5	1.3
PTCa/P(VDF-TrFE) 65/35vol%	51	26.1	57.8	1.5
PTCa/Epikote 828 50/50vol%	17	13.5	89.6	1.2
PTCa/Epikote 828 55/45vol%	25	19.2	86.4	1.7
PTCa/Epikote 828 60/40vol%	36	22.8	71.4	1.6

Table 4 Hydrostatic piezoelectric d_h, g_h and $d_h g_h$ of the composite systems and their constituent phases.

	k_t	Q_m	Z_a [MRayls]	v_s [km/s]	c^D [GPa]	h_{33}	ρ [kg/m^3]
PTCa	0.47	1200	30	4.35	183	6.6	6890
P(VDF-TrFE)	0.30	20	4.5	2.4	11	-4.7	1880
Epoxy	-	-	-	-	-	-	1160
PTCa/Epoxy 50/50	0.15	11	11	2.77	31	2.1	4025
PTCa/Epoxy 55/45	0.22	15	11	2.51	27	2.3	4312
PTCa/Epoxy 60/40	0.19	20	11	2.42	27	2.1	4598
PTCa/P(VDF-TrFE) 65/35	0.21	8.2	16	3.06	48	2.5	5136

Table 5 Table of k_t and other composite properties gained from measurements on the electrical impedances of the composite films acting as free resonators.

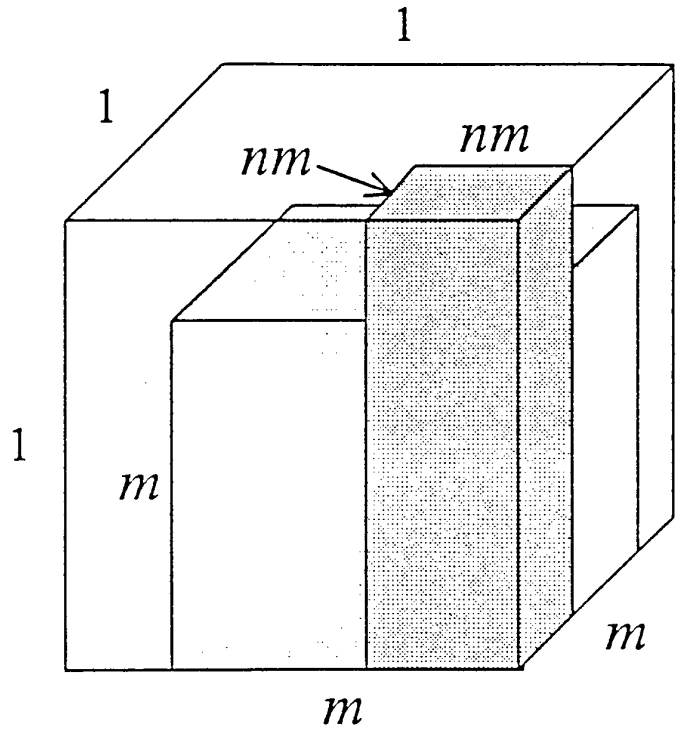

Figure 1. Mixed Connectivity Cube Model for Composites

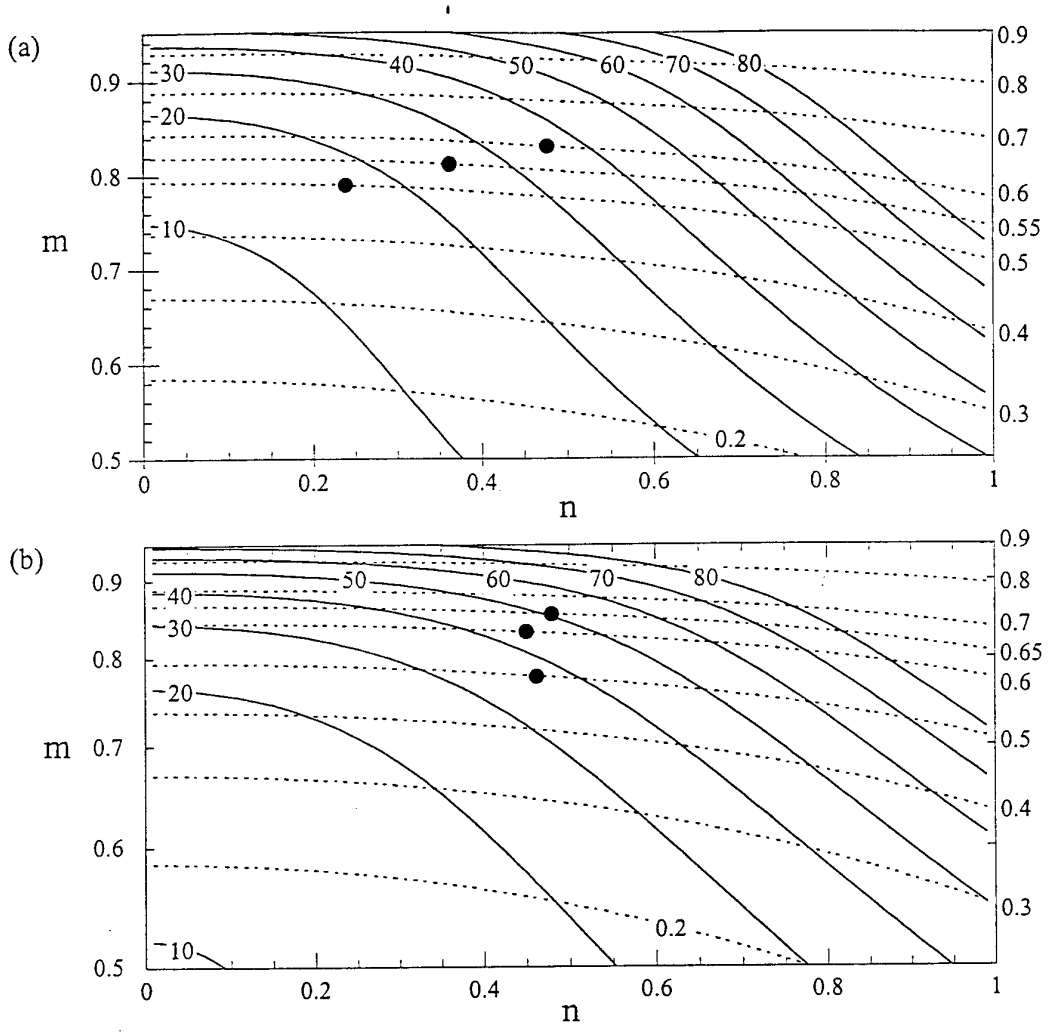

Figure 2 Permitivity contour plots in the m-n plane of the mixed connectivity cube model for (a) PTCa/Epoxy and (b) PTCa/P(VDF-TrFE) composites showing experimental points.

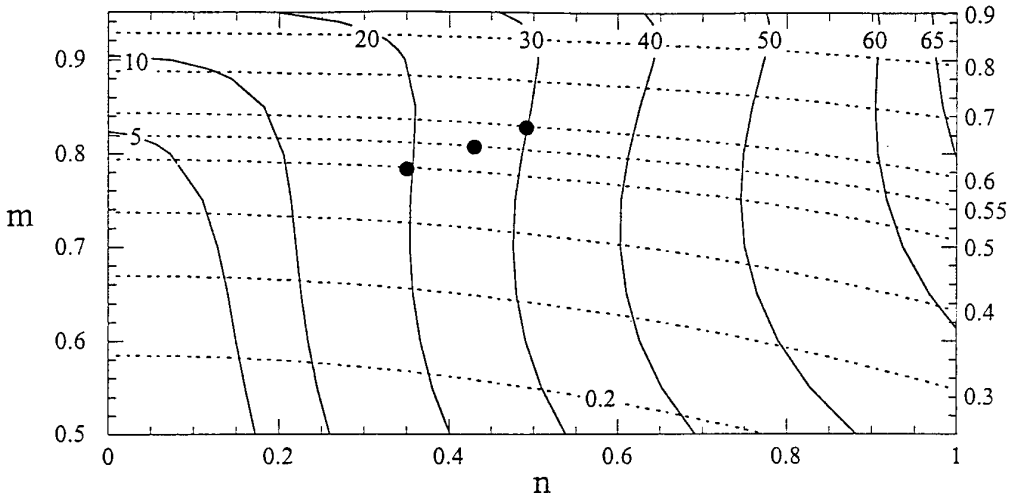

Figure 3 d_{33} contour plots in the m-n plane of the mixed connectivity cube model for composites of PTCa/Epoxy showing experimental points.

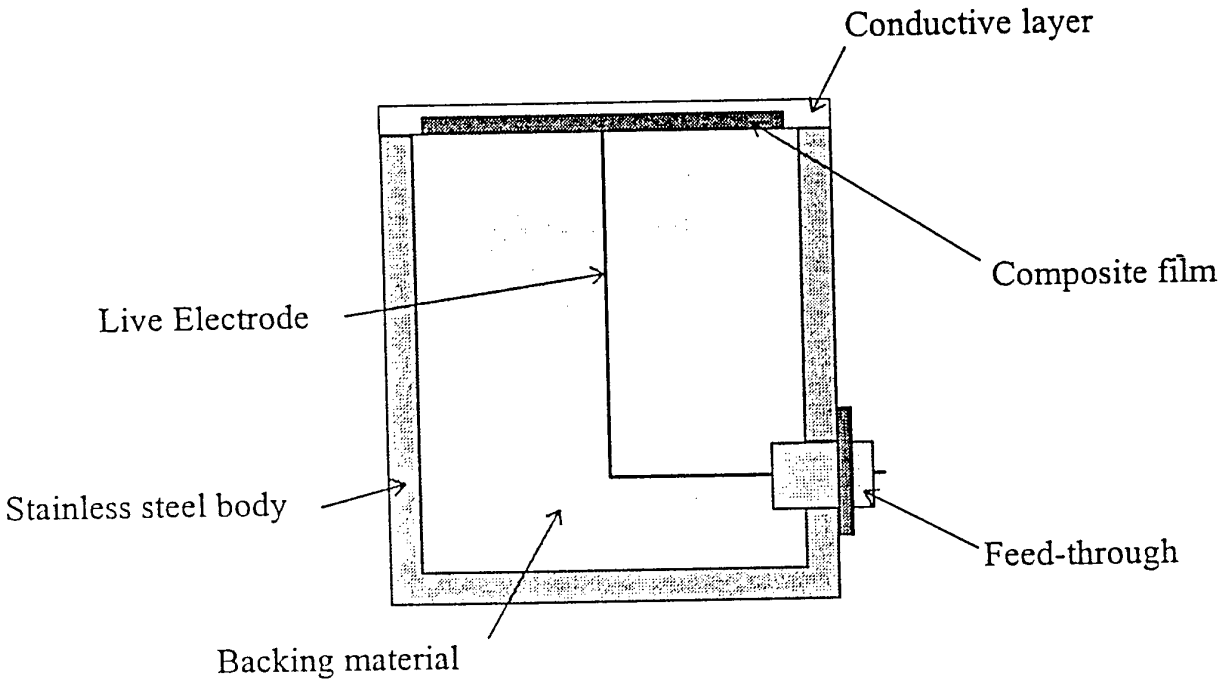

Figure 4 *Schematic diagram showing the design of a standard ultrasonic transducer.*

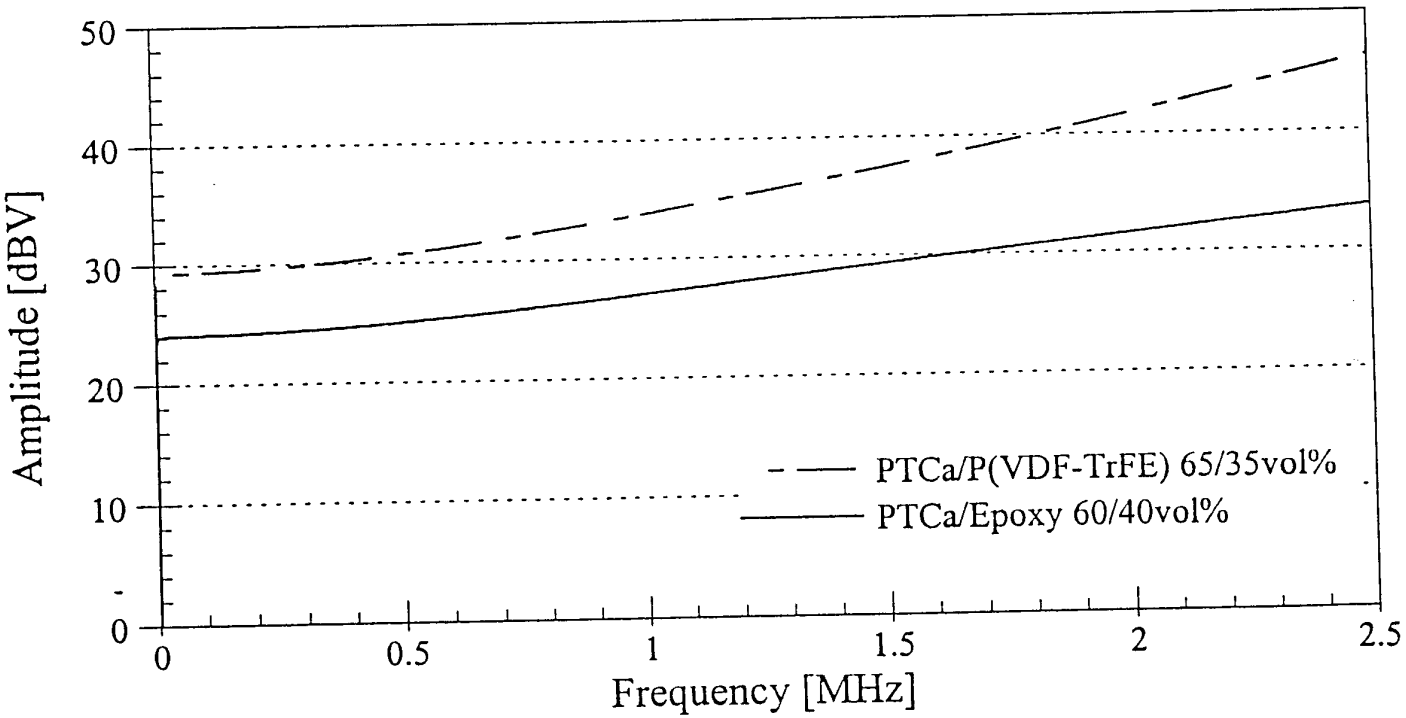

Figure 5 *Transfer functions for transducers constructed from PTCa/P(VDF-TrFE) 65/35vol% and PTCa/Epoxy 55/45vol% over the frequency range 0 - 2.5 MHz.*

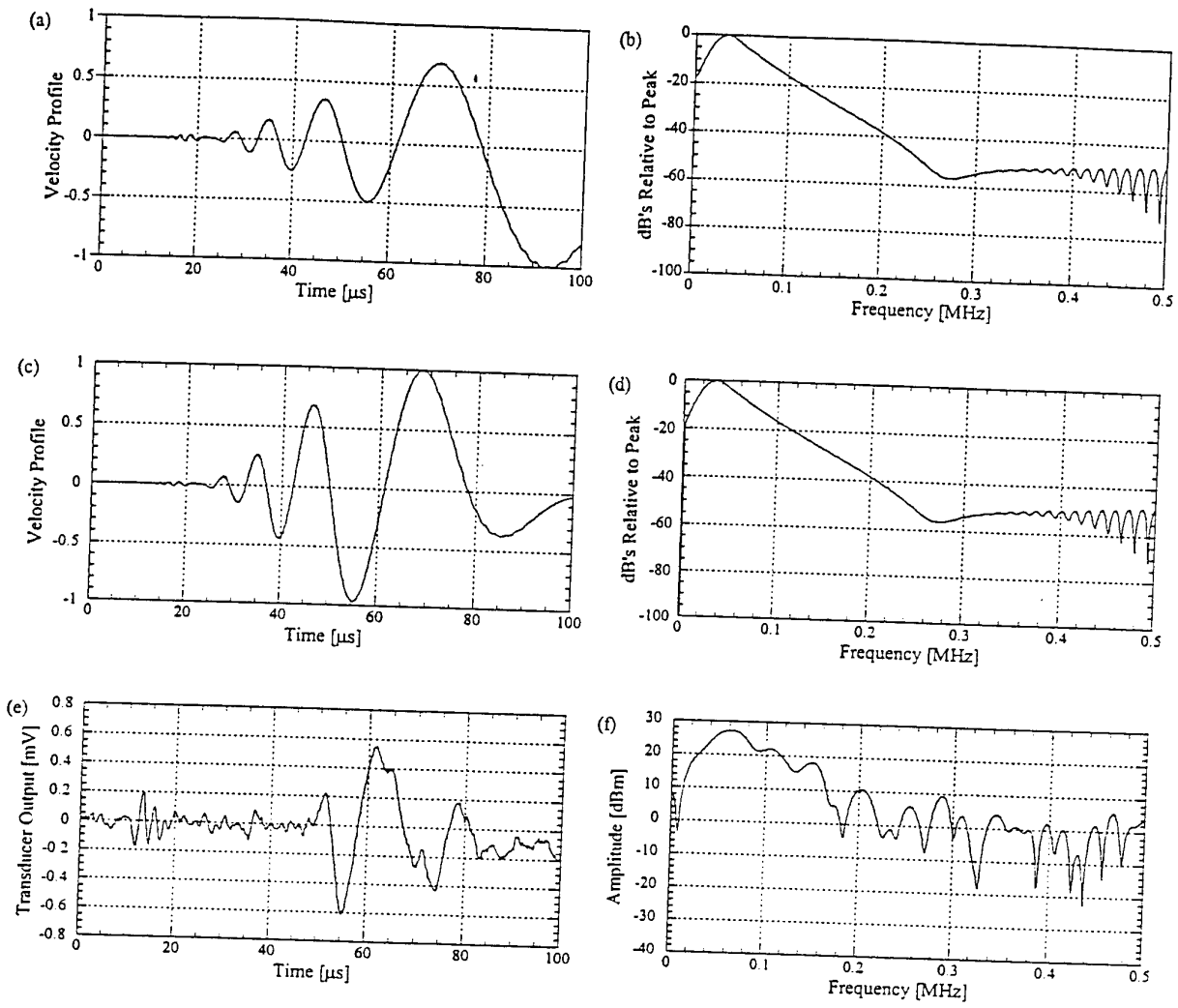

Figure 6 *(a) Predicted normal velocity component of the response to a lead break on the surface of an orthotropic FRP plate and (b) the FFT spectrum of the predicted flexural plate wave propagating along the fibre axis. (c) Inverse FFT of convoluted signal to produce the predicted output from a PTCa/Epoxy 55/45vol% surface mounted transducer, (d) corresponding frequency spectrum. (e) Output response of a real transducer and (f) corresponding frequency spectrum.*

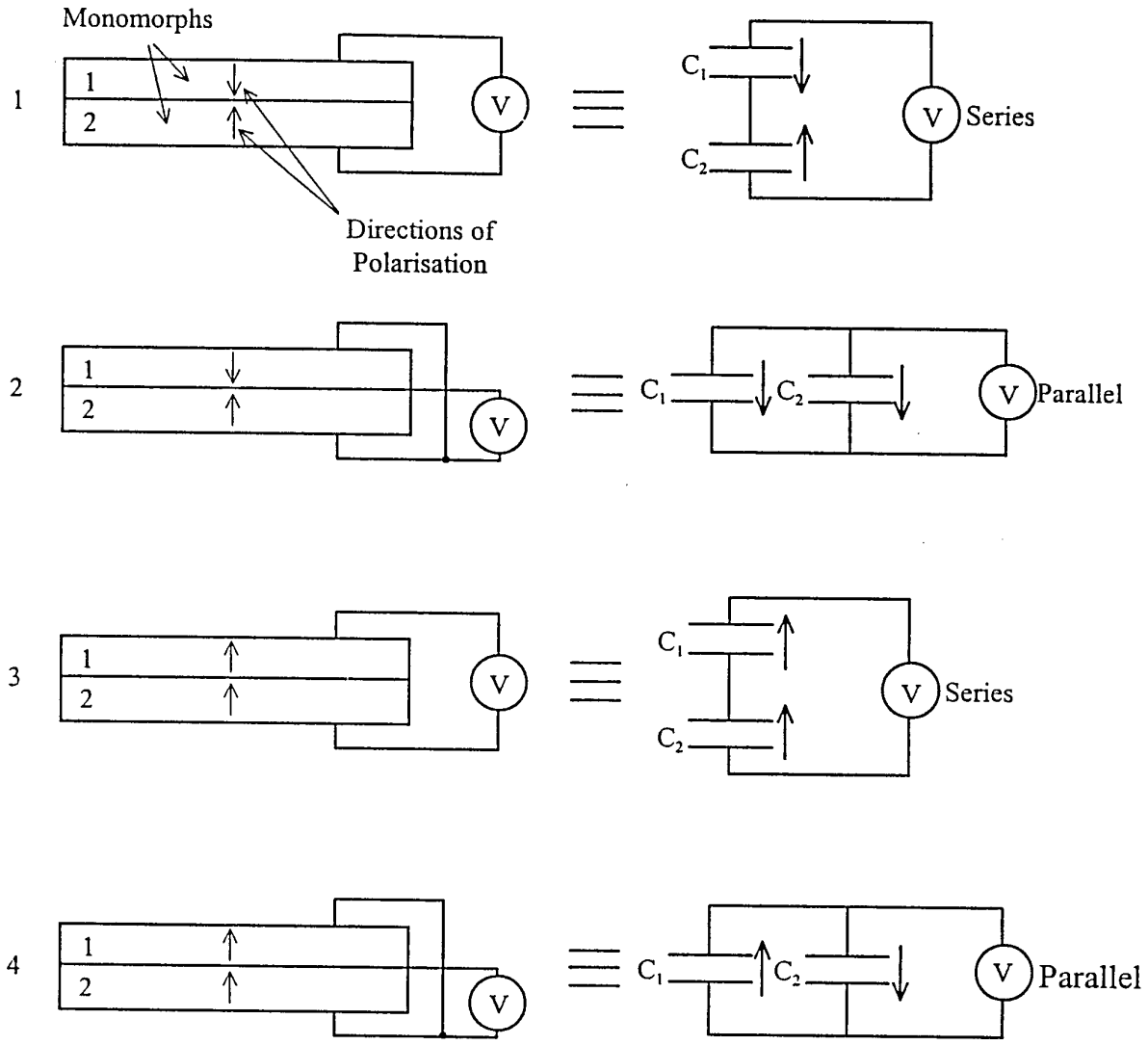

Figure 7 *Schematic representation of bimorph configurations.*

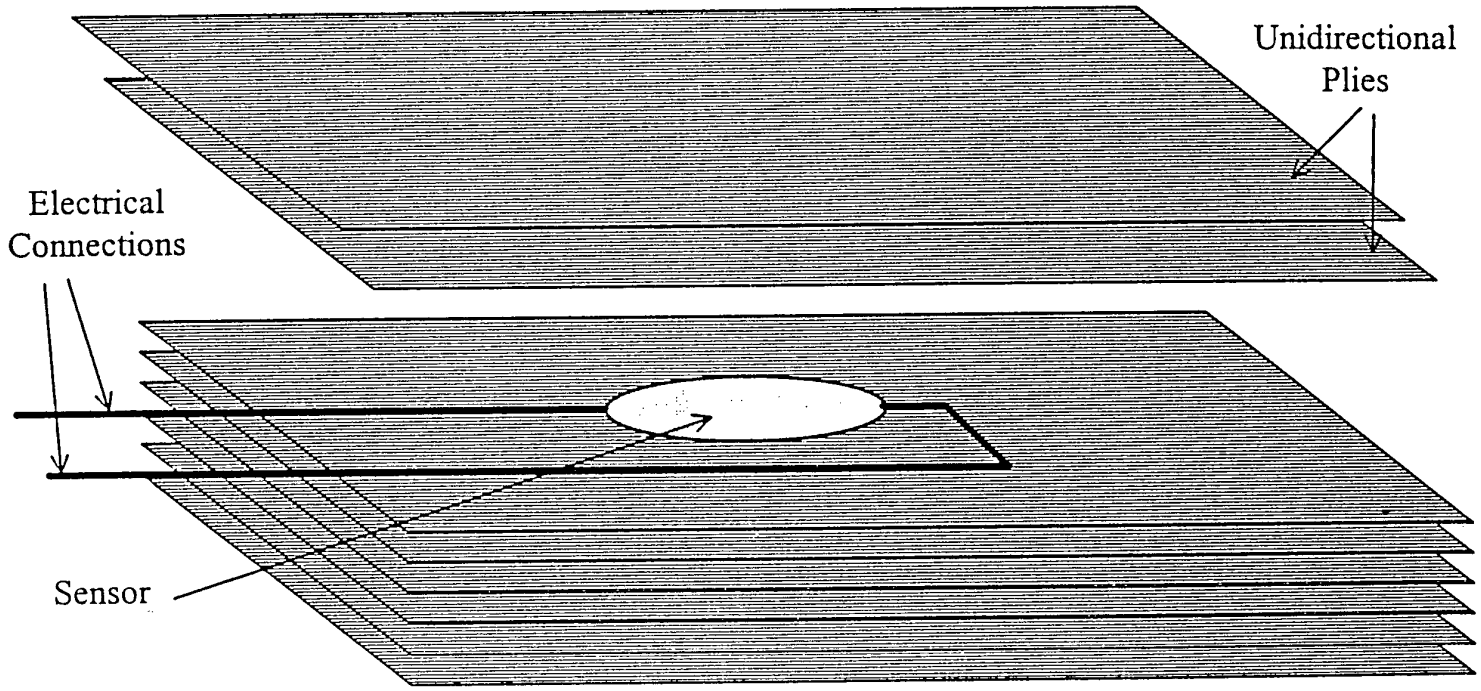

Figure 8 *Exploded view of a laminate structure containing an embedded composite transducer.*

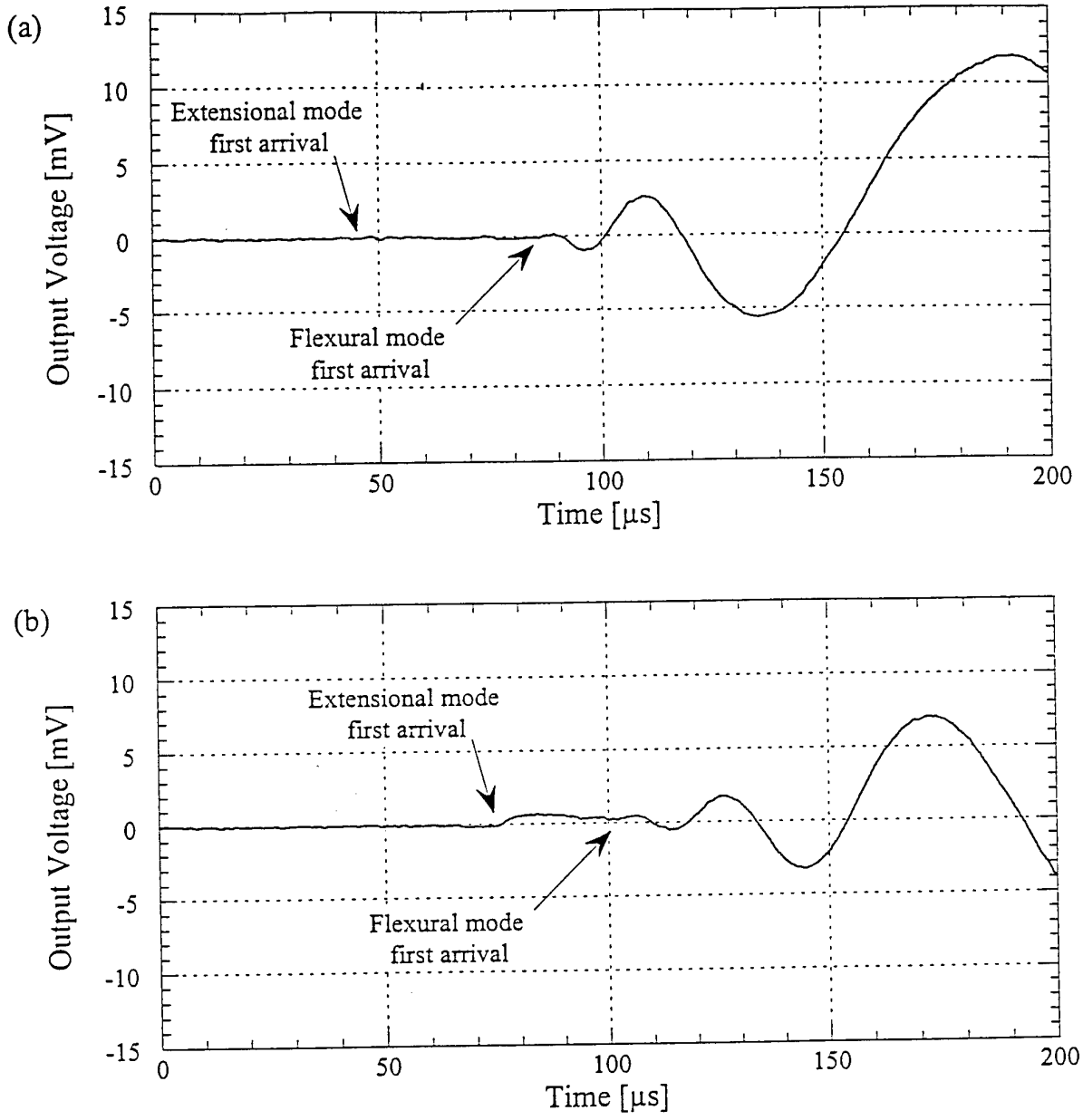

Figure 9 *Response from an embedded PTCa/P(VDF-TrFE) 65/35vol% monomorp sensor to a simulated acoustic emission 10 cm away at (a) 0° and (b) 90° to the fib axis.*

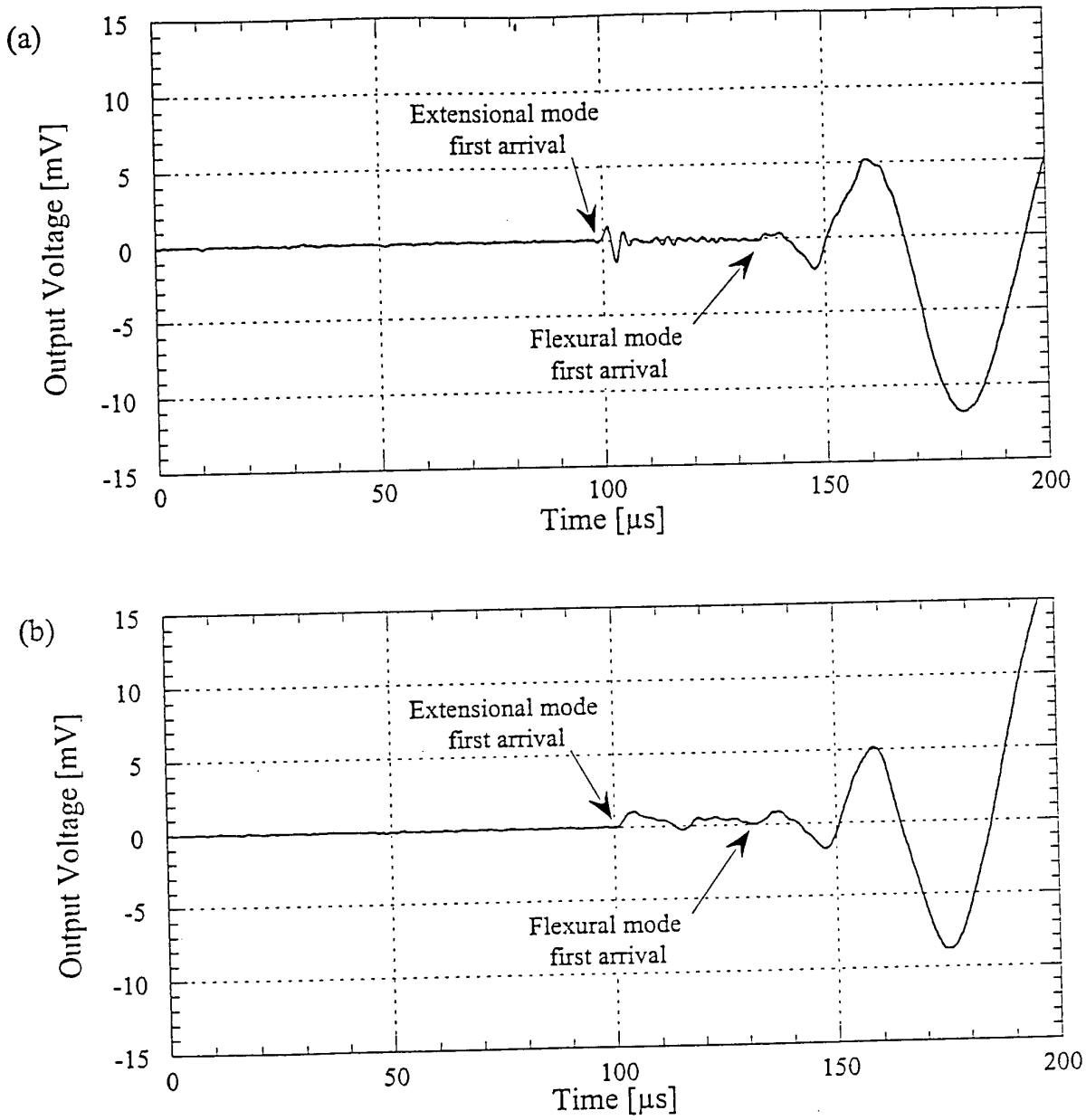

Figure 10 *Response from an embedded PTCa/Epoxy 60/40vol% monomorph sensor to a simulated acoustic emission 10 cm away at (a) 0° and (b) 90° to the fibre axis.*

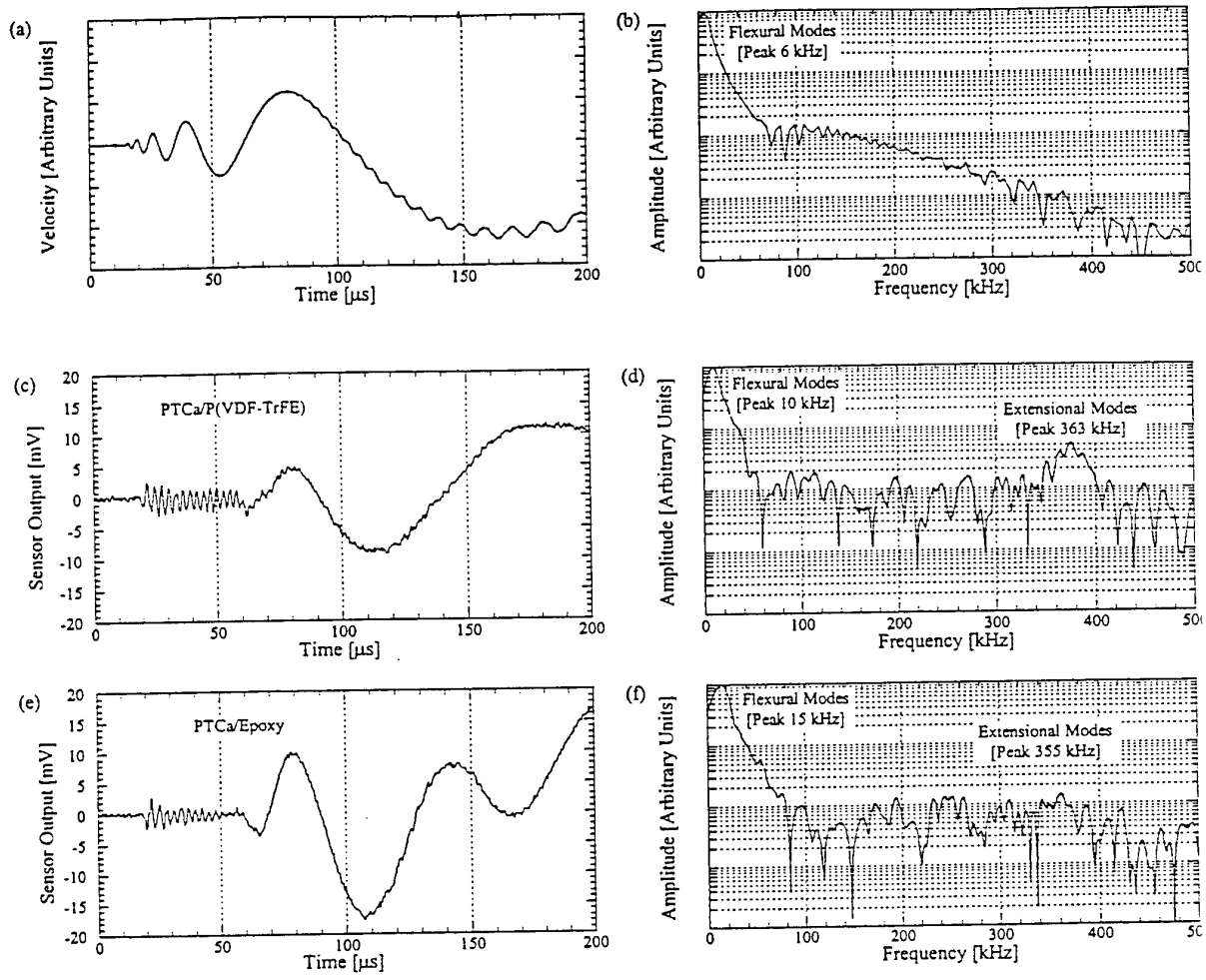

Figure 11 *(a) Theoretical plate wave and (b) its FFT frequency spectrum. (Response of an embedded PTCa/P(VDF-TrFE) 60/40vol% AE transducer and (corresponding FFT frequency spectrum. (e) Response of an embedded PTCa/Epo 55/45vol% AE transducer and (f) corresponding FFT frequency spectrum.*

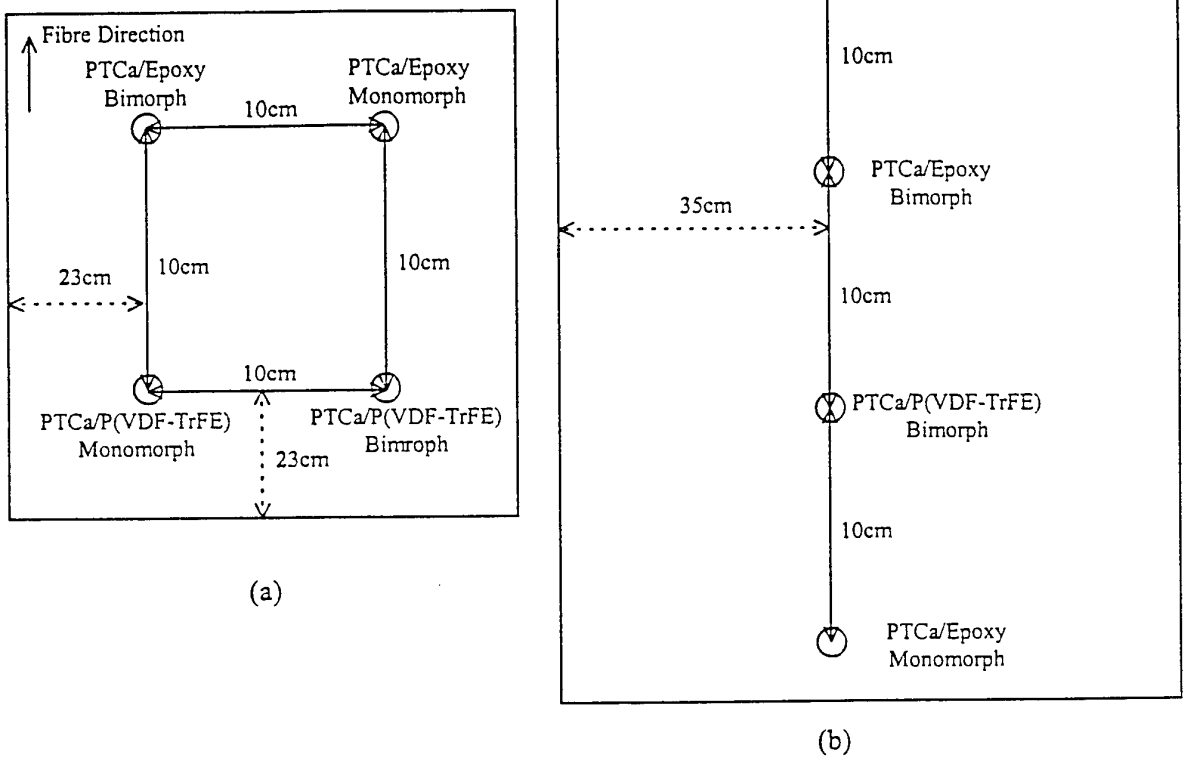

Figure 12 *Schematic diagrams showing the embedded monomorph and bimorph sensor locations (a) two layers below the surface in a composite plate of 56 x 56 x 0.3 cm and (b) four layers below the surface in a 70 x 70 x 0.3 cm.*

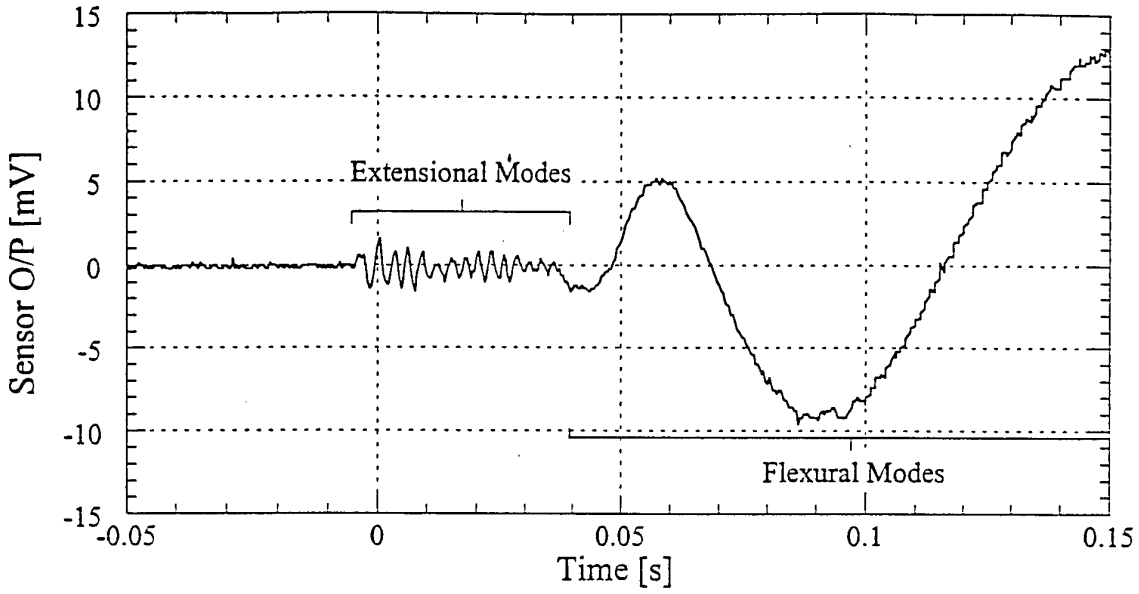

Figure 13 *Output response of an embedded PTCa/Epoxy bimorph sensor with electrode configuration 2 to a simulated AE source 10 cm away, 0° to the fibre axis in an unidirectional S-glass reinforced epoxy composites plate.*

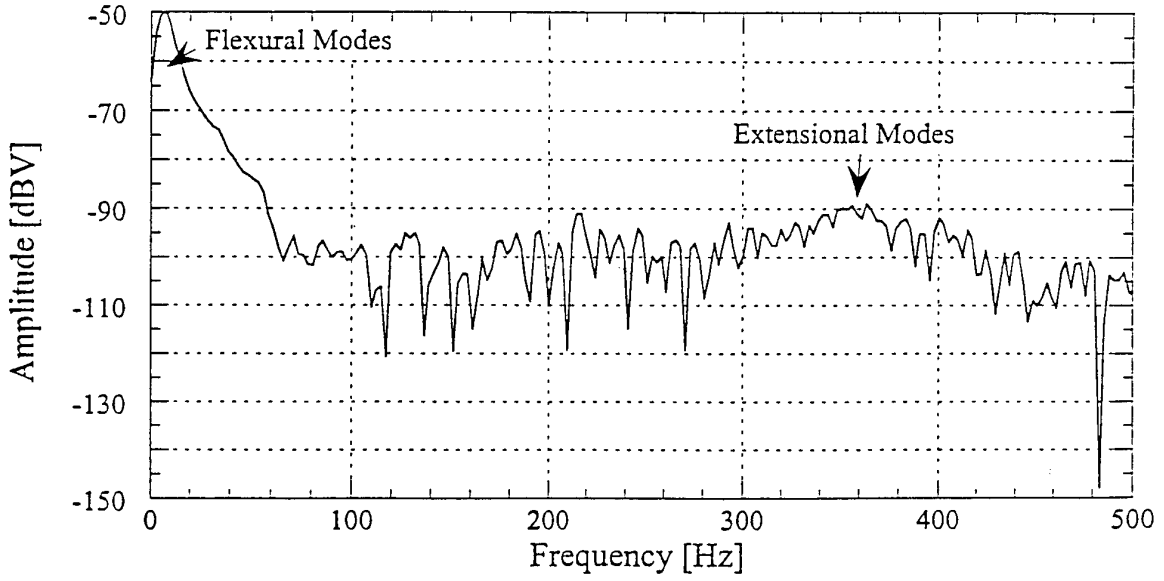

Figure 14 *FFT frequency analysis, using a Hanning window, on the signal shown in figure 8.9.*

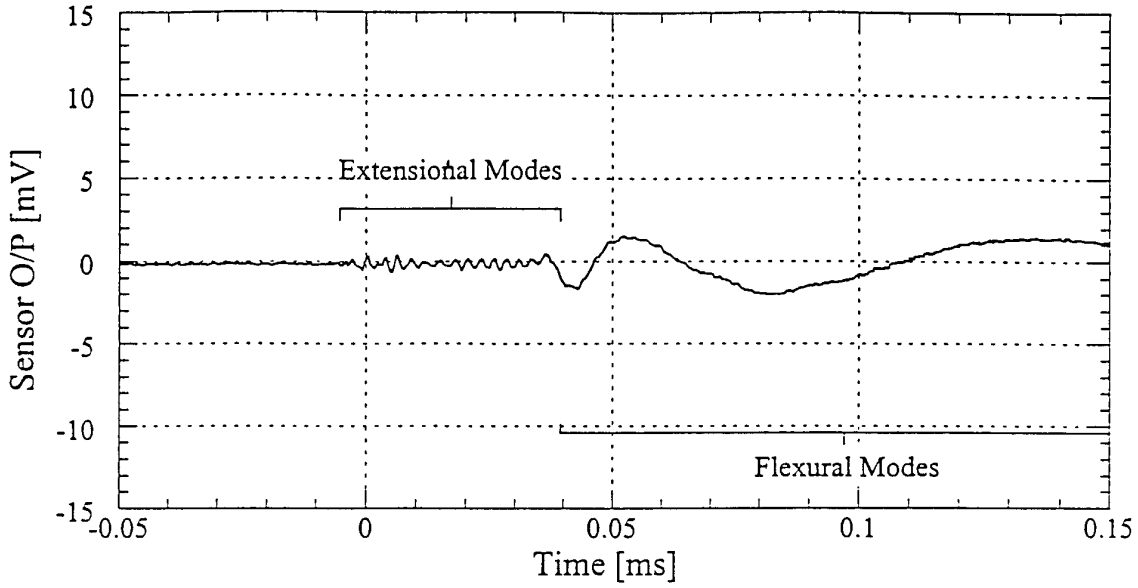

Figure 15 *Output response of an embedded PTCa/Epoxy bimorph sensor with electrode configuration 1 to a simulated AE source 10 cm away, 0° to the fibre axis in an unidirectional S-glass reinforced epoxy composite plate.*

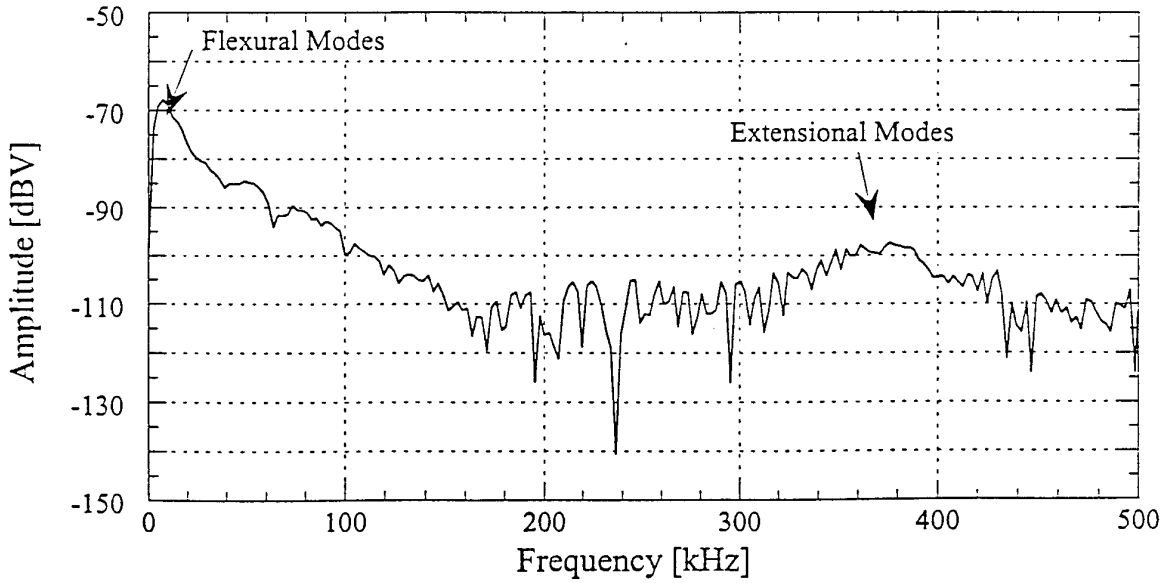

Figure 16 *FFT frequency analysis, using a Hanning window, on the signal shown in figure 8.11.*

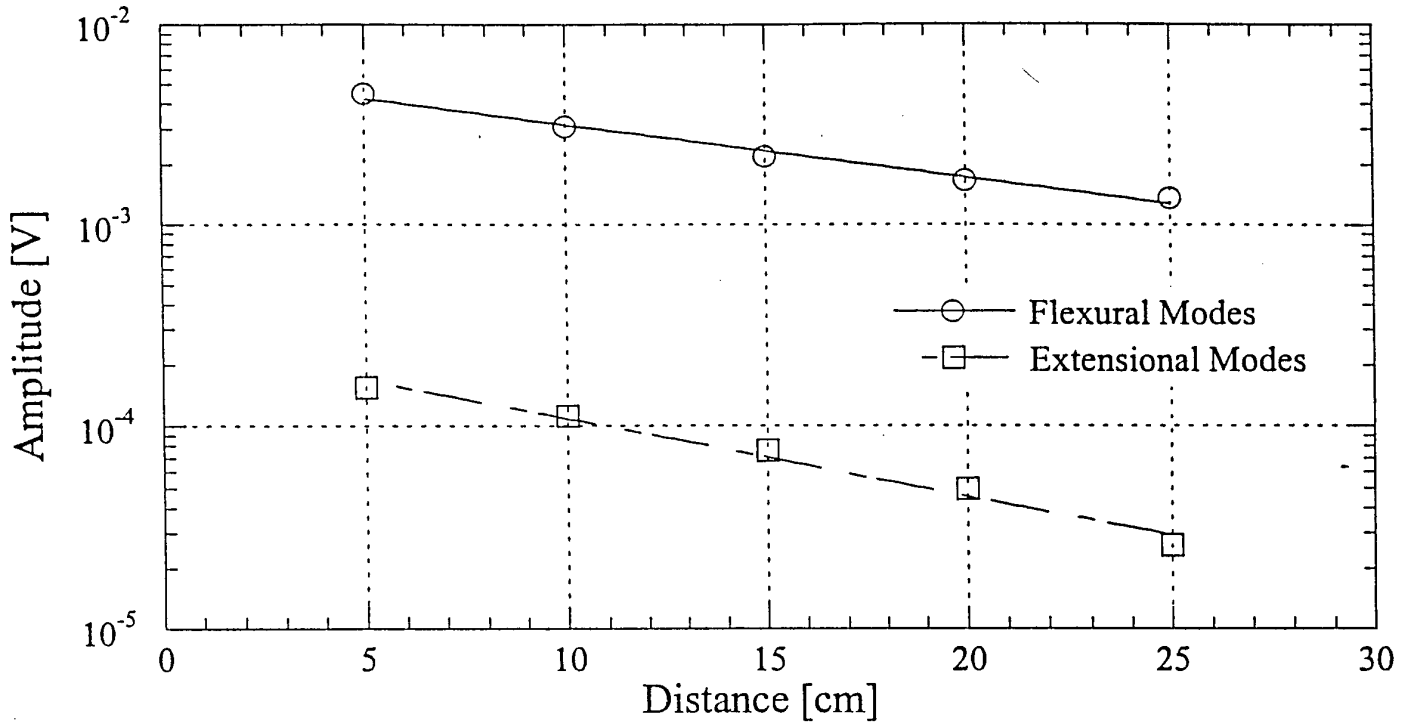

Figure 17 *Plot of the amplitudes versus distance of plate waves in a S-glass FRP composite plate as detected by an embedded PTCa/Epoxy composite monomorph sensor.*

APPENDIX 1

Finite Element Modelling of Embedded Sensors

1 Introduction

The Finite Element Method (FEM) has been proved a useful method in the modeling of piezoelectric transducers, particularly in the calculation of natural frequencies. Its main advantage over other methods is the modeling of complex geometries, which is well suited for composite transducers. In fact, the basic concept of FEM is that of founding an integral equation, defined in the transducer volume, that is equivalent to the piezoelectric equations and takes into account the static (via the elastic, dielectric and piezoelectric constants) and dynamic (via the density) properties of the material.

The integral form of this equation allows to decompose the sensor in little domains, called elements, and to define a specific set of material properties inside each element. In this way it is possible to define the connectivity of the material simply assigning the ceramic properties to a defined pattern of elements and the polymer properties to the others.

Moreover, the unknown functions - the displacement and the electric potential - inside one element are expressed in terms of their value at certain points, called nodes, of the element itself.

As a result, a set of linear algebraic equations is obtained, instead of partial differential equation. The solution of these linear equations is a vector whose components are the values of the unknowns at nodal points. The value of the unknowns between two nodes next to each other is expressed as a function of the unknowns themselves, linearly variable with the spatial coordinates. Because the size of the elements determines the distances of the nodes, it determines how good is the approximation.

The aim of the present work is to calculate the first resonant frequency of the sensor as a function of connectivity and ceramic volume fraction. However, the present study is confined to polymeric sensors only.

2 The NAG library

In the development of a Finite Element model, the first problem is given by the quite complicated mathematical theories, whose applications can be of difficult solution: first of all, the geometry of the problem, which will in turn affect the elements and nodes numbering, the shape function determination , the right hand side vector building and the numerical integration method.

1. For this reason it is a good help to the programmer a library of subroutines that gives the building blocks for a wide variety of problems and allows the relatively easy variation of the main program. Considering various software packages commercially available, the Nag (Numerical Algorithm Group) Finite Element library (NAGFE) has been chosen; it is a FORTRAN library containing subroutines that allow the modeling in two or three dimensions, in circular or orthogonal geometry, and with different kinds of system matrices (symmetric, banded, general). Furthermore, some example programs which solve purely mechanical problems have been used as the background for the construction of the model. The solution of the system equation is found using the more common Nag routines for the solution of multiple linear equations.

3. The embedded sensor

The transducer is modeled as a thin-film piezoelectric material of thickness 100 μm and surface area 1cm^2 (figure A/1). One electrode is kept at zero potential by grounding, thus the potential between the electrodes is equal to the potential of the other electrode.

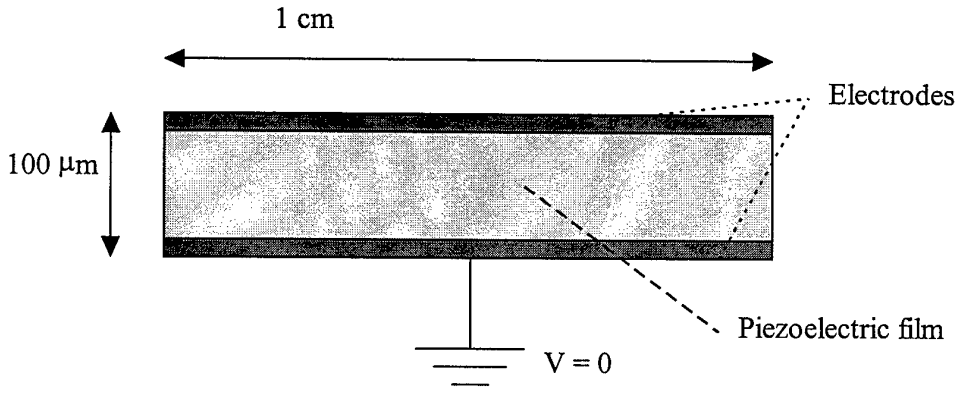

Figure A/1 Cross section of the piezoelectric film sensor

The embedded sensor is operating under hydrostatic pressure, that is a spatially uniform pressure (constant amplitude) is acting over its six surfaces (figure A/2); this pressure will be made sinusoidally variable, and the electric potential developed between the two electrodes will be calculated for different frequencies, giving the response of the sensor over the range of interest.

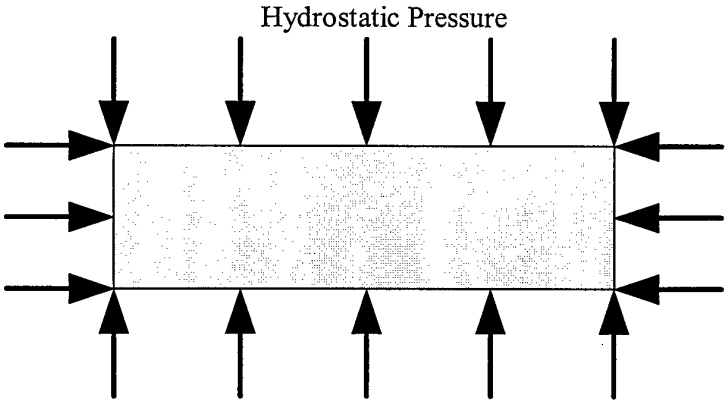

Figure A/2 Piezoelectric material under hydrostatic pressure

Because of the complexity of calculations involved in a Finite Element Model, some others conditions are initially applied in order to simplify the program that will simulate

the sensor. Removing these conditions will not affect the basic structure of the program, as it will be discussed further.

First, the transducer is modeled in two dimensions. It is assumed that this simplification, while strongly reducing the number of equations for a given lateral extension of the elements, will not affect the frequency and connectivity dependence of the potential; then a lossless case is considered in order to render real the matrix equations that model the sensor, reducing in this way the amount of memory required to run the program. Furthermore, the electrodes are not electrically connected, thus the complex impedance of the external circuit will be ignored. From the last condition follow that no free charge is allowed in the electrodes.

3 The application of these simplifications will have a strong influence on the sensor response, but can give good results in terms of the calculation of resonant frequencies of the sensor, especially for their dependence on the connectivity of the piezoelectric film material. It is intended in this work to give a good basis for the further development of a model more complete and closer to the real sensor (i.e. the addition of mechanical and electric losses and the external circuit).The Holland-EerNisse Variational Principle

As pointed out in the introduction, an integral equation equivalent to the piezoelectric equations is needed in order to consider each element on its own in the build up of the system matrix. This was first founded in the form of a variational principle by the Holland and Eer-Nisse who used a trial and error procedure. Its general form is rather complicated, and a simpler form given by Allik is usually preferred in the field of acoustic sensors:

$$\begin{aligned}&\iiint_{Vol}\{\delta S^T\cdot c\cdot S-\delta S^T\cdot e\cdot E-\delta E^T\cdot e^T\cdot S-\delta E^T\cdot\varepsilon\cdot E+\\&-\delta u^T\cdot\hat{F}+\rho\cdot\delta u^T\cdot\ddot{u}+\delta\phi\cdot\hat{\sigma}\ \}dV-\iint_{S_1}\delta u^T\cdot\hat{T}\,dS+\\&+\iint_{S_2}\delta\phi\cdot\hat{\sigma}'\,dS-\delta u\cdot P+\delta\phi\cdot Q=0\end{aligned}\qquad\textbf{(A-1)}$$

where S, u, c, E, ε, e, ϕ are respectively the strain, the displacement, the elasticity matrix, the electric field, the dielectric permittivity, the piezoelectric coefficient and the electric potential inside the material; F, T, P, σ, σ', Q are the body force, the component of stress orthogonal to the surface (pressure), the point force, the free body charge, the free surface charge and the point charge; S1 and S2 are that part of sensor surface in which respectively the orthogonal component of stress and the free surface charge are known; finally, two dot on top of a symbol means double derivation on time and the symbol δ represent a virtual displacement applied to quantities that follow it.

Because of the simplifying conditions introduced in section 1, which lead to zero free surface charge, plus the additional simplification of considering the body and point forces and charges neglectable, equation 6.1 take the following form:

$$\iiint_{Vol}\{\rho\cdot\delta u^T\cdot\ddot{u}+\delta S^T\cdot c\cdot S-\delta S^T\cdot e\cdot E-\delta E^T\cdot e^T\cdot S+ -\delta E^T\cdot\varepsilon\cdot E\}dV-\iint_{S_1}\delta u^T\cdot\hat{T}\,dS=0 \quad \textbf{(A-2)}$$

in which only the external pressure appear as a known variable.

In this application, the electrical potential and the mechanical displacement are more significant quantities than the electric field and the strain; thus the following equations are considered:

$$E=-\nabla\phi \quad \textbf{(A-3)}$$

$$S=\hat{\nabla}u \quad \textbf{(A-4)}$$

where

$$\nabla=\begin{pmatrix}\frac{\partial}{\partial x}\\ \frac{\partial}{\partial y}\end{pmatrix} \quad \textbf{(A-5)}$$

$$\hat{\nabla} = \begin{pmatrix} \frac{\partial}{\partial x} & 0 \\ 0 & \frac{\partial}{\partial y} \\ \frac{\partial}{\partial y} & \frac{\partial}{\partial x} \end{pmatrix} \tag{A-6}$$

From these equations and equation 2,we obtain the following:

$$\iiint_{Vol} \{\delta u^T(\rho \ddot{u} + \hat{\nabla}^T c \hat{\nabla} u) + \delta u^T(\hat{\nabla}^T e \nabla \phi) + \delta \phi(\nabla^T e^T \hat{\nabla} u) + - \delta \phi(\nabla^T \varepsilon \nabla \phi)\} dV - \iint_{S_1} \delta u^T \cdot \hat{T}\, dS = 0 \tag{A-7}$$

which is the form that will be used in the FEM approximation. The solution of this equation is compatible with the piezoelectric equations. Notice that the integral form of the above equation allows to write:

$$\iiint_{Vol} ....dV = \sum_{i=1}^{n} \iiint_{Vol_i} ....dV \tag{A-8}$$

$$\iint_{Sup} ....dS = \sum_{i=1}^{n} \iint_{Sup_i} ....dS \tag{A-9}$$

4 in which the subscript *i* refers to the elements (*n* is the total number of elements), and thus each element, each with its own properties (i.e. each element can be defined as made by a different material, by means of its constitutive properties), can be considered by itself to calculate the integral, and a subsequent summation over the elements will give the integral on the volume of the piezoelectric sensor as a whole.

5 Elements, nodes and numbering system

5.1 Partition of the sensor in elements

As mentioned above, the transducer volume (or area in the two-dimensional case) is divided in an arbitrary number of elements. Each element has a number associated with

it, and is then referred using this number. For instance, suppose that the transducer area is divided in four elements, each with the same extension in the axis directions (figure A/3), the elements will be numbered in the order given by following the z and x directions in turn, starting from z=0 and x=0.

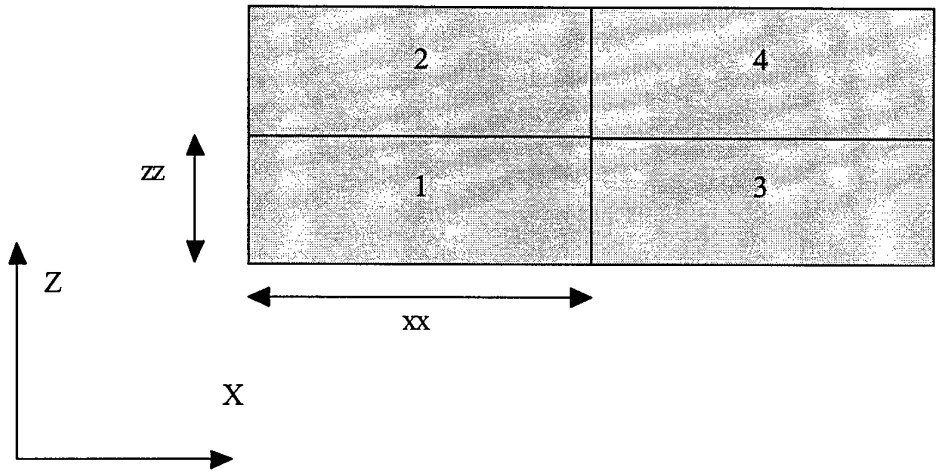

Figure A/3 Division of transducer in subdomains (elements)

The extension of the elements in the two directions, xx and zz, determine the total number of elements and the resolution obtainable by the approximation in terms of wavelength and thus frequency, as will be explained later.

5.2 Nodes and discretisation of the integral equation

In order to obtain an approximation of the solution, the unknown functions u(x,z,t), ϕ(x,z,t) are substituted by the following sum of functions:

$$u(x,z,t) \approx \hat{u} = \sum_{j=1}^{k} f_{uj}(x,z,t) \cdot u_j \qquad \textbf{(A-10)}$$

$$\phi(x,z,t) \approx \hat{\phi} = \sum_{j=1}^{k} f_{\phi j}(x,z,t) \cdot \phi_j \qquad \textbf{(A-11)}$$

In these equations, u_j and ϕ_j refer to the value of displacements and potential at one point of the sensor, f_{uj} and $f_{\phi j}$ are functions of space and time related to the same point. In the theory of FEM these points are referred to as nodes.

As stated in the last section, the left hand sides of equations 8 and 9 can be evaluated element by element and summed together before the solution procedure. In this way it is possible to give to each element the desired set of material properties, thus determining the material connectivity. WE can therefore consider only one element and define standard procedures for the calculation of one element integral.

Substituting equations 10 and 11 in one term of equation 8 we obtain:

$$\begin{aligned}&\iiint_{Vol_i}\{[\delta\hat{u}]^T\rho[\ddot{\hat{u}}]+[\delta\hat{u}]^T[\hat{\nabla}f_u]^T c[\hat{\nabla}f_u][\hat{u}]+[\delta\hat{u}]^T[\hat{\nabla}f_u]^T e[\nabla f_\phi][\hat{\phi}]+\\&+[\delta\hat{\phi}][\nabla f_\phi]^T e^T[\hat{\nabla}f_u][\hat{u}]+\\&-[\delta\hat{\phi}][\nabla f_\phi]^T \varepsilon[\nabla f_\phi][\hat{\phi}]\}dV-\iint_{S_i}[\delta\hat{u}]^T\cdot[f_{\hat{T}}][\hat{\hat{T}}]dS=0\end{aligned} \qquad \textbf{(A-12)}$$

in which the square brackets refer to a vector whose components are the values of the quantity at each node of the sensor. Because the values of u and ϕ at one node are not anymore function of space, we can take them out of the integral and write:

$$\begin{aligned}&[\delta\hat{u}]^T[M][\ddot{\hat{u}}]+[\delta\hat{u}]^T[K_{uu}][\hat{u}]+\\&+[\delta\hat{u}]^T[K_{u\phi}][\hat{\phi}]+[\delta\hat{\phi}][K_{\phi u}][\hat{u}]+\\&-[\delta\hat{\phi}][K_{\phi\phi}][\hat{\phi}]-[\delta u^T][S][\hat{\hat{T}}]=0\end{aligned} \qquad \textbf{(A-13)}$$

with

$$[M]=\iiint_{Vol}(\rho[f_u]^T[f_u])\,dV \qquad \textbf{(A-14)}$$

$$[K_{uu}]=\iiint_{Vol}([\hat{\nabla}f_u]^T[c][\hat{\nabla}f_u])\,dV \qquad \textbf{(A-15)}$$

$$[K_{u\phi}]=\iiint_{Vol}([\hat{\nabla}f_u]^T[e][\nabla f_\phi])\,dV \qquad \textbf{(A-16)}$$

$$[K_{\phi u}] = [K_{u\phi}]^T \tag{A-17}$$

$$[S] = \iint_{S_1} [f_{\hat{T}}] dS \tag{A-18}$$

As a result of the integration, the coefficients of the matrices are numbers, not functions of space. The spatial information is contained in the index *j*, that refers to a precise point of the sensor, and the coefficients that multiply the variables of index *j* are a result of integration in the elements that contain the node, thus in a region of space near the point considered.

The electrical potential at one node, as well as the two components of displacement, can be considered as another variable of the node, so we can define a generalized displacement as:

$$a = \begin{bmatrix} \hat{u}_x \\ \hat{u}_z \\ \hat{\phi} \end{bmatrix} \tag{A-19}$$

whose components are referred to as degrees of freedom of the node. Moreover, as we are considering sinusoidally variable functions on time, the double derivation of time takes the form:

$$\ddot{u} = \frac{d^2u}{dt^2} = -\omega^2 u \tag{A-20}$$

Considering the two equation above and equation 13 we can write

$$([K] - \omega^2[M'])[a] = [S]T_0 \tag{A-21}$$

where

$$[K] = \begin{bmatrix} K_{uu} & K_{u\phi} \\ K_{\phi u} & K_{\phi\phi} \end{bmatrix} \tag{A-22}$$

$$[M'] = \begin{bmatrix} M & 0 \\ 0 & 0 \end{bmatrix} \qquad \textbf{(A-23)}$$

and T_0 is a scalar representing the amplitude of the pressure.

The equations to be solved are now linear algebraic equations, and can be solved (if possible) using standard methods for linear algebra. The procedures to obtain the matrices will be discussed in the following subsections.

Notice that the matrix associated with one node is a 3*3 matrix, and this structure is reflected in the system matrix, that is symmetric by blocks, as will be discussed later.

5.3 Nodes numbering

Each node is identified by two numbers: one is the internal (to the element), which follow from the need to build, for each element, standard procedures that take into account the fact that elements have all the same structure; the other is the global number, which is different for each node and uniquely identify it in the overall system. Next figure shows the internal and global numbering systems for our example, while the arrays that keep those information in the program are shown in the following tables.

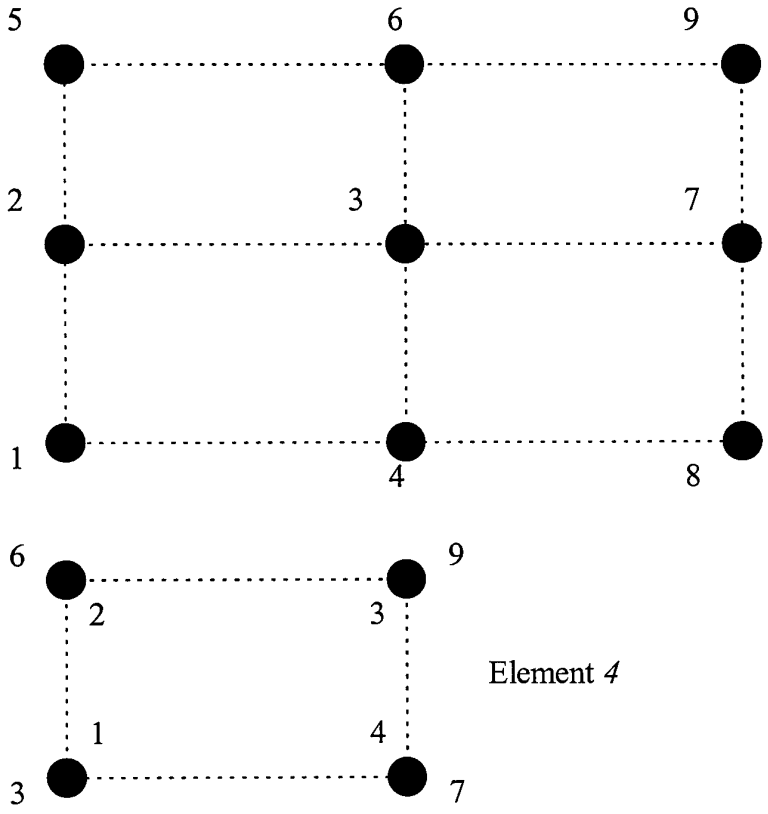

Figure A/4 Global and internal numbering system; the top picture shows the global numbering system, while the bottom picture shows global and internal numbers for nodes in element *4*

The subroutine TOPOL creates the arrays ELTOP (element topology), that contains six integer numbers: the first define the material (0 for polymer, 1 for ceramic) the second is the number of nodes for the element (4) and the other four are the global nodes

numbers arranged in an internal order; for instance, in the case shown in the above figure, the array has this form:

ELEM.	MATER.	NODES	NODE 1	NODE 2	NODE 3	NODE 4
1	0	4	1	2	3	4
2	0	4	2	5	6	3
3	0	4	4	3	7	8
4	0	4	3	6	9	7

Table A-1 ELEMENT TOPOLOGY : type of material, nodes per element, global number of nodes in internal order. The numbers of the nodes contained in the array are the global numbers, while the position (column) in the array identifies the internal numbers.

The subroutine build another array, COORD, whose row *i* correspond to the node whose global number is *i*, and the columns are the space coordinates of the nodes:

GLOBAL NUMBER	X	Y
1	0	0
2	0	zz
3	xx	zz
4	xx	0
5	0	2*zz
6	xx	2*zz
7	2*xx	zz
8	2*xx	0
9	2*xx	2*zz

Table A-2 COORD Global coordinates of the nodes.

These arrays are subsequently used to build the right hand side vector and to change the system matrix in order to take into account the fact that the nodes corresponding to one electrode have all the same potential. This is done first building four vectors that represent the four external lines of the sensor, those opposite to the axis: sx1 and sx2 are those orthogonal to x axis, at x=0 and x=2*xx respectively; in a similar way are defined sz1 and sz2, which are associated with the two electrodes. In our example the subroutine SURFACES creates the following vectors:

$$sx1 = [\ 1\ \ 2\ \ 5\ ]$$
$$sx2 = [\ 7\ \ 8\ \ 9\ ]$$
$$sz1 = [\ 1\ \ 4\ \ 8\ ]$$
$$sz2 = [\ 5\ \ 6\ \ 9\ ]$$

6 Matrix elements and right hand side vector

6.1 Element matrix and system matrix

Because each node has three degrees of freedom, a term in a matrix in equation 13 is a block of dimension 3*3. The position of a block in the element matrix correspond to a couple of nodes: the block with indices *i* and *j* correspond to nodes with internal number *i* and *j*. The element matrix has therefore dimension 12*12, because each element has four nodes.

Once the element matrix has been built, its contribution to the system matrix is made through the link between internal and global numbering. If the global number of this nodes is *h* and *k* respectively, the element block of indices *i, j* will contribute to the system block occupying the position *h, k* in the system matrix. One node belongs generally to more than one element, thus the total contribution to the system block will be the sum of the blocks that belong to the elements containing the two nodes of global numbers *h* and *k*. Moreover, the block of indices *k* and *h*, having indices corresponding to the same couple of nodes, will be the same as the former one, and the resultant system matrix will be symmetric by blocks.

6.2 Internal coordinates

The fact that the elements have all the same structure (the only differences being the position and the constitutive properties), is used in order to calculate the integration in the same way for each element.

As for the numbering system, we need a way to refer to each element in the same way, when referring to nodes and coordinates inside the element. Internal coordinates are defined in the following way:

$$\begin{cases} \xi = \dfrac{2(x - x_0)}{xx} - 1 \\ \zeta = \dfrac{2(z - z_0)}{zz} - 1 \end{cases} \qquad \textbf{(A-1)}$$

and their meaning is easily understood from figure 5

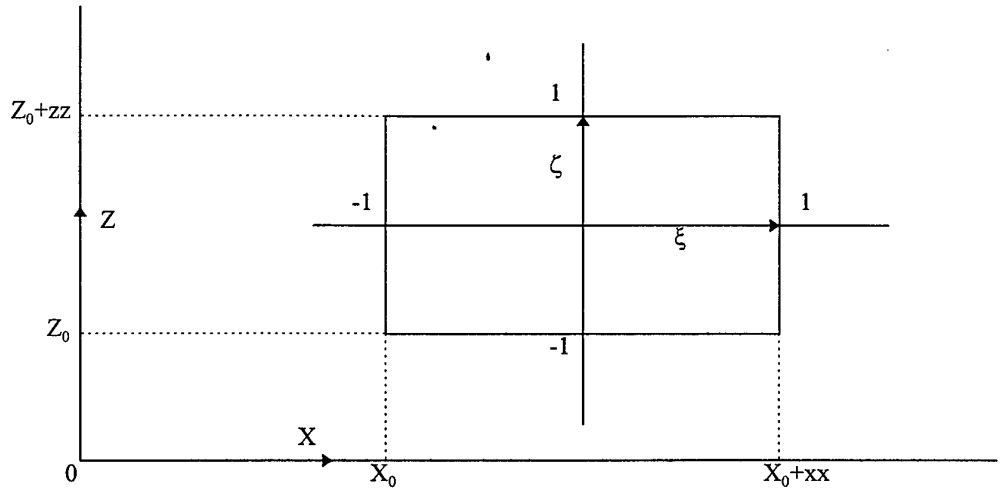

Figure A/5 Internal coordinates

A generic element has the following set of internal coordinates for its nodes:

INTERNAL NUMBER	ξ	ζ
1	-1	-1
2	-1	1
3	1	1
4	1	-1

Table A-3 Internal coordinates

The integral over an element is calculated using the following formula, valid for each transformation of coordinates:

$$\iiint f(x,y,z)\,dxdydz = \iiint f(\xi,\eta,\zeta)J(\xi,\eta,\zeta)\,d\xi d\eta d\zeta \qquad \textbf{(A-25)}$$

where

$$J(\xi,\eta,\zeta)=\det\begin{vmatrix}\frac{dx}{d\xi} & \frac{dy}{d\xi} & \frac{dz}{d\xi}\\ \frac{dx}{d\eta} & \frac{dy}{d\eta} & \frac{dz}{d\eta}\\ \frac{dx}{d\zeta} & \frac{dy}{d\zeta} & \frac{dz}{d\zeta}\end{vmatrix} \qquad \textbf{(A-26)}$$

The functions f(ξ,ψ,ζ) are expressed in terms of nodal functions and parameters:

$$f(\xi,\eta,\zeta)=\sum_{i=1}^{8} f_i(\xi,\eta,\zeta)a_i \qquad \textbf{(A-27)}$$

where the functions f_i can be made equal for each node and for each degree of freedom. In fact if the function f is for instance the potential inside an element, we can suppose that it has the following form:

$$fi(\xi,\eta,\zeta)=\frac{1}{8}(1+\xi_i\xi)(1+\zeta_i\zeta) \qquad \textbf{(A-28)}$$

where (ξ_i, ζ_i) are the internal coordinates of the node i

As can be observed by the above equation, the function value is 1 on the node i and 0 on the other nodes; thus it satisfies automatically the condition that the potential has the value ϕ_i at node i, while in all other points inside the element it varies linearly with the coordinates. Moreover, these functions satisfy the condition of continuity over the element boundary. It is then satisfied the condition of continuous electric potential and mechanical displacement over the elements boundaries.

6.3 Numerical integration

The integration is carried out numerically following the formula

$$\iiint f(\xi,\eta,\zeta)dV=\sum_{h=1}^{s} w_h f(\xi_h,\eta_h,\zeta_h) \qquad \textbf{(A-29)}$$

where the integral of a function over an element volume is evaluated multiplying the value of the function at a point inside the volume by a weight and then summing over a

set of points. In this case eight points have been taken at distances proportional to those of the nodes of the element, by a factor of $(1/3)^{1/2}$, as shown by next figure.

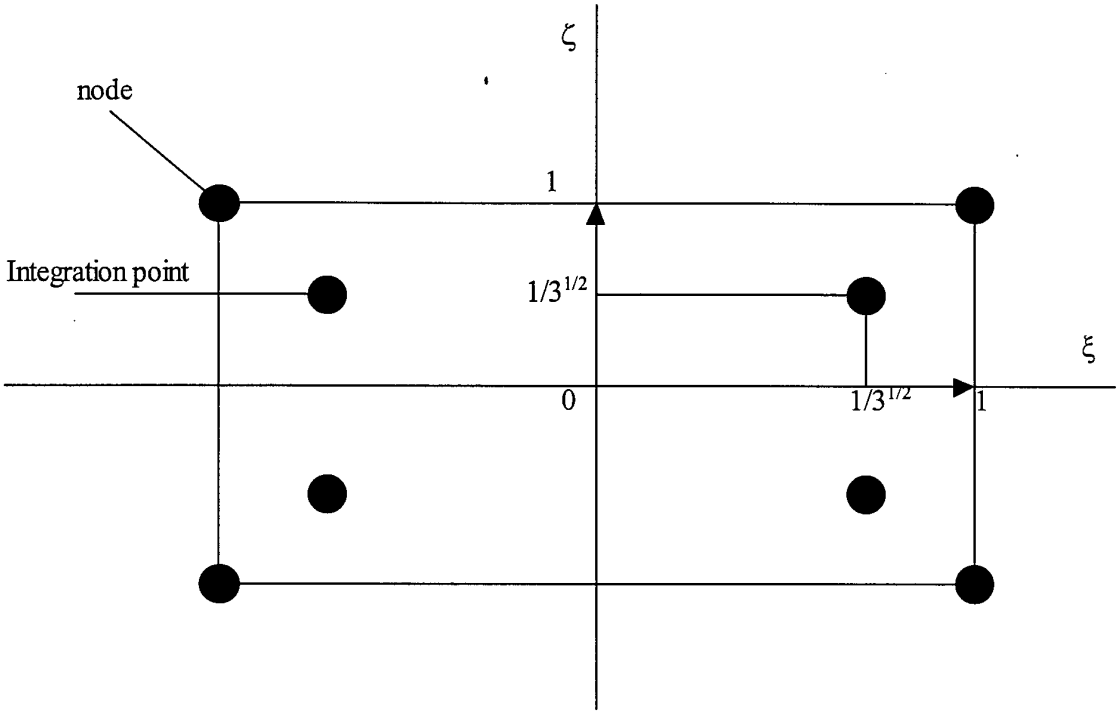

Figure A/6

7 The application of boundary conditions

There is a certain set of physical conditions over the boundaries:

1) The points of the boundary that belong to the electrodes are at constant potential.

2) One electrode is set as reference for the potential (V=0).

3) The pressure is uniform over the boundary.

As a consequence of the third condition (which is equivalent to the condition that the resultant of the external forces is zero), the center of mass of the sensor will not move. Calling x_{cm} and z_{cm} the coordinates of that point, the following equations will be valid as a consequence of condition number 3:

$$x_{cm} = \frac{1}{M}\sum_{i=1}^{n} x_i m_i = 0 \qquad \textbf{(A-30)}$$

$$z_{cm} = \frac{1}{M}\sum_{i=1}^{n} z_i m_i = 0 \qquad \textbf{(A-31)}$$

where M is the total mass of the sensor, x_i, z_i and m_i are the coordinates and the mass of the node whose global number is *i*.

These two equations can be used to express one node coordinates as function of the others nodes coordinates, allowing the reduction of the system matrix from an $n*n$ to an $(n-2)*(n-2)$ rank (subroutine REDSTIFF).

The second condition is equivalent to put all the values of the potential at the nodes that belong to the surfaces sz1 to zero; the routine REDPOT sums the rows of the system matrix whose index, say *k*, correspond to the potential at nodes contained in sz1 to the rows above them, and afterwards delete row and column *k* from the matrix.

Concerning the electrode corresponding to sz2, we only know from condition number 1 that it is constant, but this potential is what we are looking for, that is the potential difference between the two electrodes. The fact that the potential is constant over this surface, will allow to sum the variables corresponding to the potential and to consider them as one variable. The subroutine REDPOT sum the column corresponding to the potential at the nodes contained in the vector sz2 to that corresponding to sz2(1), which will be taken as reference for the potential at the electrode. Then it reduce the matrix in the same way it does for sz1, considering all points but the first one in sz2.

After the routines REDSTIFF and REDPOT have been run, the matrix will have dimension $(n-2-2*nx+1)$.

8 Frequency response

Once the system matrices [K] and [M'] have been calculated, it is possible to solve equation 21 for different values of the frequency. The subroutine SOLVE makes this calculation, accepting as parameters the starting frequency ω_0, the frequency step $\Delta\omega$ and the number of iterations ν. The frequency response of the embedded sensor,

defined as the potential developed across the electrodes by an application of an hydrostatic pressure as input, is then computed for the frequency range ω_0-ω_0+$\nu\Delta\omega$.

9 Comparison with the ABCD matrix approach

During the present work the ABCD matrix method has been successfully used to calculate the theoretical response of the transducer.

A comparison between the FEM approach and the ABCD matrix one has been made. In order to do so the same parameters for the transducer and the backing material have been used, the only difference being considering the losses in the ABCD matrix approach. The forces and velocities of the faces of the transducer (see figure A/7) are

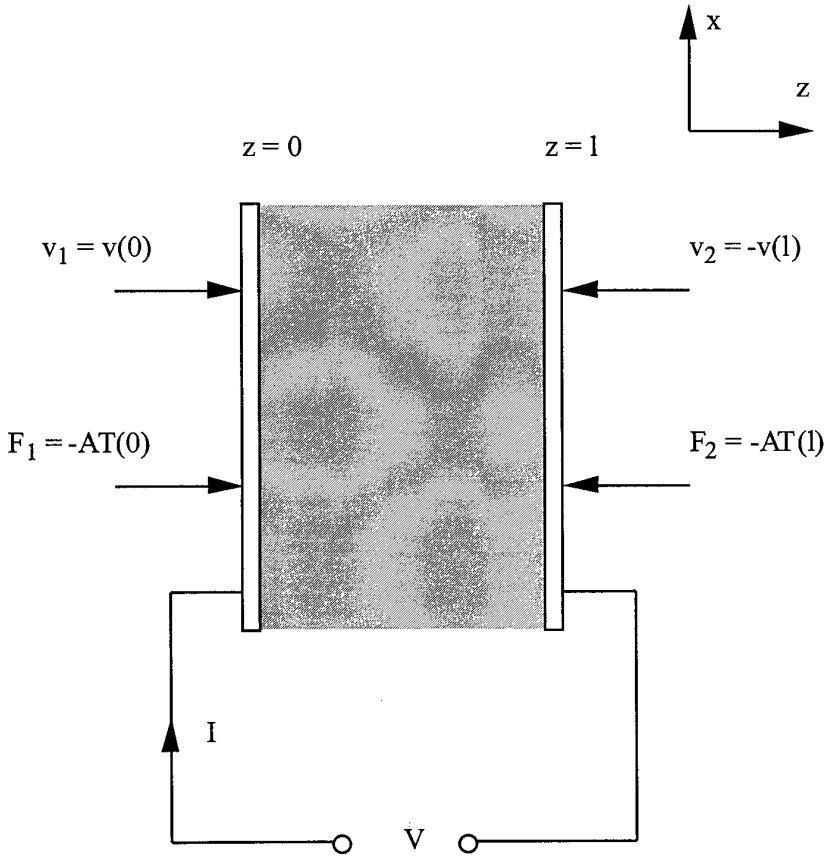

Figure A/7 Piezoelectric resonator showing the electrical and acoustical terminal variables.

related to the voltage and current of the electrodes by:

$$\begin{bmatrix} F_1 \\ F_2 \\ V \end{bmatrix} = -i \cdot \begin{bmatrix} Z_a \cot(\gamma \cdot l) & Z_a \csc(\gamma \cdot l) & \frac{h}{\omega} \\ Z_a \csc(\gamma \cdot l) & Z_a \cot(\gamma \cdot l) & \frac{h}{\omega} \\ \frac{h}{\omega} & \frac{h}{\omega} & \frac{1}{\omega \cdot C^S} \end{bmatrix} \cdot \begin{bmatrix} v_1 \\ v_2 \\ I \end{bmatrix} \quad \textbf{(A-32)}$$

where Z_a is the acoustic impedance of the resonator, γ is a complex wave propagation constant describing the acoustic wave and $h = e/\varepsilon^S$ is the piezoelectric strain coefficient, C^S is the capacitance of the sample.

If the forces applied to both faces of the transducer are the same, is

$$F_1 = F_2 \quad \textbf{(A-33)}$$

and, therefore,

$$v_1 = v_2 \quad \textbf{(A-34)}$$

From the first equation of 32 is

$$F = F_1 = F_2 = -i \cdot Z_a \cdot \left(\cot(\gamma \cdot l) \cdot v_1 + \csc(\gamma \cdot l) \cdot v_2 + \frac{h}{\omega} I \right) =$$

$$= -i \cdot Z_a \cdot \left(\left[\cot(\gamma \cdot l) + \csc(\gamma \cdot l) \right] \cdot v + \frac{h}{\omega} I \right) \quad \textbf{(A-35)}$$

As it is

$$\cot x + \csc x = \frac{\cos x}{\sin x} + \frac{1}{\sin x} = \frac{\cos x + 1}{\sin x}$$

we can reduce 32 to a two-dimension *ABCD* matrix:

$$\begin{bmatrix} F \\ V \end{bmatrix} = -i \cdot \begin{bmatrix} Z_a \frac{\cos(\gamma \cdot l) + 1}{\sin(\lambda \cdot l)} & \frac{h}{\omega} \\ 2\frac{h}{\omega} & \frac{1}{\omega \cdot C} \end{bmatrix} \cdot \begin{bmatrix} v \\ I \end{bmatrix} \quad \textbf{(A-36)}$$

If the external electric circuit between the two electrodes is open, is obviously

$$I = 0$$

From the first of 36, we obtain

$$-i \cdot v = \frac{1}{Z_a} \cdot \frac{\sin(\gamma \cdot l)}{\cos(\omega \cdot l) + 1} \cdot F \qquad \textbf{(A-37)}$$

and, from the second,

$$V = \frac{2h}{\omega} \cdot (-i \cdot v) \qquad \textbf{(A-38)}$$

Substituting 37 in 38, we finally get

$$V = \frac{2h}{Z_a \cdot \omega} \cdot \frac{\sin(\gamma \cdot l)}{\cos(\gamma \cdot l) + 1} \cdot F \qquad \textbf{(A-39)}$$

The plot for such an output voltage calculated for a P(VDF-TrFE) sensor (Figure 0.8a) shows a peak at 7.8MHz. A similar plot is given in figure 0.8b for a PTCa sensor.

10 Results

The program for the FEM method now exists in two versions: one is three-dimensional and the other is two-dimensional. The three-dimensional version is also available in three forms: a polymer sensor, a ceramic sensor and a composite (0-3) sensor. The last two versions don not produce useful results, although the reason for this is not clear.

The polymer simulation, on the contrary, presents a resonance at 7.8 MHz (as shown in figure 0.9), which is the same value obtained using the ABCD matrix approach.

The two-dimensional version of the program is not giving significant results. One possible reason is the wrong application of the boundary conditions and the subroutines that reduce the system matrix.

Subsequent work should improve the resolution obtainable, considering the two-dimensional case or applying the principles of sparse matrices. It is also important to consider the losses of the material, and the external electric circuit.

Figure A/8a Response of a P(VDF-TrFE) transducer obtained using the ABCD approach

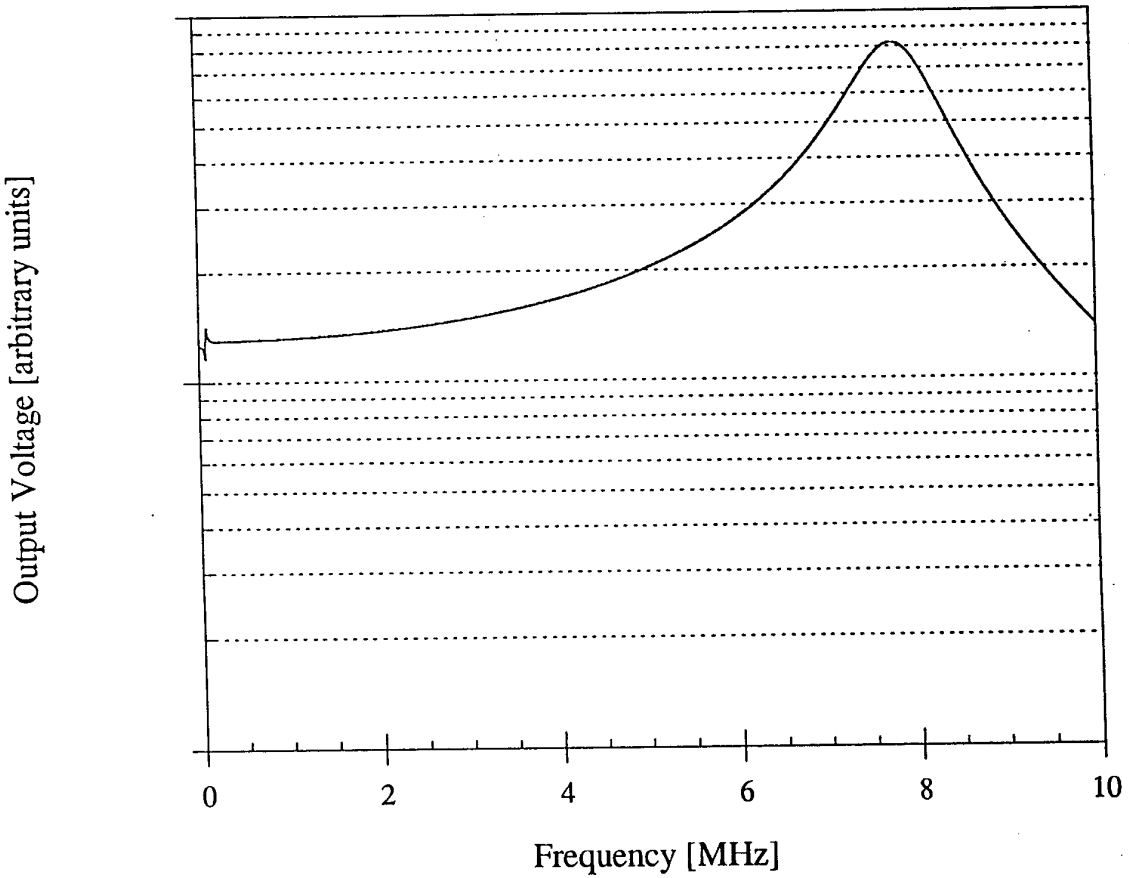

Figure A/8b Response of a PTCa transducer obtained using the ABCD approach

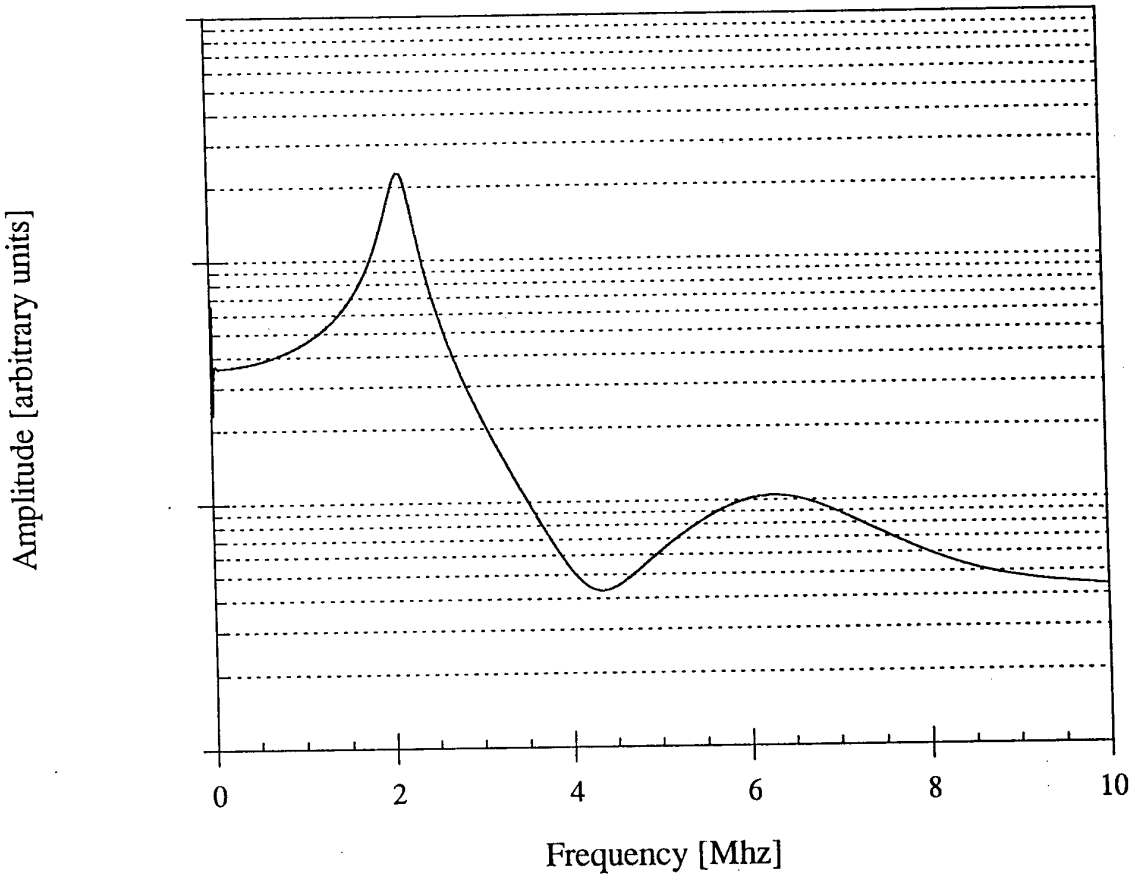

Figure A/9 Response of a lossless P(VDF-TrFE) transducer obtained using the FEM approach

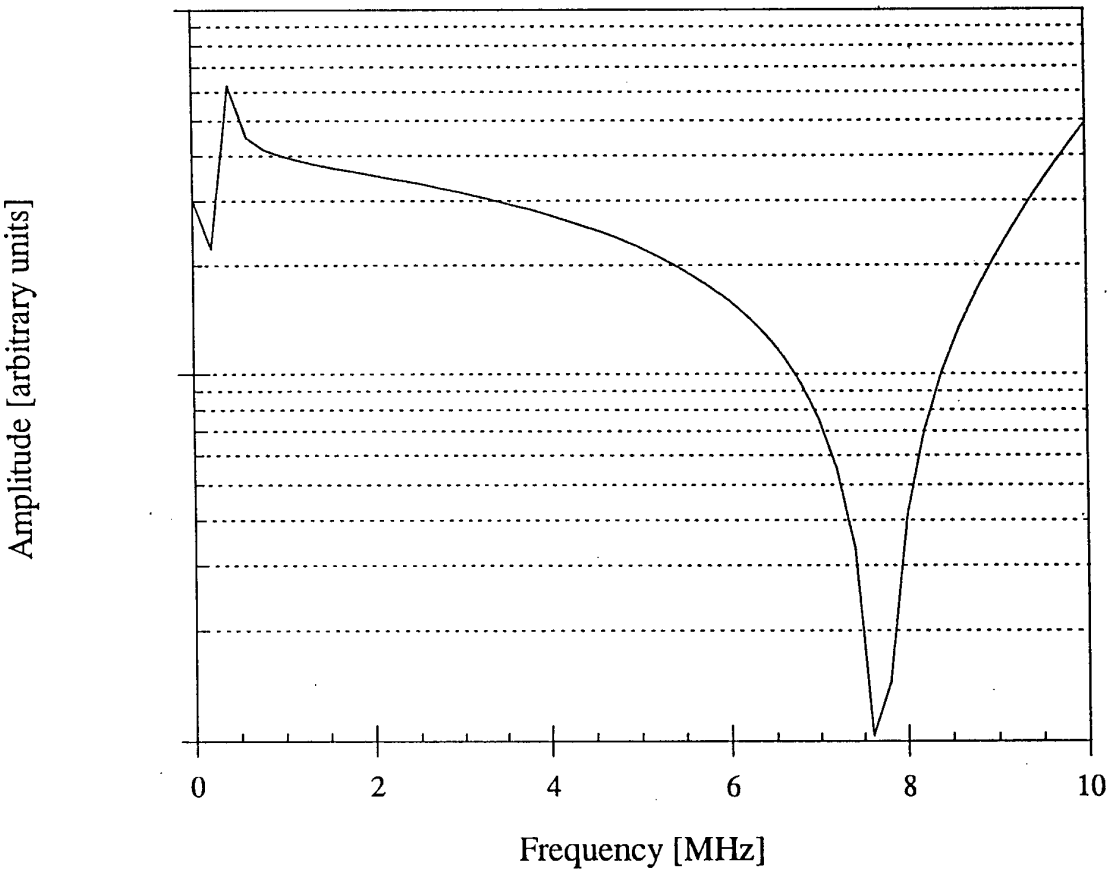

APPENDIX 2

C. Dias, M.P. Wenger, P. Blanas, R.J. Shuford, Y. Hinton and D.K. Das-Gupta, *'Intelligent piezoelectric composite materials for sensors'*, IEEE 2nd International Conference on Intelligent Materials, Williamsburg, VA, USA, pp.437-449 (5-8th June 1994)

C.J. Dias, M.P. Wenger, Y. Kaminorz, U. Hopfner and D.K. Das-Gupta, *'Electroactive properties of intelligent ferroelectric ceramic/polymer composite sensors'*, 8th International Symposium on Electrets (ISE 8), ESPCI, Paris, France, pp.589-593 (7-9 September 1994)

R. Igreja, M.P. Wenger, C.J. Dias, D.K. Das-Gupta and J.N. Marat-Mendes, *'Pyro- and piezoelectricity in sol-gel derived ceramic/polymer composites'*, 8th International Symposium on Electrets (ISE 8), ESPCI, Paris, France, pp.725-730 (7-9 September 1994)

M.P. Wenger, P. Blanas, R.J. Shuford and D.K. Das-Gupta, *'Ferroelectric ceramic and epoxy composite films as pyroelectric detectors'*, 2nd European Conference on Smart Structures and Materials, Glasgow, Scotland, SPIE vol. 2361, pp.358-361, (12-14 October 1994)

P. Blanas, M. Wenger, R.J. Shuford and D.K. Das-Gupta, *'Smart ceramic/polymer composite materials for sensors'*, 4th International Symposium on Composite Materials, Corfu, pp.468-476 (1995)

M.P. Wenger, P. Blanas, C.J. Dias, R.J. Shuford and D.K. Das-Gupta, *'Ferroelectric ceramic/polymer composites and their applications'*, Ferroelectrics, vol. 187, pp.75-86 (1996)

M.P. Wenger, P. Blanas, R.J. Shuford and D.K. Das-Gupta, *'Acoustic emission signal detection by ceramic/polymer composite piezoelectrets embedded in glass-epoxy laminates'*, Polymer Engineering Science, vol. 36, no. 24, pp.2945-2953, (December 1996)

M.P. Wenger, P. Almeida, P. Blanas, R.J. Shuford and D.K. Das-Gupta, *'The*

ferroelectric properties of piezoelectric ceramic/polymer composites for acoustic emission sensors', 5th International Conference on Polymer Characterisation (POLYCHAR5), Denton, Texas, (8-10 January 1997) (Accepted for publication in Polymer Engineering Science)

M.P. Wenger, P. Blanas, R.J. Shuford and D.K. Das-Gupta, *'Characterisation and evaluation of pieozelectric composite bimorphs for in-situ acoustic emission sensors'*, 5th International Conference on Polymer Characterisation (POLYCHAR5), Denton, Texas, (8-10 January 1997) (Accepted for publication in Polymer Engineering Science)

M.P. Wenger, P. Blanas, R.J. Shuford and D.K. Das-Gupta, *'Embedded piezoelectric composite bimorphs as non-destructive testing sensors'*, Sensors and Their Applications VIII, Glasgow, Scotland, pp 129-135 (7-10 September 1997)

Intelligent Piezoelectric Composite Materials for Sensors

C. DIAS, M. WENGER, P. BLANAS, R. J. SHUFORD, Y. HINTON AND D. K. DAS-GUPTA

ABSTRACT

Polymer/ceramic composite piezoelectric materials with 0-3 connectivity have been produced by dispersing ceramic powder of calcium modified lead titanate into the matrix of three different host polymers. The piezoelectric coefficient and the dielectric constant as well as the electromechanical coupling factor of the composite films are determined. Two piezoelectric transducers have been constructed using these films. The composite piezoelectric sensors were used to monitor strain and acoustic emission levels during tensile testing of fiber reinforced composite laminates.

INRODUCTION

Piezoelectricity is the phenomenon that couples the elastic and electric fields in piezoelectric materials. In general, materials exhibiting piezoelectricity have the ability to convert mechanical to electrical energy but also exhibit the converse electrostrictive effect. These properties enable piezoelectrics to perform both sensing and actuating functions thus classifying them as smart or intelligent materials.

At present, the standard piezoelectric materials used as sensors or actuators in a variety of applications, such as hydrophones, non-destructive evaluation transducers and shape control, are ferroelectric ceramics notably lead zirconate titanate (PZT) and some modifications of lead titanate (PT). However, these materials present some disadvantages such as acoustic impedance mismatch, high dielectric constant and lack of flexibility as well as the coupling of different vibration modes and narrow bandwidth. New materials in the form of ferroelectric polymers such as polyvinylidene fluoride (PVDF) and its copolymer poly(vinylidene fluoride/trifluorethylene) (P(VDF/TrFE)) and ferroelectric ceramic/polymer composites have emerged which attempt to bridge such disadvantages.

By mixing a ferroelectric ceramic into a polymer matrix, the compliance of the composite material increases and thus the acoustic impedance decreases to a value which

Carlos Dias, Matthew Wenger and Dilip K. Das-Gupta, University of Wales, School of Electronic Engineering Science, Dean Street, Bangor, Gwynedd LL57 1UT, UK
Panagiotis Blanas and Richard J. Shuford, U.S. Army Research Laboratory, Materials Directorate, Arsenal Street, Watertown, MA, 02172 USA
Yolanda Hinton, U.S. Army Research Laboratory, Vehicle Structures Directorate, NASA Langley Research Center, Hampton, VA, 23681 USA

depends on the ceramic loading. Also, because of the enhanced damping provided by the polymer matrix, the mechanical losses increase and the transverse modes are attenuated. As a consequence, the longitudinal piezoelectric coefficient can be tailored depending on the ceramic content. Three main variables affect the performance of a piezoelectric polymer/ceramic composite material: its connectivity, the properties of the constituent phases and the relative magnitude of the phases.

In this study we report on 0-3 connectivity composites made of ceramic powder dispersed in a polymer matrix which lends itself to easy fabrication of large area, flexible and formable piezoelectric materials. Calcium modified lead titanate (PTCa) has been used as the filler ceramic because of its low dielectric constant and highly anisotropic piezoelectric properties. A powder of this ceramic has been obtained through a quenching process which produces ceramic grain size of ~10 μm with low internal stress.

Three different polymer matrices have been used: Polyetheretherketone (PEEK), epoxy and P(VDF/TrFE). PEEK has been chosen for its high temperature capabilities thus extending the temperature range of operation of the composite transducers. The upper working temperature for a composite transducer using this polymer is thus the Curie temperature (T_C) of the ceramic which is 255°C for PTCa. Epoxy resins are commonly used as the matrix phase of fiber reinforced polymer composite materials. Therefore, epoxy/ceramic composite sensors would be compatible with and could be utilized in a wide class of fiber reinforced composites. Finally, P(VDF/TrFE) a ferroelectric polymer has also been used as the polymer host. Its polar character, which is responsible for its ferroelectricity, imparts the highest dielectric constant known in polymers peaking at ε=60 at its Curie temperature which is around 125°C for the copolymer used. This allows for easier poling of the ceramic grains near T_C due to a better dielectric constant matching between the phases.

Polymer/ceramic composite piezoelectric materials developed from this work are to be employed as multi purpose sensors for the nondestructive monitoring of fiber reinforced composite laminates. In their final configuration these films could be either surface bonded or embedded in composite laminates to monitor strain levels or be utilized as ultrasonic or acoustic emission (AE) transducers.

FABRICATION OF THE CERAMIC/POLYMER COMPOSITE FILMS WITH 0-3 CONNECTIVITY.

The mechanical, thermal and dielectric properties together with the connectivity of the two constituent phases are important factors in the choice of the most appropriate method for the fabrication of a particular composite. Many thermoplastics, i.e. polyvinylidene fluoride and its copolymers, are soluble in organic solvents and soften at some particular temperature range in such a way that they regain their properties when cooled down. The thermoset polymers, i.e. epoxy, are network polymers with mostly amorphous structure, that cannot be hot worked. In a 0-3 composite the ceramic powder is randomly distributed in the matrix of a host polymer and it is easier to fabricate in comparison with the 1-3 composites consisting of pillars of ceramic rods that are regularly spaced in the polymer.

Calcium modified lead titanate /polyvinylidene fluoride-trifluoroethylene composites, PTCa/P(VDF-TrFE), were prepared by the solvent casting technique. The copolymer P(VDF-TrFE) dissolves well in methyl ethyl ketone. The following equations have been

used to calculate the material quantities to obtain a given volume fraction, ϕ, of the ceramic in a composite

$$M_c = \phi \rho_c V \quad (1)$$

where M and ρ is the mass and density of the ceramic and V the total volume of the composite. The subscript c refers to the ceramic. Similarly,

$$M_p = \phi \rho_p V \quad (2)$$

where the subscript p refers to the polymer. The composite density ρ, is given by,

$$\rho = \phi \rho_c + (1-\phi)\rho_p \quad (3)$$

Weighed materials of the ceramic and the polymer were mixed in an agate mortar and the solvent, methyl ethyl ketone, was poured over the mixture until all the copolymer powder was dissolved. The slurry was stirred with a pestle until a uniform solid was formed due to the evaporation of the solvent. This solid mass was then used to form the composite films using the hot pressure (170°C, 4-9 tonnes) casting technique. The PTCa particle size was in the range of 5-10μm and the thickness of the composite films was ~60μm.

For the PTCa/Epoxy composite films, Epikote 828 (Shell) epoxy resin and K61B (Anchor Chemicals) curing agent have been used to produce the host thermoset polymer. A few drops of the curing agent were added to one *cc* of the epoxy resin in a small container and the mixture was stirred to ensure uniformity. A measured amount of ceramic powder (PTCa) was then gradually added to the epoxy stirring continuously until all the ceramic had been added and the mixture attained a smooth consistency. The composite was then placed on a clean and smooth piece of aluminum foil and outgassed for two hours in a vacuum oven at 60°C. Following the degassing the composite material was removed from the oven together with the aluminum foil and located onto a milled plate with thin shims placed along the edges. Another piece of clean and smooth aluminum foil was placed on top of the composite and another milled plate was located on top of the second aluminum foil. The entire assembly was then placed in the hot mechanical press (60°C, 2-6 tonnes) until the metal plates were tight against the thin shims. The composite film thus produced, was allowed to cure for a further period of four hours at 60°C. The composite film (80-300μm) was then removed from the assembly.

For the PTCa/PEEK composite, the host polymer was unoriented PEEK with the trade name Victrex (ICI) with a crystalline volume fraction ≅ 0.8. The melting temperature of PEEK is ~330°C and this polymer is not readily soluble in safe organic solvents and it also shows excellent resistance to inorganic solvents. Appropriate amounts of PTCa and PEEK grains were mixed in the solid phase and heated to 380°C when the mixture became soft. It was then stirred for one hour at this temperature and then cooled to room temperature. This material was used to produce composite films in the hot press at 370°C and at 8 to 10 tonnes pressure.

A scanning electron microscope (SEM) study of the morphology of these composite films showed that the ceramic grains were isolated from each other indicating a true 0-3 connectivity.

POLING OF COMPOSITE FILMS

For a composite with 0-3 connectivity consisting of spherical ceramic grains dispersed in a polymer matrix, the ceramic particles sense only a part of the externally applied poling field. The field E_1, acting on an isolated spherical grain for such a case is given by (Von Hippel 1954),

$$E_1 = 3\varepsilon_p E/(\varepsilon_c + \varepsilon_p) \qquad (4)$$

where E is the externally applied field and ε_c and ε_p are the dielectric constants of the ceramic and the polymer respectively. A DC field acting on a two layer capacitor, may be represented by

$$\frac{E_1}{E_2} = \frac{\sigma_2}{\sigma_1} \qquad (5)$$

where σ_1 and σ_2 are the conductivities of the polymer and the ceramic respectively. Above observations indicate that for a 0-3 connectivity system in which the dielectric constant and the conductivity of the ceramic are high and low respectively in comparison with those of the polymer host, the electric field acting on the ceramic piezoelectric particles, E_1, will be quite low and insufficient to pole ceramics efficiently. It has been claimed (Sa-Gong et al, 1986; Lee, Halliyal and Newnham, 1989) that an inclusion of a small volume fraction of conductive filler particles, e.g. silicon, carbon or germanium, as a third phase will provide a continuous electric flux path and thus enhance the conductivity of the host polymer. Unfortunately, such a procedure will lower the effective electrical breakdown field E_b, of the composite. In this respect, an approach to match the resistivities of the two phases may not achieve its expected reward. For this reason, no attempt has been made so far in this work to match the resistivity of the two constituent phases. The vacuum electroded samples were poled by a DC field in the range of $1-2.5\times10^7$ Vm^{-1} in a bath of insulating silicone oil at a temperature of 100°C for 30 minutes. The magnitude of the poling field was limited by the electrical breakdown strength, i.e. E_b.

DIELECTRIC AND PIEZOELECTRIC CHARACTERIZATION: RESULTS AND DISCUSSION

Composite films of PTCa/P(VDF-TrFE): 65/35 vol%, PTCa/Epoxy: 60/40 vol%, and ceramic discs of PTCa have been studied extensively so far to determine their dielectric constant, the piezoelectric d_{33} coefficient and the electromechanical coupling factor k_t.

The dielectric constant ε and the loss factors were evaluated from measurements of the sample capacitance and conductance by using a conventional capacitance bridge (General Radio, Model 1621) at 1kHz at room temperature and the results are given in Table 1. The

uncertainty in the values of the dielectric data, which arises from the non uniformity in the sample thickness is approximately 15%. It was observed, as expected, that for a given composite, the dielectric constant increased with the increasing volume fraction of the ceramic loading whereas the magnitude of tan δ decreased correspondingly. For example, for PTCa/P(VDF-TrFE) the ε value increased from 21 to 67 when the ceramic volume fraction was increased from 21 vol% to 65 vol%, whereas the tan δ decreased from 0.018 to 0.013 for the same range of increase in the ceramic loading.

The piezoelectric d_{33} coefficient was measured by a Pennebaker 8000 instrument that bas a range of 0 to ±1200 pC/N. The instrument is supplied with a calibrated lead titanate piezo ceramic. An internal capacitor, 0.1μF, is connected in parallel with the test sample and a voltage is developed across this capacitor by the piezoelectric sample for an applied stress and the calibrated instrument provides directly the magnitude of the d_{33} coefficient which is the ratio of the product of the voltage and the capacity to the applied stress. It may be observed from Table 1 that the d_{33} value of PTCa/P(VDF-TrFE) 65/35 vol% is comparable to that of PTCa whereas the corresponding value of PTCa/Epoxy 60/40 vol% is approximately 70% of that of the ceramic.

The piezoelectric charge coefficient d (C/N), and the voltage coefficient g (m/V), are related thus,

$$\frac{d}{g} = \varepsilon_0 \varepsilon_r \qquad (6)$$

where ε_0 is the vacuum permittivity and ε_r the dielectric constant of the material. Thus the value of the g- coefficient may be evaluated provided the values of the d- coefficient

TABLE I - PIEZOELECTRIC AND OTHER RELEVANT PROPERTIES OF PTCa AND ITS COMPOSITES WITH P(VDF-TrFE) AND EPOXY

Property	PTCa	PTCa/P(VDF-TrFE) 65/35 vol%	PTCa/Epoxy 60/40 vol%
Density, ρ (kg / m^3)	6890	5130	4600
Dielectric constant ε_r (at 1kHz)	230	67	23
tan δ (at 1kHz)	0.006	0.013	0.010
Piezoelectric d_{33} coefficient ($\times 10^{-12} C/N$)	68	43	32
Electromechanical coupling factor k_t	0.47	0.21	0.19
FOM: $d_{33} \times g_{33}$ ($\times 10^{-12}$ Pa^{-1})	2.24	3.90	5.03
Mechanical Quality Factor Q_m	80	4.3	21.7
Acoustic Impedance Z_a ($\times 10^6$ Rayls)	29.6	16.5	11.0
Acoustic Velocity (m/s)	4300	3200	2418

and ε_r are known. Furthermore, the figure of merit, FOM, of a piezoelectric transducer is given by the dg (Pa^{-1}) product. Thus,

$$dg = \frac{d^2}{\varepsilon_0 \varepsilon_r} = g^2 \varepsilon_0 \varepsilon_r \qquad (7)$$

It may be observed from Table 1 that the values of the dg product of the composites PTCa/(VDF-TrFE) 65/35 vol% and PTCa/Epoxy 60/40 vol% are 3.9×10^{-12} Pa^{-1} and 5.03×10^{-12} Pa^{-1} respectively. Generally, a piezoelectric material with an enhanced d-coefficient tends to have a reduced g- coefficient so that the dg product tends to be of a compensating nature. It may also be observed from Table 1 that the dg product of the ceramic (PTCa) is 2.24×10^{-12} Pa^{-1}. Thus, a composite transducer enjoys a superior FOM value in comparison with their ferroelectric ceramic. The dg product decreases with increasing value of the dielectric constant. Hence the composite PTCa/Epoxy 60/40 vol% appears to be an attractive transducer material for operation in the thickness mode. The hydrostatic d_h and g_h coefficient are related thus,

$$d_h = d_{33} + 2d_{31} \qquad (8)$$

$$g_h = g_{33} + 2g_{31} \qquad (9)$$

$$\frac{d_h}{g_h} = \varepsilon_0 \varepsilon_r (\equiv \varepsilon_0 \varepsilon_{33}) \qquad (10)$$

Thus the hydrostatic figure of merit FOM of a ceramic/polymer transducer will also be superior to that of a ceramic device for the reasons stated above. In addition, in the fabrication of the composite, d_{33} and d_{31} coefficients are decoupled, thus further enhancing the d_h value.

The electromechanical coupling factor k_t, is an important quantity to characterize a transducer and it is defined thus,

$$k_t^2 = \frac{\text{Electrical (mecahnical) energy converted to mechanical (electrical) energy}}{\text{Total input electrical (mechanical) energy}} \qquad (11)$$

k_t^2 is of course always less than unity. For most applications a high value of k_t is desirable as it enables a transducer to convert energy efficiently from one form into another. A piezoelectric sensor may be represented by an electrical equivalent circuit that may resonate in the thickness mode at an appropriate frequency. The k_t value may be determined from the measurement of the complex electrical impedance of a piezoelectric sample standing free in air in the frequency range around the resonance f_0. For such a case it may be assumed that the forces acting on the faces are close to zero. The electrical impedance Z, resonating in its thickness mode, is equal to the sum of two terms, i.e., the electrical impedance $Z_e(\omega)$ of the simple capacitance and the acoustic impedance $Z_a(\omega)$ (Ohigashi, 1988). The real $\mathrm{Re}[Z(\omega)]$, and imaginary parts $\mathrm{Im}[Z(\omega)]$, of the frequency

dependent total complex impedance of a piezoelectric lossy transducers are given by (Bui and Shaw, 1977; Platte, 1991; Dias and Das-Gupta, 1992; Dias et al, 1993),

$$\mathrm{Re}[Z(\omega)] = \frac{\phi}{(\phi+1)\omega C_0} + A\left(\frac{\omega_0}{\omega}\right)^2 \frac{\tanh\left(\frac{\pi\psi}{4}\right)\left[\psi\sin\left(\frac{\pi\omega}{\omega_0}\right) + 2\sinh\left(\frac{\pi\psi\omega}{2\omega_0}\right)\right]}{\sqrt{(\psi^2+4)}\left[\cos\left(\frac{\pi\omega}{\omega_0}\right) + \cosh\left(\frac{\pi\psi\omega}{2\omega_0}\right)\right]} \qquad (12)$$

$$\mathrm{Im}[Z(\omega)] = \frac{-1}{(\phi+1)\omega C_0} + A\left(\frac{\omega_0}{\omega}\right)^2 \frac{\tanh\left(\frac{\pi\psi}{4}\right)\left[2\sin\left(\frac{\pi\omega}{\omega_0}\right) - \psi\sinh\left(\frac{\pi\psi\omega}{2\omega_0}\right)\right]}{\sqrt{(\psi^2+4)}\left[\cos\left(\frac{\pi\omega}{\omega_0}\right) + \cosh\left(\frac{\pi\psi\omega}{2\omega_0}\right)\right]} \qquad (13)$$

where $\omega_0 = 2\pi f_0$, C_0 the sample capacitance, A the maximum value of the real part of the acoustic impedance at resonance, ϕ the dielectric loss and ψ the mechanical loss ($= Q_m^{-1}$, Q_m being the mechanical quality factor). From equations 12 and 13 it may be shown that,

$$k_t^2 = \frac{\pi}{4}\omega_0 C_0 A\sqrt{(\psi^2+4)}\tanh\left(\frac{\pi}{4}\psi\right) \qquad (14)$$

it is thus necessary to determine f_0, C_0, A and ψ in order to evaluate k_t.

A network analyzer, Model HP8702A was used to measure the real and imaginary components of the total impedance of the ceramic and the composite materials in the frequency range of 3.0×10^7 Hz to 5.0×10^7 Hz. Prior to the measurement, a calibration

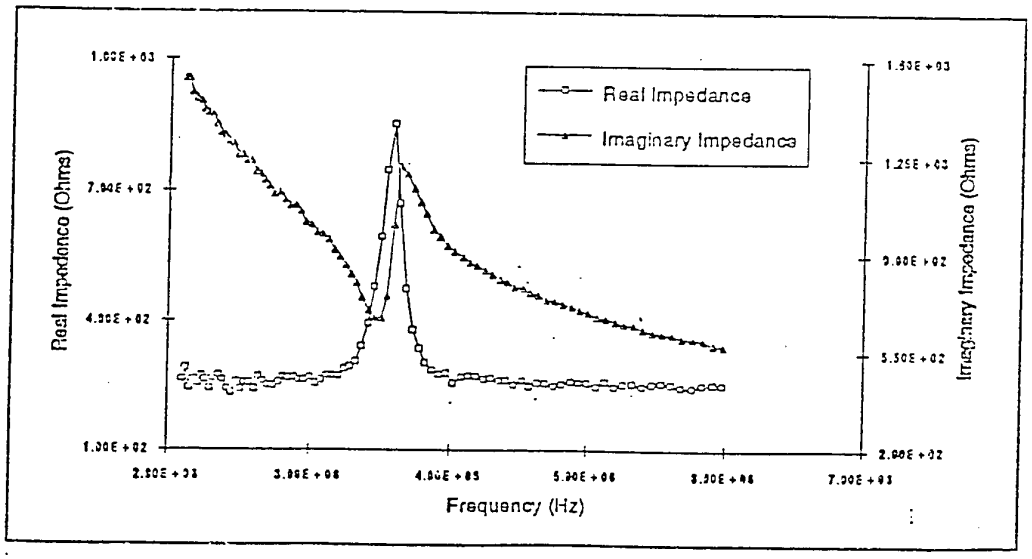

Figure 1. Real and Imaginary part of measured impedance of PTCa/Epoxy (60:40 vol%) film
Initial estimates; A=584.94 Ohms, f_o =3.57 $\times10^6$ Hz, ψ=0.057, k_t =0.21

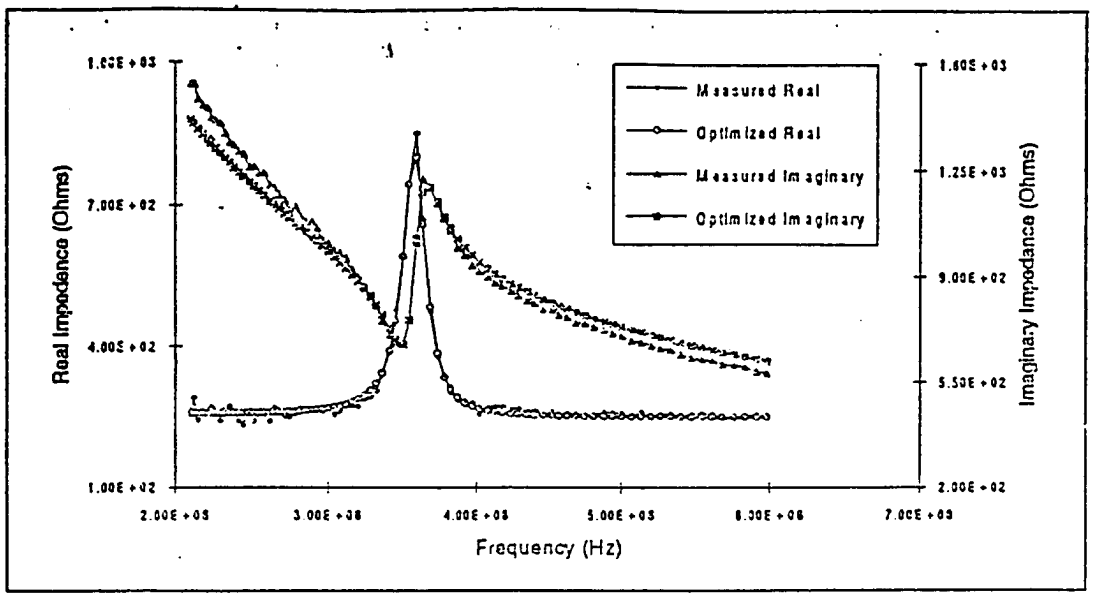

Figure 2. Real and Imaginary part of measured and calculated impedances of PTCa/Epoxy (60:40 vol%)
Optimized values; A=611.66 Ohms, f_o =3.58 ×10^5 Hz, ψ=0.046, k_t =0.19

procedure was undertaken to ensure that the true impedance of the sample was measured with no contribution from the capacitance of the cables or connectors. The experimentally determined impedance as a function of frequency yields the values of the resonance frequency f_0, the peak amplitude of the real part of the acoustic impedance A and the mechanical loss ψ which is given by the full width of the resonance at half height, measured from the base line. The behavior of the real part of the electrical impedance with frequency is, of course, given by the base line. Figure 1 shows the typical behavior of the real and imaginary parts of the complex total impedance in the frequency range of 2.0×10^6 Hz to 7.0×10^5 Hz for a PTCa/Epoxy film with a composition of 60/40 vol%. It may be observed from the resonance behavior of the real part of the complex impedance that f_0 is located at approximately 3.57×10^6 Hz for this particular film of thickness 338μm and that the values of A and ψ are 584.94 ohms and 0.057 respectively. Using these values of f_0, A and ψ and with the knowledge of C_0 and equation 13, k_t was found to be 0.21.

The measured data of the real and imaginary components of figure 1 around the resonant frequency f_0 were also analyzed using a computer algorithm to fit equations 12 and 13 of the theoretical model. The fitting process requires a prior estimation of the parameters f_0, A and ψ from figure 1. The optimization process then undertakes a finer tuning to minimize the discrepancy between the experimentally observed and the calculated curves. Figure 2 shows that there is a good agreement between the experimentally observed and the corresponding observed data that provide the best fit with equations 12 and 13. The optimized values of f_0, A and k_t were within 0.2%, 5% and 10% respectively with the experimentally determined values, whereas the optimized value of ψ (= Q_m^{-1}) was significantly different (≈24%) from the experimentally determined magnitude. The exact reason for this large discrepancy is not known yet and further work

is in progress in this respect. A similar analysis of the impedance data for PTCa/P(VDF-TrFE) composite with 65/35 vol% composition yielded a value of 0.21 for k_t.

Now the piezoelectric d- coefficient and the electromechanical coupling factor k_t are related thus,

$$d = k_t \sqrt{\varepsilon_0 \varepsilon_r S} \qquad (15)$$

where S is the compliance $\left(m^2/N = Pa^{-1}\right)$ which has the same dimension as the dg-product. Thus,

$$\frac{d^2}{\varepsilon_0 \varepsilon_r} = k_t^2 S \qquad (16)$$

Using equations 7 and 16, we get,

$$\frac{d^2}{\varepsilon_0 \varepsilon_r} = dg = k_t^2 S \qquad (17)$$

$$\text{or} \quad \frac{dg}{S} = k_t^2 \qquad (18)$$

The compliance for a given material does not change significantly with frequency and it may thus be argued that k_t^2 is proportional to the dg product.

The acoustic impedance Z_a, is defined thus,

$$Z_a = \rho V_s \qquad (19)$$

where ρ is the density and V_s is the acoustic velocity in the medium. The latter parameter is given by,

$$V_s = 2lf_0 \qquad (20)$$

where l is the sample thickness. With the knowledge of f_0 (figure 2), composite density (equation 3) and the sample thickness, the calculated value of the acoustic impedances of PTCa/P(VDF-TrFE) 65/35 vol% and PTCa/Epoxy 60/40 vol% were found to be 16.5 and 11 MRayls respectively (see Table 1). It may be observed from Table 1 that the PTCa/Epoxy composite with 60/40 vol% composition is superior to the PTCa/P(VDF-TrFE) composite with 65/35 vol% composition. Now the transmitter efficiency Y_T, in the thickness mode is given by (Silk, 1984)

$$Y_T = \frac{k_t}{1 - k_t^2} \left(\frac{\varepsilon_r}{V_s} \right)^{1/2} \qquad (21)$$

Similarly the corresponding expression for the receiver efficiency Y_R, is,

$$Y_R = \frac{k_t l}{\left(V_s \varepsilon_r\right)^{1/2}} \qquad (22)$$

It may be observed from equations 21 and 22 that it is in general beneficial to have a large value of ε_r for a transmitter whereas for a receiver, a low value of ε_r is preferable, other things being equal. The performance of a single probe is given by the $Y_T Y_R$ product for a transmit receive operation and,

$$Y_T Y_R = \frac{k_t^2 l}{\left(1-k_t^2\right) V_s} \qquad (23)$$

From equation 22 and using the appropriate values of the parameters given in Table 1, it appears that the PTCa/Epoxy composite is approximately 64% more efficient as a transducer receiver material in comparison with the PTCa/P(VDF-TrFE) composite for the same thickness of the material. It should be pointed out that the overall synergy effects of k_t, V_s, ρ and ε_r are complex and not necessarily complementary and care should be exercised in the choice of a receiver material with optimum performance.

Finally, a preliminary study of the piezoelectric d_{33} coefficient of PTCa/PEEK with 45/55 vol% composition has provided a value of 21 pC/N that may be due to an appropriate mixing of the two phases that does not conform to a proper 0-3 connectivity. Further work is in progress in this respect.

MONITORING OF COMPOSITE LAMINATES: RESULTS AND DISCUSSION

Some preliminary experiments have been conducted to show the feasibility of the polymer/ceramic films to serve as multi purpose sensors for the nondestructive monitoring of fiber reinforced composite structures. In these experiments the composite sensors have been used for strain measurements under cyclic loading, and for the detection of acoustic emission in composite laminates under tensile loading. Initial results and conclusions from these experiments are outlined in this section.

DYNAMIC STRAIN MONITORING

The strain induced in an S2-glass/epoxy $[0_2/45_2/-45_2/90]_s$ laminate by cyclic loading, was monitored using composite films of PTCa/P(VDF-TrFE) and PTCa/Epoxy, of various ceramic contents, as sensors. Poled and electroded composite sensors ~10mm in diameter were bonded onto the specimens using cyanoacrylate (LOCTITE 401). Using an Instron

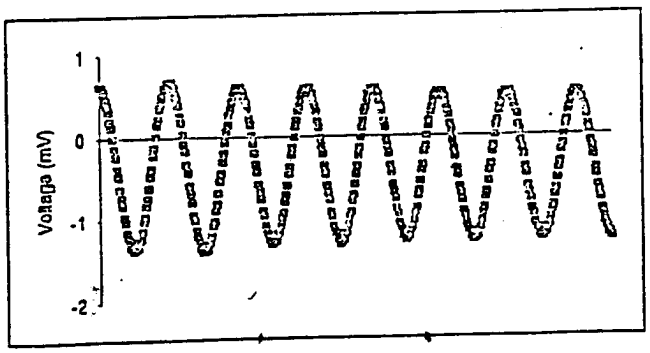

Figure 3. Response of PTCa/Epoxy sensor under cyclic load

testing machine the specimens were ramped to a mean load of 1000 lbs and immediately cycled using a sinusoidal load of 700 lbs in amplitude at a frequency of 2 Hz. A typical response from a PTCa/Epoxy composite sensor is shown in figure 3. In this case the signal from the composite sensor has a peak to peak amplitude of ~2 mV which is measurable with conventional equipment. These preliminary results indicate that these sensors could be utilized to monitor strain in composite laminates under cyclic loading.

EVALUATION AS ACOUSTIC EMISSION SENSORS

Two piezoelectric transducers have been constructed using PTCa/P(VDF-TrFE) 65/35 vol% and PTCa/Epoxy 60/40 vol% composite films as sensors. The design of these transducers consists of a grounded stainless steel case, the composite sensor an epoxy-tungsten backing and a gold-plated brass wire acting as the live electrode. The backing material consists of tungsten powder loaded epoxy in the range of 15-35/85-65 vol% ratio. The composition of the backing material was chosen appropriately to match the acoustic impedance of the ceramic/polymer composite film.

These transducers were evaluated for potential application in the detection of acoustic emission in composite materials. Two of the sensors were used to monitor glass/epoxy (SP250/E-glass) specimens during tensile testing. Each sensor was mounted on a specimen, along with a conventional Physical Acoustics Corporation (PAC) R15 acoustic emission sensor. This sensor has a piezoelectric lead-zirconate-titanate ceramic element, and is resonant at 150 KHz. The sensors were mounted on opposite faces of the specimen with vacuum grease couplant, and held by a constant force spring. They were connected to PAC 1220A preamplifiers with 100-300 KHz filters, and a PAC LOCAN 320 Acoustic Emission System. Preamplifier gain of 40 dB was used for the conventional sensor; 60 dB was used for the prototype sensors. The specimens were loaded in an Instron tensile testing machine at 0.02 inches per minute, to approximately 50% of their estimated breaking strength.

Acoustic emission data were monitored for each sensor on separate channels of the AE system. A portion of the data is shown in figures 4 and 5, plotted as histograms of number of AE hits, or signals detected by each sensor, vs. amplitude. Figure 4 shows data from the

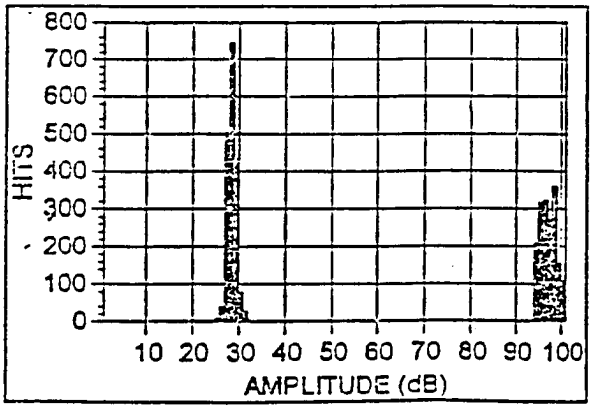

Figure 4. AE data for sensor 3 - 65% ceramic in copolymer (Hits vs. Amplitude (dB))

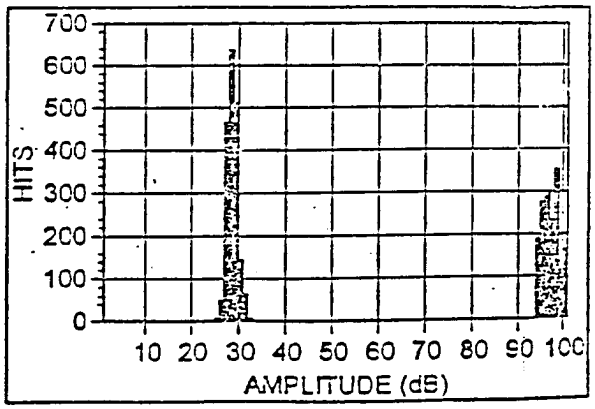

Figure 5. AE data for sensor 4 - 65% ceramic in epoxy (Hits vs. Amplitude (dB))

65% ceramic in copolymer sensor; figure 5 shows data from the 65% ceramic in epoxy sensor. The amplitude is on a dB scale where 0 dB represents 1 microvolt at the sensor with 40 dB preamp gain (10 microvolts at the sensor with 60 dB preamp gain). The prototype sensors are less sensitive than the conventional AE sensors, but very similar to one another. They detected many fewer signals, and the amplitude of the signals was significantly less. The signals from the prototype sensors ranged in amplitude from 25 to 32 dB; 25 dB is the lowest amplitude detectable above the system noise. The same signals were detected by the conventional R-15 sensors at amplitudes of 94-100 dB, the upper portion of the range, as shown in figures 4 and 5. These data indicate that the prototype sensors may find application with conventional, commercial acoustic emission systems where only higher amplitude signals are of interest. Other applications may require high gain, low noise preamplification.

The sensors were also evaluated by measuring their response to a pencil lead break on a graphite/epoxy plate. The lead break is a commonly used technique for generating a repeatable stress wave in a structure, and closely approximates an impulse load (ASTM, 1993). Figure 6 shows the response of four sensors to lead breaks on the surface of the plate. The signals were digitized at 6.25 MHz, and filtered from 20 KHz to 1.5 MHz. The units on the vertical axes are arbitrary.

The signal in figure 6c is from a Harisonic 5MHz ultrasonic sensor. It is resonant at 5MHz, but has a relatively flat frequency response at the frequencies considered here. It

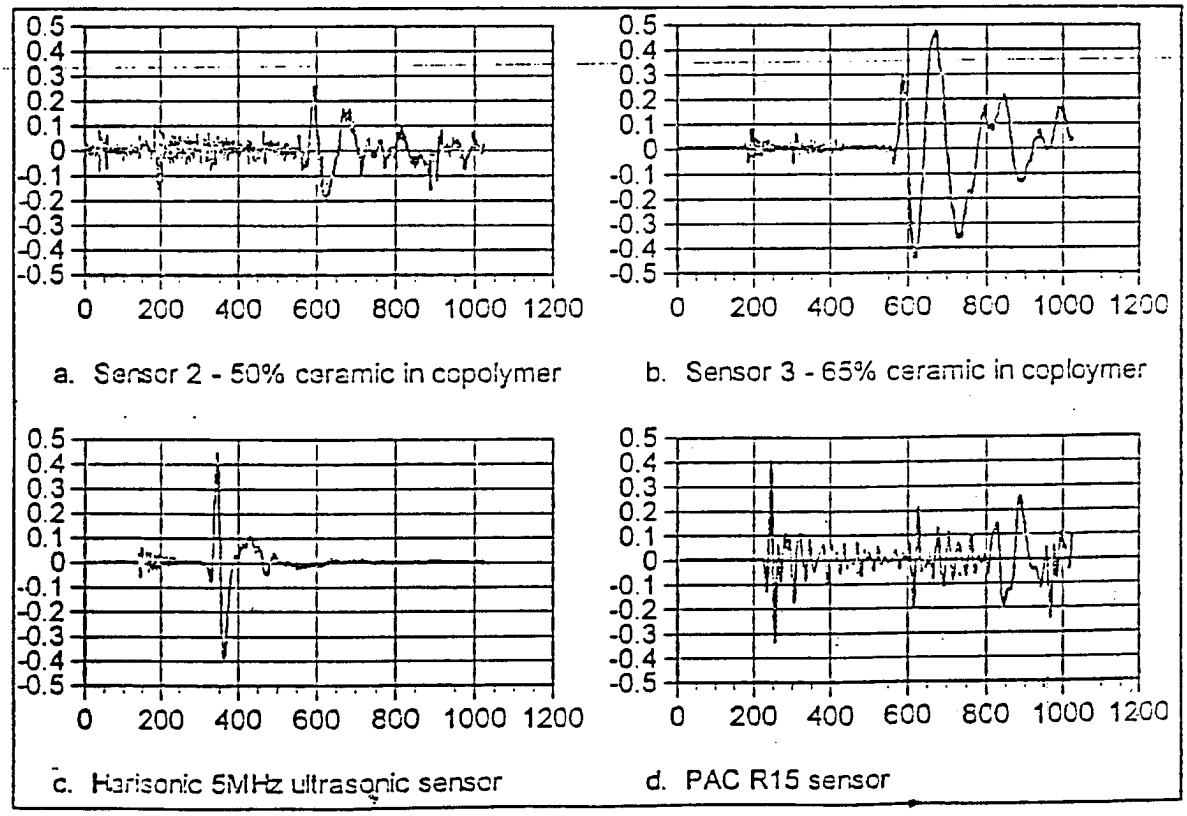

Figure 6. Waveforms from pencil lead breaks on the surface of a thin graphite/epoxy plate. Arbitrary units vs number of points digitized.

has been shown by Gorman (Gorman, 1990) that AE signals from pencil lead breaks on the surface of a thin aluminum or graphite/epoxy plate propagate as extensional and flexural plate modes. Prosser (Prosser, 1991) has shown, by comparing it to laser interferometer used to measure surface displacement, that the response of this type of sensor closely follows the surface displacement of the plate and shows both the low amplitude extensional wave, followed by the higher amplitude flexural wave. The signal in figure 6d is from an R15 sensor, and clearly shows the resonant nature of the sensor. Figure 6a shows the response of the 50% ceramic in copolymer; figure 6b is the 65% ceramic in copolymer. In both cases, both the extensional and flexural wave modes can be seen. A reflection of the extensional wave from the edge of the plate can also be seen in figures 6a and 6b resulting from the pencil lead break near the edge of the plate. The former signal was acquired with 56 dB gain before the digitization, and the electronic noise is evident in the signal. The latter signal was acquired with 50 dB gain. The noise is less, and the response to the flexural mode wave is much greater, due to the higher piezoelectric coefficient. These sensors are better suited for characterizing plate waves than are the conventional AE sensors.

REFERENCES

A.R. Von Hippel. 1954, "Dielectrics and Waves", Wiley, New York, NY.

G. Sa-Gong, A. Safari, S.J. Jang and R.E. Newnham. 1986, Ferroelectric Lett. Sect., 5, 131.

M.H. Lee, A. Halliyal and R.E. Newnham., 1989, J. Am. Ceramic Soc., 72, 986.

H. Ohigashi. 1988, "Ultrasonic Transducers in the Megahertz Range", The Application of Ferroelectric Polymers, ed. T.T. Wang, Blakie, Glasgow, 237.

L.N. Bui and H.J. Shaw. 1977, IEEE Trans. Sonics Ultrasonics, SU24, 331.

M. Platte. 1991, Ferroelectrics, 115, 229.

C. Dias and D.K. Das-Gupta. 1992, Proc. MRS Symposium on Smart Materials for Micro-Electronic-Mechanical Systems, 276, 25.

C. Dias and D.K. Das-Gupta, Yolanda Hinton and R.J. Shuford. 1993, Sensors and Actuators A, 37-38, 343.

M.A. Silk. 1984, "Ultrasonic Transducers for Nondestructive Testing", Adam Higler, Bristol, UK. 10.

ASTM E976. 1993, "Standard Guide for Determining the Reproducibility of Acoustic Emission Sensor Response", ASTM Book of Standards, Vol. 03-03.

M.R. Gorman. 1990, "Plate Wave Acoustic Emission", J. Acoust. Soc. Am., 90(1).

W.H. Prosser. 1991, "The Propagation Characteristics of the Plate Modes of Acoustic Emission Waves in Thin Aluminum Plates and Thin Graphite/Epoxy Composite Plates and Tubes", NASA TM 104187.

Electro-active Properties of Intelligent Ferroelectric Ceramic/Polymer Composite Sensors

C.J. Dias*, M.P. Wenger, Y. Kaminorz†,
U. Hopfner† and D.K. Das-Gupta
School of Electronic Engineering and Computer Systems
University of Wales, Bangor
Dean Street, Bangor, Gwynedd LL57 1UT, U.K.

†(Permanent Address) Institute of Solid State Physics,
Universität Potsdam, Neuen Palais 10, 14469 Potsdam, Germany
*(Permanent Address) Seccao de Fisica Aplicada
Universidade Nova De Lisboa, Torre, 2825 Monte de Caparica, Portugal

Abstract

The results of a study of the dielectric, piezo- and pyroelectric properties of calcium modified lead titanate (PTCa), and its composites with (i) copolymer vinylidene fluoride - Trifluoroethylene (VDF-TrFE) and (ii) Epoxy (Epicote 828) are reported. The latter composite, i.e. PTCa/Epikote 828 with 60% vol% ceramic loading appear to have superior properties for piezoelectric transducer-receiver application in comparison with the PTCa/P(VDF-TrFE) with 65 vol% ceramic loading.

1. Introduction

Ferroelectric ceramic/polymer composites enjoy the unique blending of the high electro-active(piezo- and pyroelectric and charge storage) properties of electro-ceramics and the mechanical flexibility and formability (at a low cost) of organic synthetic polymers. These composites provide an alternative to conventional ceramic sensor materials for transducer applications. Combining materials to fabricate diphasic composite films involves choosing judiciously the components with desired electroactive properties and also coupling them in the optimum way (i.e., the nature of the connectivity between the two phases). For transducer application composites with 1-3 and 0-3 connectivities are mostly used. In the 1-3 connectivity a polymer fills the space between the ceramic rods arranged in a three-dimensional matrix whereas for the 0-3 case discrete ceramic particles are introduced in a three dimensional polymer matrix. In the connectivity concept, the first digit refers to the ceramic phase.

The present work reports the results of a study of the dielectric, piezoelectric and pyroelectric properties of modified lead titanate (PTCa) ceramic particles introduced in the matrix of (i) vinylidene fluoride-trifluoroethylene (VDF-TrFE) and (ii) epoxy (Epikote 828) with the 0-3 connectivity.

2. Experimental

The method of fabrication of the composite films of 0-3 connectivity has been described elsewhere [1, 2] and will not be given here. The range of the thickness of the composite films

0-7803-1939-7/94/$ 4.00 © 1994 IEEE

was 60-90μm. Aluminium electrodes were vacuum deposited on both surfaces of the films. The following samples have been investigated in this work.

S1:	PTCa/P(VDF-TrFE)	65/35 vol%
S2:	PTCa/P(VDF-TrFE)	50/50 vol%
S3:	PTCa/P(VDF-TrFE)	40/ vol%
S4:	PTCa/Epikote 828	60/40 vol%
S5:	PTCa/Epikote 828	50/50 vol%
S6:	PTCa	
S7:	P(VDF-TrFE)	

The dielectric data were obtained in the temperature range of ~ 20°C to 120°C at 1kHz. The nature of the behaviour of the real (ε') and imaginary (ε") parts of the complex permittivity was also investigated in the frequency range 10^{-5} Hz to 10^{5} Hz. A General Radio Bridge (Model 1621) was used to evaluate ε' and ε" from 10Hz to 10^{5} Hz. The low frequency behaviour of ε " below 10Hz to 10^{-5}Hz was determined from the time dependent discharge current data and an appropriate truncated Fourier transform operation.

The composite samples were poled by the conventional thermal poling technique. The piezoelectric D_{33}- coefficient was measured with a Pennebaker apparatus (Model 8000). The evaluation of the electromechanical coupling coefficient was made from the measurement of complex impedance in the range of 300 kHz to 50 MHz using a network analyser (Model HP8702A). Finally the pyroelectric coefficient was determined both by the direct [3] and the dynamic methods [4].

Results and Discussion

The dielectric properties of constituent materials of a composite will have a significant influence on the electroactive properties of a composite. Table 1 shows the values of the dielectric constant and tanδ of some of the fabricated composites and their constituent materials offer poling at 30°C, 1kHz [5, 6].

Table 1: Dielectric Properties of Composites and their Constituent Materials at 30°C at 1kHz (after poling).

Material	Ceramic Volume fraction %	ε_r	tanδ
PTCa		220	0.006
P(VDF-TrFE)		7.9	0.011
PTCa/P(VDF-TrFE)	65	67	0.013
PTCa/P(VDF-TrFE)	50	40	0.021
PTCa/Epikote 828	50	24	0.009
PTCa/Epikote 828	60	30	0.010

All the materials show an enhancement of permittivity with temperature, the highest variation occurring with P(VDF-TrFE). The composites with a higher volume fraction of ceramic show a higher permittivity as is expected. In the low temperature range at ~ 10°C the composite S1 with 65% vol. loading shows a relaxation peak (ε″) which is attributed to the β- relaxation of P(VDF-TrFE). The ε″- values of composites decreases in the low temperature range following an analogous behaviour of the copolymer, whereas in the high temperature range the dielectric loss rises as in the case of PTCa.

Table 2 shows the values of the piezoelectric constants of the composites and the constituent materials [5].

Table 2: Piezoelectric Constants D_{33} and k_t of Composites

Material	Ceramic Volume fraction %	d_{33} p.c./N	k_t
PTCa		68	0.47
P(VDF-TrFE)		-33	0.30
PTCa/P(VDF-TrFE)	65	48	0.24
PTCa/P(VDF-TrFE)	50	25	0.09
PTCa/Epikote 828	50	24	0.14
PTCa/Epikote 828	60	30	0.19

The largest D_{33}- and k_t values are provided by the PTCa/P(VDF-TrFE), 65/35 vol% composite. However, the acoustic impedance for this composite is also largest (16.5 MRayl).

k_t- values were determined from the measurement of the electrical impedance of a poled composite vibrating as a free resonator. Now the transmitter efficiency y_T, of a piezoelectric transducer is given by [7],

$$y_T = \frac{k_t}{1-k_t^2}\left(\varepsilon_r / v_s\right)^2 \qquad \ldots(1)$$

and the corresponding expression for the receiver efficiency y_R, is [7],

$$y_R = \frac{k_t l}{\left(v_s \varepsilon_r\right)^{1/2}} \qquad \ldots(2)$$

where v_s is the acoustic velocity in the medium and l the sample thickness. It is thus necessary to have a high value of ε_r for a transmitter, whereas for a receiver, a small value of ε_r is preferable. The measured values of v_s for PTCa/P(VDF-TrFE), 65/35 vol%, and PTCa/Epikote 828, 60/40 vol% are 3200 m/s and 2418 m/s respectively. Using these values of v_s and the appropriate magnitude of ε_r (see Table 1), it appears that PTCa/Epikote 828 composite is approximately 64% more efficient as a receiver than PTCa/P(VDF-TrFE) composite [7].

Table 3 shows [5] the values of pyroelectric coefficients and the figure of merit $(FOM)_p$ of PTCa, P(VDF-TrFE) and PTCa/P(VDF-TrFE) composites.

The pyroelectric coefficients, shown in Table 3, were obtained by using the direct method [3].

Table 3: Pyroelectric coefficients of the two constituents and the composites

Material	Ceramic Volume fraction %	p at 30°C ($\mu C/m^2k$)	$(FOM)_p$ at 30°C ($\mu C/m^2k$)
PTCa		380	1.73
P(VDF-TrFE)		17	2.1
PTCa/P(VDF-TrFE)	65	130	1.94
PTCa/P(VDF-TrFE)	50	79	1.97
PTCa/Epikote 828	50	20	0.84
PTCa/Epikote 828	60	30	0.99

$(FOM)_p = p/\varepsilon_r$, is roughly proportional to the responsivity of a detector. It is necessary to have a high p- value and low ε_r in order to obtain a high $(FOM)_p$.

The observed piezo- and pyroelectric properties of the composites can be explained by a modified [5, 8] cube model [9].

Acknowledgement

One of the authors (MPW) expresses his gratitude for a maintenance grant from the European Research Office of the US Army which is also financially supporting the present work.

References

1. C. Dias, D.K. Das-Gupta, Y. Hiuton & R.J. Shuford, Sensors and Actuators A, 37-38, 343-347 (1993).

2. C.J. Dias & D.K. Das-Gupta, J. Appl. Phys., 74, 6317-6321 (1993).

3. R.L. Byer & C.B. Roundy, Ferroelectrics, 3, 333-338 (1972).

4. M. Simhony & A. Shanlov, J. Appl. Phys., 42, 3741-3744 (1971).

5. C.J. Dias, PhD Thesis, University of Wales, 1994.

6. C.J. Dias, M. Wenger, P. Blanas, R.J. Shuford and D.K. Das-Gupta, Proc. 2nd Internat. Conf. on Intelligent Materials, Williamsburg, VA, USA, 437-449 (1994).

7. M.G. Silk, "Ultrasonic transducers for non-destructive testing", Adam Hilger Ltd., Bristol, UK (1984).

8. C.J. Dias & D.K. Das-Gupta, "Piezo- and Pyroelectricity in ferroelectric ceramic-polymer composites" in 'Ferroelectric Polymers and Ceramic-Polymer Composites', Ed. D.K. Das-Gupta, Trans-Tech Publications, Switzerland, 1994, 92, Chapter 8, pp217-248.

9. H. Banno, Jap. J. Appl. Phys., 24 (suppl. 2), 445-447 (1985).

Pyro- and Piezoelectricity in Sol-Gel Derived Ceramic / Polymer Composites

Igreja R., Wenger M.P.†, Dias C.J., Das-Gupta D.K.† and Marat-Mendes J.N.

Universidade Nova de Lisboa, Faculdade de Ciências e Tecnologia / Secção de Física Aplicada, Torre, 2825 Monte de Caparica, Portugal
†School of Electronic Engineering Science, University of Wales, Dean Street, Bangor, Gwynedd, LL57 1UT, UK

Abstract
Electroactive ceramic/polymer composites with 0-3 connectivity pattern have been studied recently in view of their attractive properties for smart sensors applications.

Sol-gel is a convenient technique to obtain ceramics of high purity and molecular homogeneity. A further advantage is the use of lower processing temperatures than that of the conventional mixed oxides route. In this work we have synthesized lead titanate (PT) and calcium modified lead titanate (PTCa) ceramic powders by this technique. Various techniques have been used to evaluate the characteristics of the resulting ceramics.

Introduction

The work presented here stems from an effort to produce calcium modified lead titanate (PTCa) powders via the sol-gel method for use in the formation of ceramic/polymer composites for sensing materials.

PTCa has long been know to possess ferroelectric characteristics which are more suitable to practical applications than lead titanate (PT) alone [1]. High Curie temperature Tc, low permittivity e_r, large anisotropy of the electromechanical coupling coefficients d_{33} and d_{31} and high pyroelectric coefficient p, all make PTCa an appealing material for use in various transducers.

The addition of a ferroelectric ceramic powder to a polymer matrix with 0-3 connectivity, produces materials which combine the desirable ferroelectric properties of the ceramic with the good properties of the polymer. Polymers possess lower dielectric constants with respect to ceramics, acoustic impedances closer to that of water which makes composites appealing to ultrasonic diagnosis and sonar applications, as well as having the added property of being easily formed into a variety of shapes or large area thin films.

The sol-gel method for preparation of ferroelectric ceramics can offer many advantages over conventional processing techniques. Ceramics produced via the sol-gel method show high degrees of purity and homogeneity, can produce fine powders as well as being able to be formed into a variety of structures and they possess the ability to be processed at lower temperatures.

0-7803-1939-7/94/$ 4.00 © 1994 IEEE

Thin films of composite materials using PTCa, produced by conventional mixed oxide processing methods, and PVDF-TrFE have been produced and shown to be of practical use as sensor materials [2]. This paper reports on the production of PTCa powders via the sol-gel method for use in ceramic/polymer composites.

Experimental Methods

In this work we have prepared PT and PTCa ferroelectric ceramic powders, using complexed alkoxide precursors, formed by the reaction of lead acetate trihydrate, $Pb(CH_3COO)_2 \cdot 3H_2O$, calcium acetate hydrate, $Ca(CH_3COO)_2 \cdot nH_2O$, with titanium isoproxide, $Ti(OC_3H_7)_4$.

Gel of PT was prepared by the following method. The lead acetate trihydrate and titanium isoproxide were dissolved separately in solutions of propanodiol-(1,3) in a 0.05M ratio of total reagents to solvent. Once the acetate had dissolved completely the two solutions were mixed together and water for hydrolysis was added. This solution was left to reflux at 80°C and a viscous gel was formed in approximately two hours. The amounts of metal-alkoxides were chosen to achieve a 1:1 molar ratio of lead to titanium and the amount of water added was calculated using a method described by Lipeles, Coleman and Leung [3].

A gel of PTCa was also prepared using this method and the amounts of metal-alkoxide reagents were chosen so as to form $(Pb_{1-x}Ca_x)TiO_3$ with a value of x=0.24.

The gels were dried under vacuum at approximately 80°C to remove excess solvents. The gels were then allowed to dry for one week in the open air. After one week the gels showed shrinkage and had become solid like i.e., would not flow. These gels were then heated in an oven at various temperatures in order to obtain the crystalline ceramic powders. The drying of the gels was performed in stages to ensure the removal of excess solvents and unwanted organics, therefore the initial heating was performed very slowly.

The gels were analysed by TGA and DTA methods and the ceramic powders studied by X-ray diffraction methods and DSC analysis.

Results and Analysis

Thermal gravimetric analysis (TGA) and differential thermal analysis (DTA) techniques were performed on the gels which had been left to dry whilst exposed to the atmosphere. A heating rate of 5°C/min was used for both techniques. The TGA analysis shows a loss of weight due to solvent evaporation at temperatures below 250°C for both PT and PTCa. The DTA results indicate a crystallisation temperature of 240-280°C, of the amorphous gel, due to a sharp exothermic response, for PT and PTCa.

The powders of the ceramics after being prepared at various temperatures were formed into pellets which enabled X-ray diffraction to be performed using Cu-K_α radiation. The results showed that both ceramics possess a high degree of crystallinity, corresponding to a perovskite phase, when fired above 500°C. It was observed that the

powders crystallised at about 250-300°C for PT and PTCa, below which the powders were amorphous. This agrees with the DTA results indicating the crystallisation temperatures. The resulting diffraction patterns can be seen in figure 1 for various times and temperatures (PT: 2h at 150°C, 2h at 450°C, 2h at 800°C; PTCa: 2h at 150°C, 15 min at 450°C, 2h at 800°C).

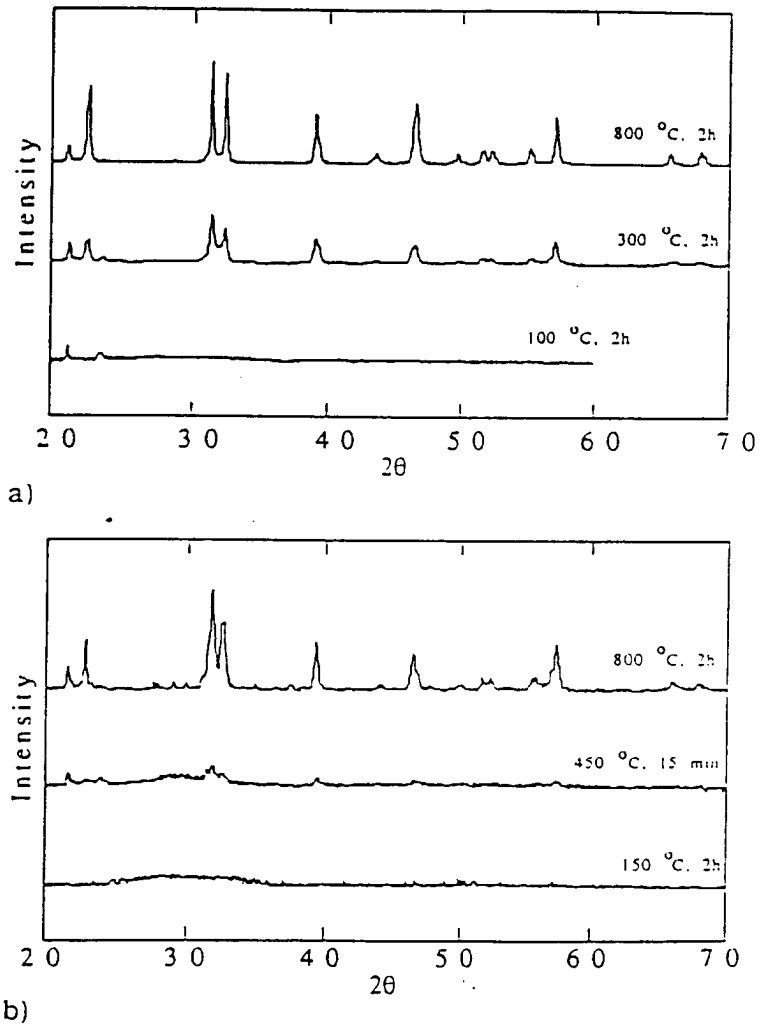

Figure 1. - X-ray diffraction paterns (CuK_α): a) lead titanate: b) calium modified lead titanate.

The tetragonality (c/a ratio) of the crystal lattice was calculated from the 002 and 200 diffraction peaks and are shown in table 1. The value of the c/a ratio for PT is in good agreement with other published results [4]. The value for PTCa is lower than that of PT but differs from other results from similar ceramics of calcium modified lead titanate [5]. This could be due to a difference in stoichiometry.

	PT	PTCa
T_C °C	487	412
tetragonality (c/a)	1.066	1.052

Table 1. - Curie temperature and tetragonality for PT and PTCa.

Differential scanning calorimetry (DSC) analysis was performed on powders which had been fired at temperatures above 500°C. Endothermic peaks, corresponding to the detection of a ferroelectric transition from the tetragonal to cubic crystal structures, were observed for both PT and PTCa ceramics. The transition temperature for PT was observed to be approximately 487°C which agrees with reported data on lead titanate [6]. The observed endothermic peak for PTCa was approximately 1/5 of the intensity of that for PT and appeared at 412°C as can be seen from fig 2.

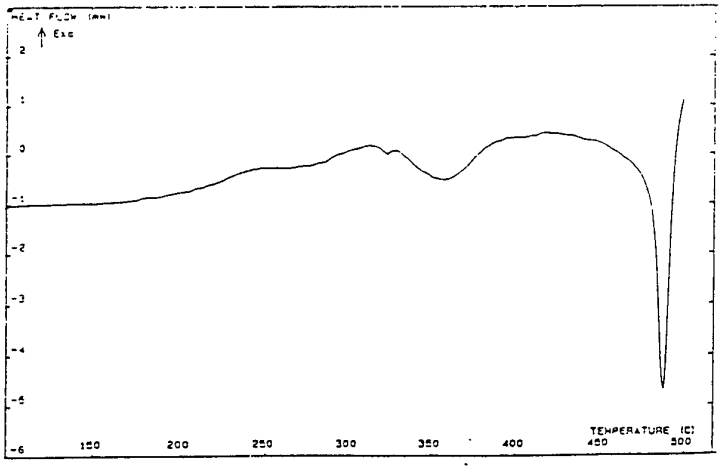

a)

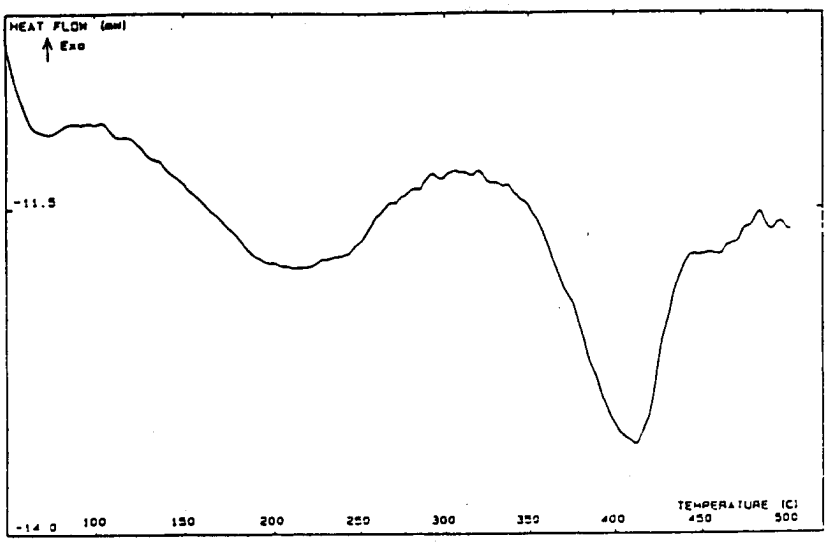

b)

Figure 2. - DSC of ceramic powders fired above 500°C: a) lead titanate, b) calcium modified lead titanate.

Conclusion

It has been shown that PTCa can be synthesised via sol-gel method, used in the past for the production of PT. The results of X-ray, TGA and DSC analysis show that PTCa produced in this way posses a perovskite structure and a comparable temperature of crystallisation to that of PT. The anisotropy of crystal lattice has been reduced by the addition of modifier ions of Ca^{2+} within the crystal lattice which produce a ceramic less susceptible to cracking during cooling through the Curie temperature.

The observed Curie temperature from DSC measurements of $(Pb_{1-x}Ca_x)TiO_3$ (x=0.24), produces a broadened peak which could be due to a spread of **x** values. Varying **x** values would have the effect of reducing the homogeneity of the bulk ceramic and therefore resulting in a ceramic with a less well defined Curie temperature. This could be explained by a difference in the hydrolysis rates of the various alkoxides [7].

Further work is being undertaken to the control of the hydrolysis-condensation reaction by the study of the kinetics of the multicomponent sol-gel process to improve the stoichiometry of PTCa. The results of combining these ceramics into polymer matrices with 0-3 connectivity to form pyro- and piezoelectric composites and the effects of other isovalent substitutions will be reported at a later date.

References

1. Liao, J.H., Cheng, S.Y., Wang, H.C., Wang, C.M., *Microstructure and Poperties of Modified $PbTiO_3$ Ceramics*. Ferroelectrics, vol. 127, pp. 101-106, 1992.

2. Dias, C.J., *Ferroelectric Composites for Pyro- and Piezoelectric Applications*. PhD Thesis, University of Wales, Bangor, 1994.

3. Lipeles, R.A., Coleman, D.J., Leung, M.S., *Metallorganic Solution Deposition of Ferroelectric PZT Films*. IEEE Transactions on Ultrasonics, Ferroelectrics & Frequency Control, vol. 38, No. 6, November 1991.

4. Durán, P., Fernández, J. F., Recio, P., Moure, C., *Processing and Properties of Modified - Lead Titanate Ceramics*. Materials & Manufacturing processes, vol 5(3), pp. 427-443, 1990.

5. Yamushita, Y., Yoshida, S., Takahashi, T., *Effects of MnO Additive on Piezoelectric Properties in Modified $(Pb,Ca)TiO_3$ Ferroelectric Ceramics*. Japanese Journal of Applied Physics, vol 22-2, pp. 40-42, 1983.

6. West, A. R., Solid State Chemistry and its Applications, John Wiley & Sons, 1984.

7. Re, N.,*Kinetics of Bicomponent Sol-Gel Process*. Journal of Non-Crystalline Solids, vol. 142, pp. 1-17, 1992.

Paper presented at the Second European Conf. on Smart Structures and Materials, Glasgow 1994, Session 1(

Ferroelectric Ceramic and Epoxy Composite Films as Pyroelectric Detectors

M.P. Wenger, P. Blanas†, R.J. Shuford† and D.K. Das-Gupta

School of Electronic Engineering Science, University of Wales, Dean Street, Bangor, Gwynedd, LL57 1UT, UK

†U.S. Army Research Laboratory, Materials Directorate, Arsenal Street, Watertown, MA. 02172-0001, USA

Abstract

Thin films of ferroelectric ceramic and epoxy composites with 0-3 connectivity have been produced by dispersing a ceramic powder in a thermosetting epoxy resin. Calcium Modified Lead Titanate [PTCa] powder with grain size of less than 10μm was mixed with an epoxy resin and curing agent and then formed into thin films of approximately 100μm. The pyroelectric behaviour of these composites with 50% and 60% volume loading of ceramic is reported in this present work.

Introduction

The use of the piezoelectric and pyroelectric properties of ferroelectric ceramic and polymer composites as sensors in transducers has gained much interest in the past years. Ferroelectric ceramics have a tendency to possess high pyroelectric coefficients and a correspondingly high permittivity. Polymers can be either ferroelectric or not, but tend to have low values of permittivity. The suitability of a pyroelectric material as a detector is usually determined by its Figure of Merit (FOM_p) and is defined for a thin film composite as

$$FOM_p = \frac{p}{\varepsilon} \qquad \ldots(1)$$

where p is the pyroelectric coefficient and ε the permittivity of the composite. The FOM_p for a composite material can thus be determined by the properties of the constituent materials and reflects the responsivity of the material. The permittivity, due to the ceramic alone will be lowered by the inclusion of the ceramic into a low permittivity polymer matrix. The corresponding pyroelectric coefficient will also be lowered but the value of the FOM_p may be greater than that of the constituent materials alone.

Other determining factors in the choice of materials for certain applications can be the size of the sensing material. Composite materials possess an advantage over ceramics alone in their ability to be formed into large area targets. The use of a thermosetting epoxy as a polymer matrix provides ease of composite manufacture as well as providing low manufacturing cost.

0-8194-1700-9/94/$6.00

Fabrication of Composite Films

In a 0-3 connectivity ceramic/polymer composite, ceramic powder is dispersed randomly in a polymer matrix. The quantity of the ceramic can be calculated using the following equation

$$M_c = \left(\frac{\phi}{1-\phi}\right)\rho_c V_p \qquad ...(2)$$

to obtain the mass M, of the ceramic for a given ceramic volume fraction ϕ, where ρ_c is the density of the ceramic and V_p the volume of the epoxy resin used. The subscripts c and p refer to the ceramic and the polymer respectively. The composite density is then given by

$$\rho = \phi\rho_c + (1-\phi)\rho_p \qquad ...(3)$$

where ρ_p is the density of the polymer.

Epikote 828 (Shell) and curing agent K61B (Anchor Chemicals) were used to produce a matrix of a thermosetting polymer. A few drops of the curing agent were added to 1 cc of the epoxy resin in a small container. The measured amount of the ceramic powder was gradually added to the epoxy whilst stirring continuously to ensure an even distribution of ceramic throughout the polymer.

The composite mixture was placed in a vacuum chamber and outgassed at room temperature for two hours. At this stage it was removed from the container and placed on a clean, smooth piece of aluminium foil and replaced into the vacuum chamber. The composite was outgassed for a further two hours at 60°C.

The composite was then removed from the vacuum chamber, together with the foil, and another piece of foil was placed on top of the composite. These were located between two milled steel plates and the assembly was placed in a temperature controlled mechanical press at 60°C. A maximum pressure of 250 kg cm^{-2} was gradually applied. The composite was left to cure for another 2 - 4 hours at 60°C.

The cured material was removed from the assembly and the foil gently peeled away to expose a smooth thin film, (80 - 300μm). Aluminium electrodes were evaporated onto the surface of the films which were poled by applying a DC electric field in the range of 15 - 30 MVm^{-1} between the electrodes. The poling process was performed with the sample immersed in a bath of insulating silicon oil at 100°C. The magnitude of the poling field was limited by the electrical breakdown strength of the composite.

Pyroelectricity: Results and Discussion

Composite films of PTCa/P(VDF-TrFE) and PTCa/Epoxy of varying ceramic volume fraction have been studied extensively so far to determine their piezoelectric and pyroelectric properties. The piezoelectric properties of these composites have been reported [1] and their suitability as sensing materials in transducers has been considered.

The pyroelectric properties of these composites were measured using a direct method [2]. The phenomenon of pyroelectricity arises from the temperature dependency of the spontaneous polarisation present in ferroelectric materials. Thus a change in temperature produces a change in spontaneous polarisation which manifests itself as surface charge on the electrodes of the sample. If the electrodes are short circuited a current will flow from one electrode to the other via the external circuit. The pyroelectric coefficient, p in this configuration is defined as

$$p = \left(\frac{dP_s}{dT}\right)_{E,X} = \left(\frac{dQ/A}{dT}\right)_{E,X} \equiv \frac{1}{A}\left(\frac{dQ}{dT}\right)_{E,X} \qquad \ldots(4)$$

where P_s is the polarisation of the sample, Q the surface charge produced, A the area (assumed not to vary significantly) and T the temperature. The subscripts E and X refer to the electric and stress fields respectively which are kept constant. By suitable manipulation of equation (4) the pyroelectric coefficient becomes

$$p = \frac{1}{A}\left[\left(\frac{dQ}{dt}\right)\left(\frac{dt}{dT}\right)\right]_{E,X} = \frac{I}{A}\left(\frac{dt}{dT}\right)_{E,X} \qquad \ldots(5)$$

where t is the time. Therefore while knowing the rate of change of temperature and measuring the current, the pyroelectric coefficient can be determined.

The samples were placed in a cryostat and heated/cooled at a constant rate of 1.5 ^{o}C/min between 10 - 70 ^{o}C. The electrodes of the samples were shorted circuited via a Keithley 616 Digital Electrometer to monitor the current. The output of the electrometer was read directly by a computer via an analogue to digital converter at temperature intervals of 0.5 ^{o}C. The temperature ramp was controlled by an Eurotherm 818P Model.

This procedure is the same for the Thermally Stimulated Discharge Current measurements and therefore it was necessary to ensure that the contribution due to space charge was kept to a minimum. The sample was therefore annealed, for an extended period of time by keeping the electrodes short circuited whilst the temperature was held above the measuring temperature (@ 80 ^{o}C). A number of temperature cycles were performed to ensure the value of the pyroelectric coefficient was reversible on the heating and cooling part of the cycle (figure 1).

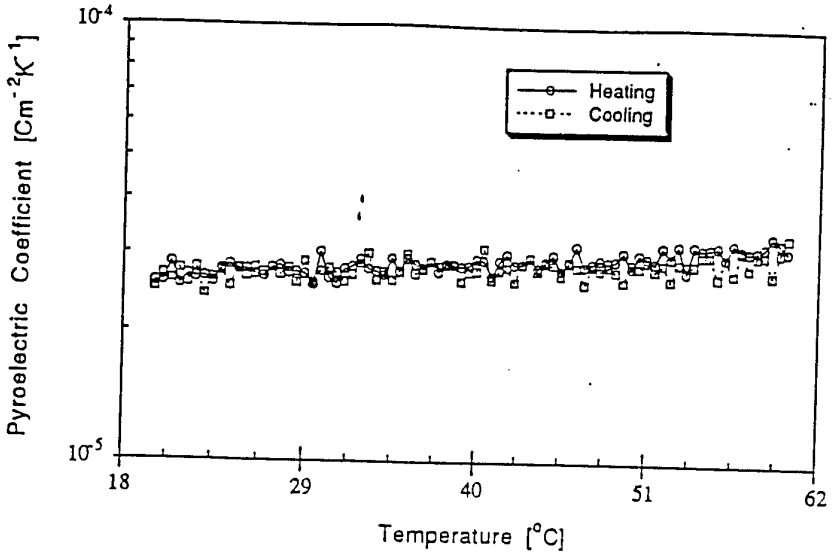

Figure 1 - Plot of the pyroelectric coefficient against temperature on a heating cycle and cooling cycle for PTCa/Epikote 60/40vol%. True reversibility can be seen from the graph.

As stated earlier the pyroelectric figure of merit, FOM_p can be used to characterise the suitability of a material for use as a sensor. The permittivity of the samples were obtained from measurements of their capacitance and conductance by using a conventional capacitance bridge (General Radio, Model 1621) at 1 kHz at a variety of isothermal temperatures. Values of the pyroelectric coefficient, permittivity and FOM_p for composites of PTCa/Epoxy and their individual constituent materials can be seen in table 1.

Material	p @ 30°C (x10^{-3})	ε_r @ 1 kHz	FOM_p
PTCa	380.0	220.0	1.73
Epikote 828	-	4.1	-
PTCa/Epikote 50/50vol%	20.4	24.0	0.85
PTCa/Epikote 60/40vol%	29.7	30.1	0.99

Table 1 - Pyroelectric properties of PTCa, Epikote 828 and composites of the constituent materials at 50/50vol% and 60/40vol%.

Acknowledgements

This work is financially supported by the US. Army Research Laboratory (Watertown - US) and we are grateful to Siemens (Munich - Germany) and GEC - Marconi Materials Research (Caswell - UK) for supplying the ceramic used in the research.

References

1. C. Dias, M.P. Wenger, P. Blanas, R.J. Shuford, Y. Hinton , D.K. Das-Gupta, *Intelligent Piezoelectric Composite Materials for Sensors*. To be presented at the 1994 International Conference on Intelligent Materials, Williamsburg, Virginia, USA.

2. Byer, R.L. and C.B. Roundy, *Pyroelectric coefficient direct measurement technique and application to a nsec response time detector*. Ferroelectrics, 1972. 3: p. 333-38.

SMART CERAMIC/POLYMER COMPOSITE MATERIALS FOR SENSORS

P. Blanas, R. J. Shuford
U.S. Army Research Laboratory, Materials Directorate
Arsenal Street Watertown, MA. 02172-0001, USA

M. Wenger, D. K. Das-Gupta
University of Wales, School of Electronic Engineering Science
Dean Street, Bangor, Gwynedd, LL57 1UT, UK

Abstract

Polymer/ceramic composite materials have been produced by mixing calcium modified lead titanate powder into two different polymer matrices. Thin films of the composites have been obtained and characterized to determine their dielectric and piezoelectric properties. Furthermore, an initial evaluation of the piezoelectric films as multipurpose sensors for the nondestructive monitoring of fiber reinforced composites has been made.

1. INTRODUCTION

Smart materials and structures can be defined as those possessing the capability to respond in an advantageous manner to their environment. As such, these structures must in general have the ability to sense a stimulus, compute a reaction and actuate the structural system. Currently, smart structures incorporate passive and active components to perform their function. In many instances the passive, load carrying components consist of advanced fiber reinforced composites. Reliable nondestructive evaluation methods to monitor the integrity of these components are necessary. The active components of the smart structure can be utilized for the nondestructive structural health monitoring of the composite parts.

Piezoelectric materials have the ability to convert mechanical to electrical energy but also exhibit the converse electrostrictive effect. These properties enable piezoelectrics to perform both sensing and actuating functions thus classifying them as active or smart materials. The standard piezoelectric materials used as sensors or actuators in a variety of applications, such as nondestructive evaluation transducers, are ferroelectric ceramics notably lead zirconate titanate (PZT). However, these materials present some disadvantages such as acoustic impedance mismatch, high dielectric constant and lack of flexibility as well as the coupling of different vibration modes and narrow bandwidth. New materials in the form of ferroelectric polymers such as polyvinylidene fluoride (PVDF) and ferroelectric ceramic/polymer composites have emerged which attempt to bridge such disadvantages [1,2].

By mixing a ferroelectric ceramic into a polymer matrix, the compliance of the composite material increases and thus the acoustic impedance decreases to a value which depends on the ceramic loading. Also, because of the enhanced damping provided by the polymer matrix, the mechanical losses increase and the transverse modes are attenuated. As a consequence, the longitudinal piezoelectric coefficient can be tailored depending on the ceramic content.

In this study we report on mixed connectivity composites made of ceramic powder dispersed in a polymer matrix which lends itself to easy fabrication of large area, flexible and formable piezoelectric materials. Calcium modified lead titanate (PTCa) has been

used as the filler ceramic because of its low dielectric constant and highly anisotropic piezoelectric properties.
Two different polymer matrices have been used; Epoxy and P(VDF/TrFE). Epoxy resins are commonly used as the matrix phase of fiber reinforced polymer composite materials. Therefore, epoxy/ceramic composite sensors would be compatible with and could be utilized in a wide class of fiber reinforced composites. Finally, P(VDF/TrFE), a ferroelectric polymer, has also been used as the polymer host. Its polar character, which is responsible for its ferroelectricity, imparts the highest dielectric constant known in polymers peaking at $\varepsilon = 60$ at its Curie temperature which is around 125°C for the copolymer used. This allows for easier poling of the ceramic grains near T_c due to a better dielectric constant matching between the phases.
In this paper we report on the piezoelectric constants and dielectric properties obtained for the ceramic/polymer composites with various ceramic contents. We also report on their application as multi purpose sensors for the nondestructive monitoring of laminated fiber reinforced composites. The response of these sensors to cyclic loading is investigated and results from the detection of acoustic emission signals in composite plate structures are presented.

2. FABRICATION OF FERROELECTRIC CERAMIC/POLYMER COMPOSITE FILMS

A great deal of versatility in the properties of ferroelectric ceramics is obtained by introducing suitable dopants so that the Curie temperature T_c, dielectric constant ε_r and polarization P_s, can be manipulated. Lead titanate (PT) has a perovskite tetragonal structure with $T_c = 490$°C, $\varepsilon_r \sim 150$ and $P_s = 0.6\ C/m^2$[3]. Due to its high tetragonal distortion, considerable internal stresses are induced during the phase transition which fractures the ceramic [4]. It was observed that by doping PT with calcium oxide (CaO) appropriately, the sinterability of the ceramic improves [5]. An optimum doping of 24 mol% of Ca together with a modification in the B-site with one of the following pairs, Ni-Nb, Co-W or Fe-W provides an optimum electromechanical anisotropy [3] with an ε_r-value in the 200 range. The modified PTCa employed in this work, contains this mol% of Ca together with Co-W doping.
The copolymer based PTCa/P(VDF-TrFe) composites were prepared by the solvent casting technique. The composition of the copolymer P(VDF-TrFe) was 73-27 *mol%*. Weighted amounts of the two constituents were dissolved in methyl-ethyl ketone, i.e. butanone, and a uniform slurry was formed. The slurry was stirred to form a solid which was used to cast films of thickness in the range of 50-80 μm in a hydrostatic press at a temperature of 170°C and pressure of 9 *MPa*. The PTCa particle size was in the range of 5-10 μm. The following equations were used to obtain a desired volume fraction, φ, of the ceramic in the composite film.

$$M_c = \varphi \rho_c V \tag{1}$$

$$M_p = (1 - \varphi)\, \rho_p V \tag{2}$$

$$\text{and } \rho = \varphi \rho_c + (1 - \varphi)\rho_p \tag{3}$$

where M, ρ and V are the mass, density and total volume. Subscripts c and p refer to the ceramic and polymer respectively.
Epicote 828 (Shell) epoxy resin and K61B (Anchor Chemicals) hardener were used to produce the host thermoset polymer for the PTCa/Epoxy composite. After mixing the

ceramic into the epoxy, an outgassing procedure, in a vacuum oven both at room temperature and 60°C, was followed to remove air trapped during mixing. Thin films of the composite were then obtained by the above discussed method.

3. CONNECTIVITY OF THE COMPOSITE FILMS

The composites of ceramic/polymer are a mixture of two components, i.e. phases, and the concept of connectivity [6] classifies different types of mixtures. In a two phase composite each phase may be spatially self-contained in zero, one, two or three dimensions. The diphasic composite films, produced by dispersing randomly fine ceramic grains, as in the present case, are expected to have a 0-3 connectivity in which ceramic grains are isolated from each other, 0-dimension, with the polymer phase around them, 3-dimension. If the ceramics are well connected with each other in the polymer, the composite material will have a 1-3 connectivity. The scanning electron microscopy of the composite films used in the present work, shows a presence of both 0-3 and 1-3 pattern of mixed connectivity which possibly originates from the wide distribution of the ceramic particle size and a possible agglomeration of the ceramic grains. This is not detrimental as the electro-active properties are expected to be enhanced by the presence of 1-3 connectivity.

4. POLING OF THE COMPOSITE FILMS

Aluminum electrodes of ~1 μm thickness were vacuum deposited on both surfaces of each film sample which was poled at a DC field of $1 - 2.5 \times 10^{-} \; Vm^{-1}$ for 30 minutes at 100°C. The magnitude of the poling field was restricted by the electrical breakdown strength of the samples. In order to prevent Paschen discharge and/or surface breakdown, the samples were immersed in insulating silicone oil during the poling process.

With a 0-3 connectivity the ceramic grains in the composite will only sense part of the applied poling field. The magnitude of the induced polarization will thus be dependent on the connectivity pattern, volume fraction of the ceramic phase and the relative values of the resistivity of the constituent phases. In a mixed connectivity case the two phases may exist simultaneously both in series, 0-3 case, and parallel, 1-3 case, connections. The ceramics in the parallel branch will certainly be subjected fully to the poling field and will be polarized provided the poling field is greater than the coercive field, usually a few MV/m. For the series case, however, the composite may be described as a two layer capacitor in which the field will be shared thus,

$$\frac{E_p}{E_c} = \frac{\sigma_c}{\sigma_p} \qquad (4)$$

where E and σ are the poling field and the electrical conductivity respectively. In general, $\sigma_p << \sigma_c$, and as a result, the voltage drop across the polymer phase is much higher than that across the ceramic phase. For example, at 90°C the resistivities of PTCa and P(VDF-TrFe) are 6.5×10^{9} ohm-meter and 4.5×10^{12} ohm-meter respectively. Such a large difference in resistivity will produce a voltage drop across the polymer approximately 690 times greater than that across the ceramic phase. The importance of the connectivity of the phases with respect to the poling efficiency can thus be appreciated. Attempts have been made to improve the degree of poling by decreasing the resistivity of the polymer by doping with carbon, silver, silicon or germanium [7]. However, this approach has been unsatisfactory as it increases the dielectric loss of the composite and thus decreases its signal-to-noise ratio. An increase in ceramic resistivity is not an option as its electro-active properties are generally maximized and dielectric

TABLE 1
Piezoelectric and other relevant properties of PTCa and its composites PTCa/P(VDF-TrFe) and PTCa/Epoxy.

Property	PTCa	PTCa/P(VDF-TrFe)		PTCa/Epoxy	
		50/50 vol%	65/35 vol%	50/50 vol%	60/40 vol%
Density (g/cm^3)	6.89	4.40	5.13	4.03	4.60
Dielectric constant ε_r, at 1kHz, RT	230	40	67	17	23
Tanδ, at 1kHz, RT	0.006	0.013	0.013	0.009	0.010
Piezoelectric $d_{3,3}$ coefficient ($\times 10^{-12} C/N$)	68	43	48	28	32
Electromechanical coupling factor k_t	0.47	0.09	0.21	0.15	0.19
FOM: $d_{33} \times g_{33}$ ($\times 10^{-12}$ Pa^{-1})	2.24	5.20	3.90	5.21	5.03
Mechanical Quality Factor Q_m	80	4.1	4.3	11.0	21.7
Acoustic Impedance Z_a ($\times 10^6$ Rayls)	29.6	13.8	16.5	11.0	11.0
Acoustic Velocity (m/s)	4300	3100	3200	2767	2418

loss minimized.

5. RESULTS AND DISCUSSION: DIELECTRIC AND PIEZOELECTRIC CHARACTERIZATION

Composite films of PTCa/P(VDF-TrFe) with 65/35 and 50/50 vol% and PTCa/Epoxy with 60/40 and 50/50 vol% compositions have been investigated to determine their dielectric constant ε_r, piezoelectric d_{33}-coefficient and the electromechanical coupling factor k_t. The dielectric properties were evaluated from capacitance and conductance measurements at 1 *kHz* and room temperature (RT) using a capacitance bridge (General Radio Model 1621). The results are given in Table 1 and are an extension of our previous work [8]. It may be observed that for a composite, the ε_r value increases with increasing volume fraction of the ceramic content which is to be expected.

The piezoelectric d_{33}-coefficient was measured with a Pennebaker Piezo-Tester (Model 8000) and the results are also given in Table 1. Now the piezoelectric d- and g-coefficients are related thus,

$$\frac{d}{g} = \varepsilon_o \varepsilon_r \tag{5}$$

where ε_o is the free space permittivity. The g- coefficient values were calculated using

the measured values of ε_r, d- coefficient and eqn 5, and are given in Table 1. Furthermore, the piezoelectric figure of merit, FOM, is given by,

$$\text{FOM } (m^2/N = Pa^{-1}) = d_{33}\, g_{33} = \frac{d_{33}}{\varepsilon_o\, \varepsilon_r} = g^2\, \varepsilon_o\, \varepsilon_r \qquad (6)$$

The FOM values are given in Table 1 from which it may be observed that the ceramic polymer composites are superior to ceramics for piezoelectric transducers in the receiver mode of operation. The ceramics with high ε_r values, on the other hand are desirable for piezoelectric transducers for application in the transmitter mode of operation. In general, a piezoelectric material with a high d- coefficient, tends to have a low g- coefficient so that the d_s- product is of compensating nature.

An important parameter of a piezoelectric material is the electromechanical coupling factor k which is a measure of the efficiency of mechanical, or electrical, to electrical, or mechanical, energy conversion. This physical quantity is a tensor so that its magnitude depends on the direction of the stress and electric fields. The electromechanical coupling factor in the thickness direction is denoted by k_t and is an important parameter in the design of hydrophones and other piezoelectric detectors.

A piezoelectric sensor may be represented by an electrical equivalent circuit that may resonate at a frequency f_o. The k_t value may be determined from a measurement of the real and imaginary parts of the complex impedance of a piezoelectric sample standing free in air in the frequency range around f_o [9]. It may be shown [8-12] that,

$$k_t^2 = \frac{\pi}{4}\omega_o\, C_s\, A \sqrt{(\psi^2 + 4)}\, \tanh\left(\frac{\pi}{4}\psi\right) \qquad (7)$$

where $\omega_o = 2\pi f_o$, C_s the sample capacitance, A the maximum value of the real part of the impedance at resonance and ψ the mechanical loss ($= Q_m^{-1}$), where Q_m is the mechanical quality factor. A network analyzer, Model HP8702A was used to measure the real and imaginary parts of the complex impedance in the frequency range of $10^6 - 10^7 Hz$. Figure 1 shows the typical behavior of the real and imaginary parts of the complex impedance of a PTCa/Epoxy film with a composition of 50/50 vol% from which it may be observed that A = 19.15 *ohms*, measured from the base line. $f_o = 1.34 \times 10^7$ *Hz* and $\psi = 0.09$. The calculated value of k_t for this composite is 0.15. The k_t values of PTCa and the composites are given in Table 1.

It may be shown that [8],

$$\frac{dg}{S} = k_t^2 \qquad (8)$$

where S is the compliance which has the same dimension as that of the dg- product. The compliance of a material does not change appreciably with frequency and it may thus be argued that k_t^2 is also a measure of a piezoelectric sensor. The acoustic velocity V_s in a medium is given by,

$$V_s = 2lf_o \qquad (9)$$

where l is the sample thickness. With the knowledge of f_o (Fig. 1) the magnitude of the acoustic velocity was calculated. Using this value of V_s the magnitude of the acoustic

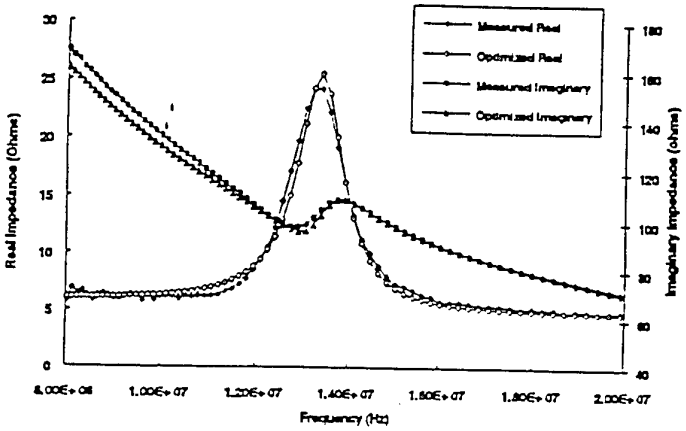

Figure 1. Real and Imaginary part of measured and optimized impedances of PTCa/Epoxy 50:50 vol%

impedance Z_t was determined. The values of V_t and acoustic impedance Z_a for PTCa and the composites are also given in Table 1. It should be noted that the overall synergy effects of ε-, d- and g- coefficients, k_t and V_t values are complex because of their frequency dependence in an active piezoelectric material and care should be exercised in the choice of intelligent materials in order to obtain an optimum performance [8].

6. NONDESTRUCTIVE MONITORING OF COMPOSITE LAMINATES

One of the objectives of this effort is to employ the ceramic/polymer ferroelectric materials as multipurpose intelligent sensors for the nondestructive monitoring of fiber reinforced composites. The monitoring function will be enhanced when the sensors are incorporated within the composite laminate. In that respect, the resulting structure becomes an integrated smart system with sensing as well as health monitoring capabilities. The composition of the piezoelectric composites can be varied to achieve the desired coupling between the mechanical and electrical fields and also match the matrix phase of the fiber reinforced composite. Composite sensors have been embedded in glass/epoxy laminates to study their cyclic load and acoustic emission monitoring capabilities. In this section some data obtained from the composite sensors will be presented and some initial results and conclusions will be outlined.

7. DYNAMIC RESPONSE

Both epoxy and copolymer based ceramic/polymer sensors were utilized to monitor the response of quasi-isotropic S2-glass/epoxy laminates to cyclic loading. The laminate was subjected to a tensile sinusoidal load of 700 lbs in amplitude at a frequency of 2 *Hz*. Typical responses from the PTCa/P(VDF-TrFe) and PTCa/Epoxy sensors are shown at Figs 2 and 3 respectively. The signals produced from the composite sensors have amplitudes of ~2 *mV* and ~7 *mV*, for the epoxy and copolymer composite respectively, which are sufficient for monitoring with conventional equipment. These preliminary results indicate that the composite sensors could be utilized as spectrum or transient load monitoring devices.

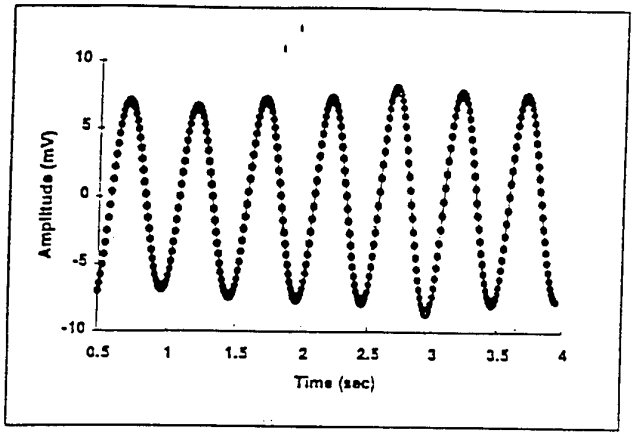

Figure 2. Response of PTCa/P(VDF-TrFe) 65:35 vol% to sinusoidal load (2 *Hz*)

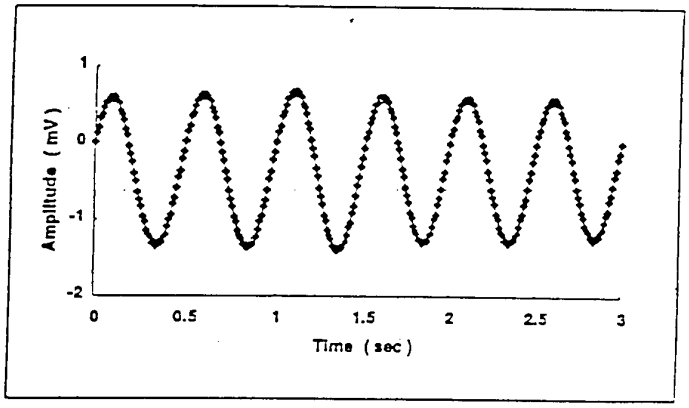

Figure 3. Response of PTCa/Epoxy 50:50 vol% to sinusoidal load (2 *Hz*)

8. ACOUSTIC EMISSION

Acoustic emission (AE) can be defined as the transient elastic waves generated in materials by the release of energy due to changes in the localized stress and strain fields. Such acoustic emission events can be initiated in fiber reinforced composites by damage mechanisms such as matrix cracking and fiber breakage [13]. Acoustic emission transducers have been constructed by using the composite thin films as sensors. These transducers were utilized with a conventional, commercial AE system and were compared to commercial acoustic emission transducers. Acoustic emission signals in composite materials during tensile testing were monitored and their AE parameters identified. Results showed that these prototype sensors could be used with commercial

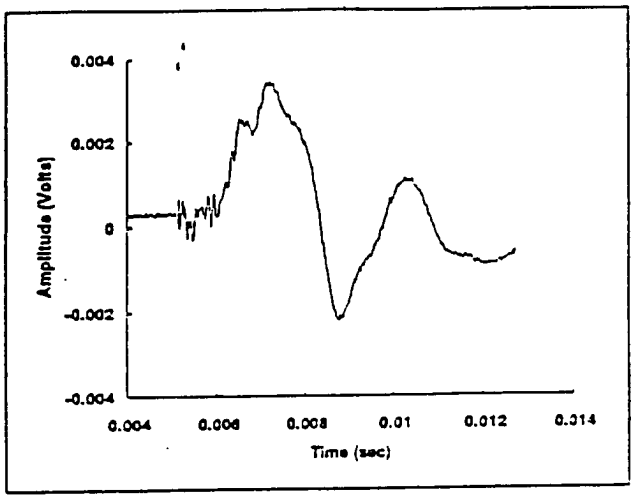

Figure 4. Response of PTCa/P(VDF-TrFE) 65:35 vol% sensor to lead break on the surface of a thin glass/epoxy plate

AE systems, especially when higher amplitude signals are of interest [8].
It has been suggested that plate waves can be used to detect and quantify damage in composite plate like structures [13,14]. The prototype composite transducers have been also used to capture plate waves generated by lead breaks (Hsu-Nielsen source). Results showed that the composite sensors have broad bandwidth characteristics and high sensitivity [8]. In this paper we report on the feasibility of embedded composite sensors to monitor acoustic emission events in composite laminates. Composite sensors of PTCa/P(VDF-TrFe) with a ceramic volume fraction of 65%, were embedded in a glass/epoxy $[0_2/90]_s$ laminate. The poled composite films, with thickness of ~130 μm, were embedded in between the plies. Pencil lead breaks on the surface of the thin glass/epoxy plates, 8 *cm* away from the sensor, were used to generate simulated acoustic emission signals. It has been shown [15] that these types of AE signals propagate as extensional and flexural plate modes. A typical response of the embedded sensor to the lead break is shown in Fig. 4. Both the extensional and flexural wave modes can be identified in this figure. However, the extensional mode is quite small and electronic noise is evident on the signal. Further work is in progress to better characterize the embedded ceramic/polymer films as acoustic emission sensors. It seems, however, that the embedded sensors are capable of characterizing plate waves and as such can be utilized for detecting such waves generated by AE events in plate like structures.

REFERENCES

1. J.F. Campbell, E.G. Vanderheiden, L.A. Martinez, D.S. Cairns, M.G. Abdallah, *J. of Composite Materials*, **26** (3), 334 (1992).
2. E. Egusa, N. Iwasawa, *Proc. 2nd Int. Conf. on Intelligent Materials* (ICIM'94), 486 (1994).
3. W. Wersing, K. Lubitz, J. Mohaupt, *IEEE Ultrason. Ferroelec. Freq. Contr.* **36**, 424 (1989).
4. H. Jaffe, *IEEE Trans. Electron. Devices*, **ED-16**, 557 (1968).
5. Y. Yamashita, K. Yokoyama, H. Honda, T.Takahashi, *Jap. J. Appl. Phys.*, **20** (suppl.

4), 183 (1981).
6. R.E. Newnham, D.P. Skinner, L.E. Cross, *Mat. Res. Bul.*, **13**, 525 (1978).
7. G. Sa-Gong, A. Safari, R.E. Newnham, *Proc. IEEE 6th Int. Symp. on Applied Ferroelectrics* (ISAF 86), 281 (1986).
8. C. Dias, M. Wenger, P. Blanas, R.J. Shuford, Y. Hinton, D.K. Das-Gupta, *Proc. 2nd Int. Conf. on Intelligent Materials* (ICIM'94), 437 (1994).
9. H. Ohigashi, Ultrasonic Transducers in the Megahertz Range, *The Application of Ferroelectric Polymers*, ed. T.T. Wang, Blakie, Glaskow, 237
10. L.N. Bui, H.J. Haw, *IEEE Trans. Sonics Ultrasonics*, SU24, 331 (1977).
11. M. Plate, *Ferroelectrics*, **115**, 229 (1991).
12. C. Dias, D.K. Das-Gupta, Y. Hinton, R.J. Shuford, *Sensors and Actuators A*, **37-38**, 343 (1993).
13. M.R. Gorman, S.M. Ziola, *Ultrasonics*, **29**, 245 (1991).
14. M.R. Gorman, W.H. Prosser, *J. of Acoustic Emission*, **9** (4), 283 (1990).
15. M.R. Gorman, *J. Acoust. Soc. Am.*, **90** (1), 358 (1991).

Ferroelectrics, 1996, Vol. 187, pp. 75-86
Reprints available directly from the publisher
Photocopying permitted by license only

FERROELECTRIC CERAMIC/POLYMER COMPOSITES AND THEIR APPLICATIONS

M.P. WENGER, P. BLANAS†, C.J. DIAS*, R.J. SHUFORD† & D.K. DAS-GUPTA

School of Electronic Engineering and Computer Systems, University of Wales, Bangor, Dean Street, Bangor, Gwynedd, LL57 1UT, U.K. †U.S. Army Research Laboratory, Materials Directorate, Arsenal Street, Watertown, MA 02172-0001, USA *Now at Universidade Nova de Lisboa, Faculdade de Ciências e Tecnolgia / Secção de Física Aplicada, Torre, 2825 Monte de Caparica, Portugal

(Received August 31, 1995)

Abstract Thin composite films of calcium modified lead titanate (PTCa)/copolymer of vinylidene fluoride-trifluoroethylene P(VDF-TrFE) and PTCa/Epoxy have been produced and their piezoelectric d_{33}- and electromechanical coupling coefficient k_t, have been measured. These composite sensors have been used to monitor strain induced in a glass/epoxy laminate produced by cyclic loading. PTCa/P(VDF-TrFE) was embedded in a laminate structure to detect acoustic emission (AE) signals generated on the surface of the laminate by a conventional lead-break technique. The results show that the composite sensor is able to detect AE signals over a wide bandwidth.

INTRODUCTION

The principal objective in the design of ferroelectric ceramic/polymer composites, which could provide both sensing and actuating functions for intelligent structural systems, is to achieve optimum mechanical, electroactive (i.e., piezoelectric and pyroelectric) and thermal properties together with appropriate coupling between these properties. The desired properties of the composite sensor material are achieved by an appropriate choice of the two constituent components, (viz., electroceramic and polymer), their relative amounts and connectivity[1,2]. By introducing a ferroelectric ceramic into a polymer

matrix, the compliance of the compósite material increases in comparison with that of the ceramic alone and thus the acoustic impedance decreases to a value which depends on the ceramic loading. However, the mechanical losses increase resulting in an attenuation of transverse mode propagation. As a consequence, the hydrostatic piezoelectric coefficient can be tailored depending on the ceramic content. The concept of connectivity [1,2] is that each phase in a mixture may be self connected in zero, one, two or three directions. Hence, ceramic particles, randomly dispersed and separated from each other will have a connectivity of zero while the host polymer surrounding them has a connectivity of three. Such a composite material has 0-3 connectivity. Similarly, a composite material consisting of arrays of ceramic rods extending between the major surfaces of a polymer block will have 1-3 connectivity.

The present work reports the results of characterization of piezoelectric and other related properties of two different composite materials of 0-3 connectivity which were prepared by dispersing fine grains of ferroelectric calcium modified lead titanate (PTCa) ceramic in the matrices of (i) thermoplastic and ferroelectric copolymer of vinylidene fluoride-trifluoroethylene P(VDF-TrFE) and (ii) thermosetting epoxy. Both types of composite films were used to detect tensile cyclic loading of a laminate structure. The ability of these materials to detect acoustic emission signals is investigated and the results of these studies are also reported in this paper.

EXPERIMENTAL

The chemical composition of the PTCa, which was kindly provided by GEC-Marconi (UK) is

$$Pb_{0.76}Ca_{0.24}\left[(C0_{0.5}W_{0.5})_{0.04}Ti_{0.96}\right]0_3 + Mn0_2$$

Its Curie temperature T_C is 260°C and the grain size was in the range 10-60μm. The copolymer P(VDF-TrFE) with a composition of 75:25 mol% was obtained from Piezotech. The epoxy resin was Epikote 828 (Shell) and the curing agent K61B was obtained from Anchor Chemicals. Thin films (>60μm) of PTCa/P(VDF-TrFE) were prepared by a hot-rolling and high pressure casting technique, described in our earlier work[3-5] and will not be described further here. PTCa/Epikote films were prepared by manual mixing followed by high pressure casting and curing at 60°C[6]. The minimum thickness and the maximum area of the composite films prepared in this work are 60μm

and 10cm x 10cm respectively. The ceramic loading for each of the two types of composite films was varied in the range of 20-65 vol%. Scanning electron microscopy (SEM) was employed to study the morphology of these films. An aluminium electrode of 1cm in diameter and 1000°A in thickness was vacuum deposited on each surface of a film. The electroded samples were subsequently poled by a dc field in the range 1-2.5 x 10^7 Vm^{-1} in a silicone oil bath at 100°C for 30 minutes and cooled down to room temperature before the field was removed.

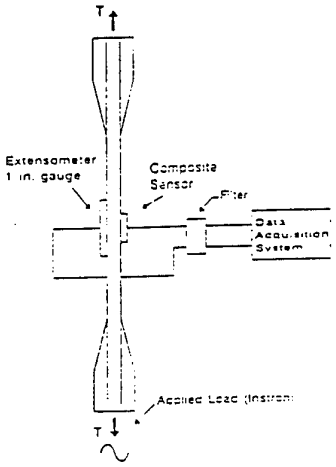

FIGURE 1 Setup for strain monitoring experiments.

The piezoelectric d_{33}- coefficients of the poled films were measured at room temperature using a Pennebaker Model 8000 instrument which is supplied with calibrated lead metaniobate ceramics which allow repeatable measurements up to a d_{33}- value of 1200 x $10^{-12}CN^{-1}$. The electromechanical coupling coefficient k_t was determined from the measurement of the real and imaginary parts of the complex electrical impedance by a Network analyser (Model HP8702A) around the fundamental resonant frequency f_0, of the samples in the frequency range of 10^5Hz - 5.0 x 10^7 Hz.

The strain induced in a S2-glass/epoxy $(0_2/45_2/-45_2/90)_s$[1] laminate by a cyclic loading was monitored using composite films of PTCa/P(VDF-TrFE) and PTCa/Epoxy and the results compared with that from an extensometer (see figure 1). The test was set to run at 2Hz on an Instron testing machine (Model 1331). The specimens were ramped

[1] The notation $(X_1y_1/X_2y_2/\text{etc.})_S$ describing the lay-up of glass reinforced epoxy laminates indicates the direction of the glass fibre by the X value and the number of subsequent layers by the y value. The symmetry of the system is then given by the value of S.

to a mean load of 455 kg and immediately cycled using a sinusoidal load of 318kg amplitude at a frequency of 2Hz. Each test was run for a total of 30 cycles. The feasibility of the PTCa/P(VDF-TrFE), 65/35 vol% composition as an acoustic emission detector has also been studied by embedding it between two 0° piles of a glass laminate structure $(0_2/90)_S$ of area 20cm^2 (see figure 2). The source was located at a distance of 8.5cm from the embedded sensor. A commercially available transducer (PAC R15) was located on the surface of the laminate plate at the same distance from the AE source. A 2H pencil lead of diameter 0.5mm protruding 6.7mm from a convex plastic receptacle was used to generate the AE signal by breaking it against the surface of the laminate. A digital storage oscilloscope (Gould 4050) was used to monitor the detected AE response.

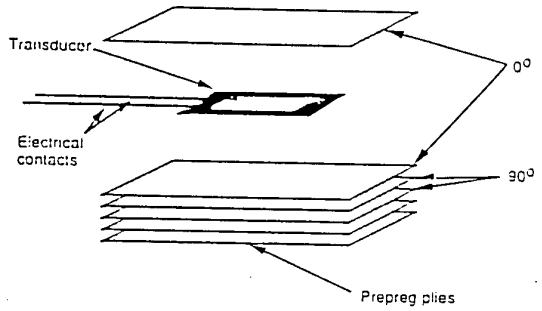

FIGURE 2 Exploded view of a laminate structure containing a composite transducer.

RESULTS AND DISCUSSION

A great deal of versatility in the properties of ferroelectric ceramics is obtained by introducing suitable dopants to manipulate the relative dielectric constant ε_r, the Curie temperature Tc, and the saturation polarisation Ps. Lead titanate (PT) has a tetragonal - Perovskite structure with lead at the A-site. Its ε_r and Ps values at room temperature[7] are ~ 300 and 0.6 Cm^{-2} respectively. Its Tc is ~ 490°C and it has no major transitions at lower temperatures. Due to its structure, a considerable internal stress is induced during the phase transition which tends to fracture the ceramic[8]. By doping PT appropriately with calcium oxide (CaO), the sinterability of the ceramic improves [9]. A doping of 24 mol% of Ca together with a modification of B-Site with Ni-Nb, Fe-W or Co-W provides an optimum electrochemical anisotropy[7] with an ε_r- value of ~200. The modified PTCa, employed in this work, contains this mol% of Ca together with Co-W doping. Although the composite films were fabricated with ceramic loading in the range of 20 vol% to a

maximum of 65 vol% and characterised, the best piezoelectric responses were observed with 65/35 vol% for PTCa/P(VDF-TrFE) and 60/40 vol% for PTCa/Epoxy sensors and only their dielectric and piezoelectric properties are reported here.

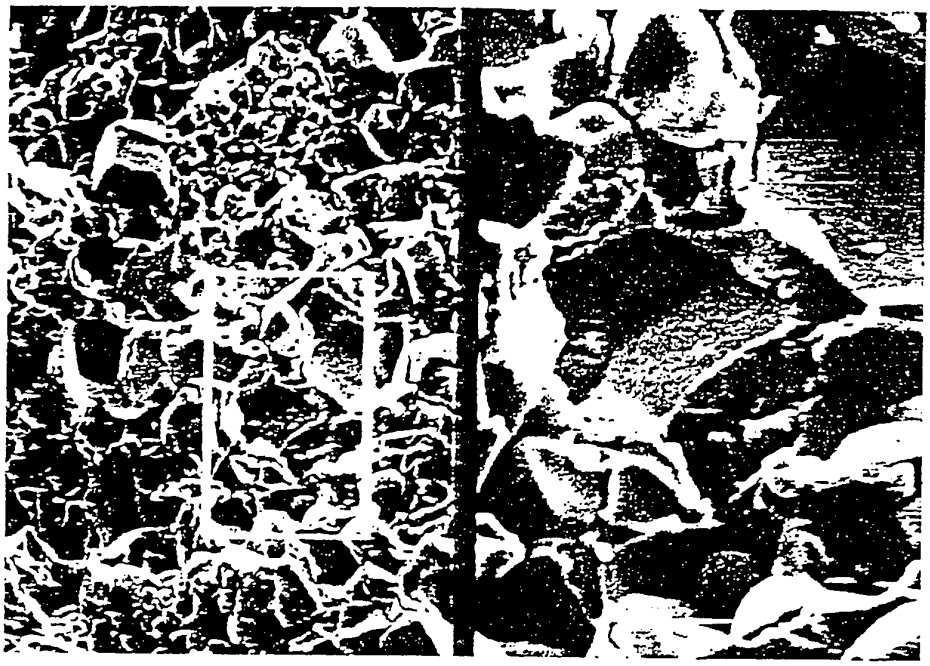

FIGURE 3 Morphology of PTCa/Epoxy composite (60/40 vol%). Film thickness 228μm. Magnifications x2640 and x7920.

Figure 3 shoes a typical SEM micrograph of PTCa/Epoxy (60/40 vol%) film of thickness 228μm. The left half of the figure was taken at a magnification of X2640 whereas the right half is the micrograph of the white bordered in-set section but with a magnification of X7920. Similar micrographs were also taken from both types of the composites fabricated with different loading (vol%) of the ceramic powder showing that with low volume fractions, most of the ceramic particles are separated from each other by polymer layers, indicating a good 0-3 connectivity. However, with increasing volume fraction and particularly with large particle sizes of the ceramic, the connectivity between the ceramic grains increases, smaller grains clustering between the larger grains, which thus brings about a presence of 1-3 connectivity in addition. This is not detrimental as such because its presence provides an enhanced piezoelectric response[10]. Voids and

defects were not observed provided the pressing operation was performed correctly. Figure 3 also shows that there was a wide distribution of the ceramic grain size. The piezoelectric voltage coefficient g(V-mN^{-1}) was determined from a knowledge of the measured values of piezoelectric charge coefficient d (CN^{-1}) and the relative permittivity using the expression,

$$\frac{d}{g} = \varepsilon_0 \varepsilon_r \qquad ...(1)$$

The piezoelectric figure of merit (FOM) was determined from,

$$FOM(m^2N^{-1} = Pa^{-1}) = d_{33}g_{33} = \frac{d_{33}}{\varepsilon_0 \varepsilon_r} = g^2 \varepsilon_0 \varepsilon_r \qquad ...(2)$$

The measured values of ε_r and d_{33} and the calculated values of g_{33} together with the FOM- values of PTCa, PTCa/P(VDF-TrFE), 65/35 vol% and PTCa/Epoxy, 60/40% are given in Table 1 from which it may be observed that the latter composite has the highest (FOM)- value. For receiver applications, a high g- value is desirable although in general, a material with a high g value tends to have a low d value depending on it's permittivity.

A piezoelectric sensor may be represented by an equivalent circuit of a free resonator at its resonance frequency f_0[11].

It may be shown[10-13] that the real (i.e. Re[Z(ω)]) and imaginary (i.e. Im[Z(ω)]) parts of the frequency dependent total complex impedance are given by

$$\mathrm{Re}[Z(\omega)] = \frac{\beta}{(\beta+1)\omega C} + A\left(\frac{\omega_o}{\omega}\right)^2 \frac{\tanh\left(\frac{\pi\psi}{4}\right)\left[\psi \sin\left(\frac{\pi\omega}{\omega_o}\right) + 2\sinh\left(\frac{\pi\psi\omega}{2\omega_o}\right)\right]}{\sqrt{(\psi^2+4)}\left[\cos\left(\frac{\pi\omega}{\omega_o}\right) + \cosh\left(\frac{\pi\psi\omega}{2\omega_o}\right)\right]} \qquad ...(3)$$

$$\mathrm{Im}[Z(\omega)] = \frac{-1}{(\beta+1)\omega C} + A\left(\frac{\omega_o}{\omega}\right)^2 \frac{\tanh\left(\frac{\pi\psi}{4}\right)\left[2\sin\left(\frac{\pi\omega}{\omega_o}\right) - \psi \sinh\left(\frac{\pi\psi\omega}{2\omega_o}\right)\right]}{\sqrt{\psi^2+4}\left[\cos\left(\frac{\pi\omega}{\omega_o}\right) + \cosh\left(\frac{\pi\psi\omega}{2\omega_o}\right)\right]} \qquad ...(4)$$

where β is the dielectric loss tangent (i.e. $\tan\delta_e$), $\omega_o = 2\pi f_o$, C the capacitance, A the maximum value of the real part of the acoustic impedance at resonance and ψ the mechanical loss (i.e. $\tan\delta_m = Q_m^{-1}$, Q_m being the mechanical quality factor). The magnitude of ψ is given by the full width at the half height of the maximum value of $Re[Z(\omega_o)]$. This method requires the determination ω_o, A and ψ which gives the best fit to the impedance curves. The relationship between these parameters and k_t is,

$$k_t^2 = \frac{\pi}{4}\omega_o CA\sqrt{(\psi^2+4)}\tanh\left(\frac{\pi}{4}\psi\right) \qquad ...(5)$$

The values of f_o, A and ψ can be determined from a plot of the real part of the measured electrical impedance against the frequency, the magnitude of ψ being given by the full width at half height of the resonance curve. The value of k_t with Q_m was thus determined in this work and are given in Table 1 for the two composites and PTCa. Figure 4 shows a typical complex impedance/frequency plot of PTCa/Epoxy, 60/40 vol% composite with A = 584.94 Ohms, $f_o = 3.57 \times 10^6$Hz, $\psi = 0.057$ and $k_t = 0.21$. It should be noted that the value of k_t^2, which is always less than 1, does not represent the absolute efficiency of a transducer but the ratio of useful converted power to the input power. The efficiency may be lower than k_t^2 at lower frequencies and higher than k_t^2 at resonance. However, k_t^2 is proportional to the dg- product if the compliance of a material does not change significantly with frequency as in the case of a ceramic. For such cases k_t^2- value may also represent a figure of merit criterion.

In a 0-3 composite with a wide distribution of ceramic grain size, as in the present case, the particles will resonate at slightly different frequencies and as a result the mechanical quality factor will be reduced. This has been observed, particularly with PTCa/P(VDF-TrFE) composite (see Table 1), in the present work. It should be noted that the overall synergy effects of the ε, d and g coefficients, k_t and v_s values are complex because of their frequency dependence in an active piezoelectric material. Care should be exercised in the choice of materials in order to obtain an optimum performance[14].

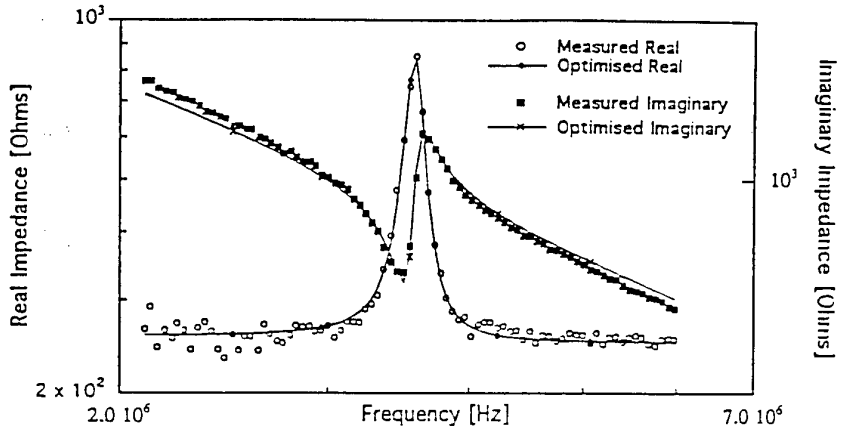

FIGURE 4 Real and imaginary part of measured and calculated impedance of 60/40 vol% PTCa/epoxy composite thin film.

The measured values of d_{33}- coefficient, ε_r and k_t of the composites agree well with the mixed connectivity model[10] which is an extension of the modified 'Cube' model due to Banno[15,16]. It should be noted that PTCa/Epoxy composites have been extensively studied by other workers[17-20] who have reported of the dependence of the piezoelectric activity on the grain size of the ceramic particles. It has been observed that similar to the PZT composite case, a higher grain size to thickness ratio was beneficial to the piezoelectric properties[21]. Furthermore, piezoelectric properties may also depend on the alignment of the long axis of the nonspherical grains along the perpendicular direction to the composite film surface[22,23].

The resonance frequency f_o, of a freely resonating piezoelectric material is given by,

$$f_o = v_s/2l \qquad ...(6)$$

where v_s is the velocity of sound in the material at f_o and l the thickness of the material. From a knowledge of f_o, obtained from the impedance measurement for the determination of k_t, v_s was calculated and the acoustic impedance $Z_a(=\rho v_s)$ was determined, ρ being the density of the material. The composite density ρ, is given by,

$$\rho = \phi\rho_c + (1-\phi)\rho_p \qquad ...(7)$$

where ϕ is the volume fraction of the ceramic and the subscripts c and p refer to the ceramic and the polymer respectively. The values of v_s and Z_a are also given in Table 1 for PTCa, PTCa/P(VDF-TrFE), 65/35 vol% and PTCa/Epoxy, 60/40% composites. It may be observed that the values of v_s and Z_a and $d_{33}g_{33}$ for the PTCa/Epoxy composite would make if it an attractive sensor material for ultrasound applications in comparison with PTCa.

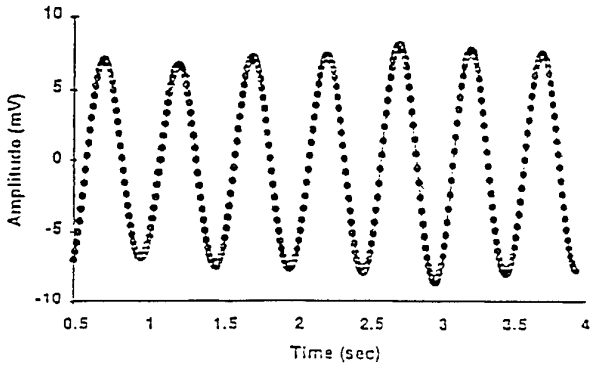

FIGURE 5 Response of PTCa/P(VDF-TrFE) 65/35 vol% to sinusoidal load (2Hz).

Figure 5 shows a typical response of PTCa/P(VDF-TrFE) 65/35 vol%, sensors for the tensile load tests and similar results were also observed for the PTCa/Epoxy composite sensors[14], the signal amplitudes being ~7mV and 2mV respectively for the two cases. These signals are comparable to that of an extensometer which was also mounted simultaneously on the specimen under test with each of the composite sensors. These preliminary results indicate that the composite sensors are suitable for transient load monitoring devices.

One of the objectives of this effort is to employ ceramic/polymer sensors as multipurpose intelligent sensors for the non-destructive monitoring of fibre reinforced composite. The monitoring function will be reinforced when the sensors are incorporated within the composite laminate. In this respect the resulting structure becomes an integrated smart system. Figure 6 shows the response of a PTCa/P(VDF-TrFE) sensor embedded into a test piece of glass fibre reinforced epoxy plate to an acoustic emission

signal generated by a lead break on the surface of the test plate at a distance of 8.5cm away from the composite sensor. This technique of generating AE signals is commonly

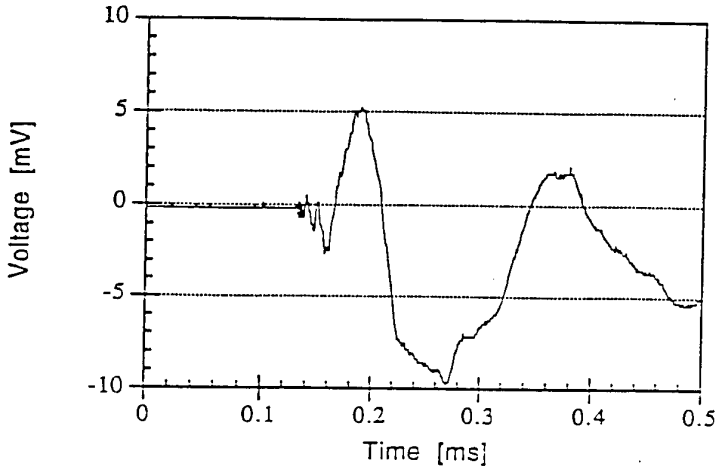

FIGURE 6 Response of an embedded ceramic/copolymer composite transducer to a lead break on the surface of the epoxy plate a distance of 8.5cm from the transducer.

used to provide repeatable stress waves in a structure and it closely approximates an impulse load[24]. It has been suggested that plate waves may be used to detect and quantify damage in composite plate like structure[25-26] and it has been shown that AE signals propagate as extensional and flexural plate modes[27]. Both the extensional and flexural modes can be identified in figure 6 which shows the output of the composite embedded sensor directly recorded on a digital oscilloscope at a sampling rate of 20MHz. The extensional modes have higher velocities than the flexural modes, which have frequencies predominantly above 300kHz as compared with those of the flexural modes with frequencies less than 300kHz. The higher frequencies of the extensional mode suffer from greater attenuation than those of the flexural mode. The response, shown in figure 4 agrees with the above observation, the frequencies of the flexural and extensional modes in the present case being 120kHz and 660kHz respectively. This ability to discern the differences in frequency from mode to mode exhibits the wideband nature of the composite sensor. Further work is in progress to improve the ability of the embedded bimorph sensor to detect plate waves in composite structure and to fabricate transducers with composite sensors and front matching layer.

Poperty	PTCa	PTCa/P(VDF-TrFE) 65/35 vol%	PTCa/Epoxy 60/40 vol%
Density, ρ (kg/m^3)	6890	5130	4600
Dielectric constant, ε_r (at 1kHz)	230	67	23
tan δ (at 1kHz)	0.006	0.013	0.010
Piezoelectric d_{33} coefficient (x10^{-12}C/N)	68	33	26
Electromechanical coupling factor, k_t	0.47	0.21	0.19
FOM: d_{33} x g_{33} (x10^{-12} Pa^{-1})	2.24	1.84	3.32
Mechanical Quality Factor, Q_m	80	4.3	21.7
Acoustic Impedance, Z_a (x10^6 Rayls)	29.6	16.5	11.0
Acoustic Velocity (m/s)	4300	3200	2418

TABLE 1 Piezoelectric and other relevant properties of PTCa and its composites with P(VDF-TrFE) and Epoxy.

ACKNOWLEDGMENT

This work is financially supported by a research grant (DAJA 45-93-C-0017) from the European Research Office of the US Army.

REFERENCES

1. R.E. Newnham, D.P. Skinner and L.E. Cross, Mat.Res.Bull., 13, 525 (1978)
2. D.P. Skinner, R.E. Newnham and L.E. Cross, Mat.Res.Bull, 13, 599 (1978)
3. C.J. Dias, D.K. Das-Gupta, Y. Hinton and R.J. Shuford, Sensors & Actuators A, 37-38, 343 (1993)
4. C.J. Dias and D.K. Das-Gupta, Ferroelectrics, 157, 405 (1994)
5. C.J. Dias, PhD Thesis, Ferroelectric Composites for Pyro & Piezoelectric Applications, (PhD Thesis, University of Wales, 1994)
6. M.P. Wenger, P. Blanas, R.J. Shuford and D.K. Das-Gupta, Second European Conference on Smart Structure & Materials, SPIE, 2361, 358 (1994)

7. W. Wersing, K. Lubitz and J. Mohaupt, IEEE Ultrason.Ferroele.Freq.Centr, 36, 424 (1989)
8. H. Jaffe, IEEE Trans.Electron Devices, ED-16, 557 (1968)
9. Y. Yamashita, K. Yokoyama, H. Honda and T. Takahashi, Jap.J.Appl.Phys, 20 (suppl.4), 183 (19891)
10. C.J. Dias and D.K. Das-Gupta, Ferroelectric Polymers & Ceramic-Polymer Composites, edited by D.K. Das-Gupta (Trans Tech Publications, Zurich, Switzerland 1994), Chapter 8, pp217-248
11. H. Ohigashi, The Application of Ferroelectric Polymers, edited by T.T. Wang (Blackie, Glasgow, U.K., 1988), Chapter 11, pp237-273
12. L.M. Bui and H.J. Shaw, IEEE Trans.Sonics Ultrasonics, SU-24, 331 (1977)
13. M. Plate, Ferroelectrics, 115, 229 (1991)
14. C. Dias, M. Wenger, P. Blanas, R.J. Shuford, Y. Hinton and D.K. Das-Gupta, Proc.Second Internat.Conf.on Intelligent Materials, ICIM '94, (Williamsburg, Virginia, USA), 437 (1994)
15. H. Banno, Jap J.Appl.Phys, 24 (Suppl.2), 445 (1985)
16. H. Banno, K. Ogura, H. Sobue and K. Ohya, Jap J.Appl.Phys., 26 (Suppl.1), 153 (1987)
17. J.A. Chilton, G.M. Garner, R.W. Whatmore and F.W. Ainger, Ferroelectrics, 109, 217 (1990)
18. J.A. Chilton, GEC Review, 6(3), 156 (1991)
19. G.M. Garner, N.M. Shorrocks, R.W. Whatmore, M.T. Goosey, P. Seth and F.W. Ainger, Ferroelectrics, 93, 169 (1989)
20. A.A. Shaulov, W.A. Smith and R. Ting, Ferroelectrics, 63, 177 (1989)
21. L. Pardo, J. Mendiola and C. Alemany, Ferroelectrics, 93, 183 (1989)
22. T. Yamada, T. Ueda and T. Kitayama, J.Appl.Phys., 53, 4328 (1982)
23. H.J. Lee and H-G Kim, J. Appl.Phys., 67, 2024 (1990)
24. ASTM Handbook of Sensors Standard Guide for Determining the Reproducibility of Acoustic Emission on Sensor Response. ASTM E976 03-03(1993)
25. M.R. Gorman and S.M. Ziola, Ultrasonics, 29, 245 (1991)
26. M.R. Gorman and W.H. Prossor, J.Acoust.Emission, 9, 283 (1990)
27. M.R. Gorman, J.Acoust.Soc.Am. 90, 358 (1991)

Acoustic Emission Signal Detection by Ceramic/Polymer Composite Piezoelectrets Embedded in Glass-Epoxy Laminates

M. P. WENGER, P. BLANAS,* R. J. SHUFORD,* *and* D. K. DAS-GUPTA

School of Electronic Engineering & Computer Systems
University of Wales, Bangor
Bangor, Gwynedd, LL57 1UT, U.K.

**U.S. Army Research Laboratory*
Materials Directorate
Aberdeen Proving Ground, Maryland 21005-5069

Piezoelectric composites, consisting of a ferroelectric ceramic powder of calcium-modified lead titanate dispersed in two different polymer matrices, viz. from vinylidene fluoride trifluoroethylene and an epoxy, have been fabricated. The composites show a mixed connectivity structure, and the results of electromechanical characterization are given. Thin films of these materials have been incorporated into surface mounted acoustic emission sensors and their frequency response and ability to detect plate waves, generated by a simulated acoustic emission source, has been examined. In situ transducers embedded into glass-reinforced laminate plates have also been examined and have been shown suitable for acoustic emission sensors.

INTRODUCTION

Intelligent (i.e. Smart) materials have the capability to respond to changes in their environment and actuate a desired response in an advantageous manner. Ferroelectric materials can convert mechanical and thermal energies into electrical signals (i.e. piezo- and pyroelectric effect). These materials can also exhibit the converse effects and hence can be regarded as intelligent materials. The conventional piezoelectric and pyroelectric sensors and actuators are ferroelectric ceramics, notably lead zirconate, lithium tantalate and lead niobate which offer high values of the piezoelectric charge (i.e. d-) coefficient, electromechanical coupling (k-) coefficient, pyroelectric (p-) coefficient, relative permittivity (ϵ_r) and low dielectric loss ($\tan\delta$). These advantageous properties have been exploited in diverse applications including underwater, biomedical and thermal imaging. However, these electroceramics have some disadvantages, such as high acoustic impedance, mechanical quality factor, low piezo- and pyroelectric figure of merit and a lack of mechanical flexibility. Ferroelectric polymers, viz., poly(vinylidene fluoride) (PVDF) and its copolymer, vinylidene fluoride trifluoroethylene P(VDF-TrFE), and ferroelectric ceramic/polymer composites have emerged as new electroactive and intelligent materials, which attempt to bridge some of the disadvantages of the electroceramics mentioned above (1–3). By introducing ferroelectric ceramic in a polar or nonpolar polym matrix, the compliance of the composite, compared the ceramic alone, increases and thus the acous impedance decreases to a value which depends on t ceramic loading. Also, because of the enhanced dam ing provided by the polymer matrix, the frequen dependent mechanical losses increase and the tran verse mode of the acoustic wave propagation is atte uated. As a consequence, the longitudinal piezoele tric coefficient, d_{31}, can be tailored.

Most materials designed to withstand high stre levels emit acoustic energy when stressed. Structur rearrangements at a molecular and/or atomic lev which occur within a material during deformati delamination, bond breaking and cracking produ elastic waves. An acoustic emission sensor detects t dynamic motion resulting from acoustic emission (A and converts the detected motion into a voltage-tim signal. Nondestructive evaluation (NDE) of materia using the AE method, employs the detection of t elastic waves generated by the rapid release of energ from localized sources within the material. AE differ from most other NDE methods in two significant way First, the energy detected is released from within t material under test, rather than being supplied exte nally. Second, the AE method is capable of detecti

the dynamic processes associated with the degradation of structural integrity. AE monitoring of fiber reinforced composite materials is an attractive method for the detection and location of fiber breakage, delamination and other types of structural degradation. Most commercially available AE sensors are used to detect the motion of the surface of the material at a point some distance from the source of emission.

Many structures tested using the AE method are plate-like in geometry, i.e., the thickness of the structure is much smaller than the other two dimensions. When considering only linearly elastic displacements away from the source, the propagating waves will be governed by Lamb's homogeneous equations (4), the solutions to which are known as Lamb waves. In the limit when the wavelength is much larger than the plate thickness, a simpler set of governing equations can be used to understand the motion. In this case the waves are called plate waves and are derived from classical plate theory. There are two dominant modes of propagation, the extensional and the flexural. The symmetrical extensional mode has the larger of its two displacement components in the plane of the plate, while the asymmetrical flexural mode has its larger component perpendicular to the plane of the plate. Both modes have components in the plane of the plate and perpendicular to the plate. Conventionally, the acoustic emission method detects the out of plane component as the transducers are usually situated on the surface of the material. Most commercially available AE transducers employ piezoelectric ceramics as sensors.

This work reports the results of a study of the dielectric, piezoelectric and pyroelectric properties of two different types of composite films that have been fabricated in our laboratory. The composite materials are calcium-modified lead titanate (PTCa) with a copolymer of vinylidenefluoride-trifluoroethylene, P(VDF-TrFE) in a 65/35 vol% and PTCa/epoxy with a 60/40 vol%. Both composites possessing 0-3 and 1-3 mixed connectivity (1, 5). Furthermore, surface mounted AE transducers have been fabricated from PTCa/P(VDF-TrFE) 65/35 vol% and PTCa/epoxy 60/40 vol% composites. The transducers have been comparatively evaluated to determine their frequency response over the frequency range 300 kHz to 50 MHz using a face-to-face technique previously used by other workers (6). The performance of the composite transducers have been compared to the performance of a commercially available AE sensor, (Panametrics V109-RM), in their ability to detect the modes of propagation of plate waves. Embedding of composite transducers in glass reinforced epoxy laminate plates has been achieved and the ability of these sensors to detect plate waves generated by a simulated acoustic emission source has been studied.

EXPERIMENTAL

A great deal of versatility in the properties of ferroelectric ceramics is obtained by introducing suitable dopants so that the Curie temperature T_c, the permittivity ϵ_r and the saturation polarisation P_s, can be manipulated. Lead titanate (PT) has a perovskite tetragonal structure with values of T_c, ϵ_r and P_s of 490°C, 250 and 0.6 C/m^3 respectively (7). Owing to its high tetragonal distortion, considerable internal stresses are induced during the phase transition, which fractures the ceramic (8). By doping PT with calcium oxide (CaO) appropriately, the sinterability of the ceramic improves (9). An optimum doping of 24 mol% of Ca together with a modification in the B-site with one of the following pairs Ni-Nb, Co-W or Fe-W provides an optimum electrochemical anisotropy (7) with an ϵ_r-value ~230. The modified PT employed in this work (GEC Marconi) contains this mol% of Ca together with Co-W doping. The electromechanical properties of PTCa/P(VDF-TrFE) composites have been investigated with respect to their ceramic volume content (10). It was found from these studies that a ceramic volume fraction of 65% produced the highest piezoelectric figure of merit. The PTCa/P(VDF-TrFE) composites in this study have thus been chosen with this ceramic volume fraction. As the ceramic is the only electroactive phase in the composites of PTCa/epoxy, a volume fraction of 60% was chosen, which was the maximum volume fraction obtainable. A volume fraction greater than this produced films of unacceptable electrical and mechanical properties.

The ceramic/copolymer composite PTCa/P(VDF-TrFE) was prepared by a hot-rolling technique (11, 12). The composition of the copolymer P(VDF-TrFE) was 73-27 mol%. Epikote 828 (Shell) epoxy resin and K61B (Anchor Chemicals) hardener were used to produce the host thermosetting polymer for the PTCa/epoxy composite (13).

An aluminum electrode of ~1000Å thickness was vacuum deposited on each surface of the composite films which were subsequently poled in a DC field of 1-2.5 × 10^7 V/m for 30 min at 100°C in an insulating silicone oil bath. The dielectric properties, the piezoelectric d_{33}- coefficient, the electromechanical coupling factor k_t, and the pyroelectric coefficient p, were then determined for these films (14). The dielectric properties were evaluated from the capacitance and the conductance measurements at 1 kHz and room temperature (RT) using a capacitance bridge (General Radio Model 1621). The pyroelectric coefficient of these composite films were determined using a direct method (15).

The surface mounted AE sensors were fabricated using the composite transducers. The poled composite material was cemented to a backing material by a thin layer of epoxy adhesive. The backing material was constructed from a tungsten powder dispersed in an epoxy matrix, so as to match the acoustic impedance of the composite film (16, 17). Electrical connections were made to the electroactive film by way of a live electrode running through the center of the backing material and to the earthed stainless steel casing (*Fig. 1*).

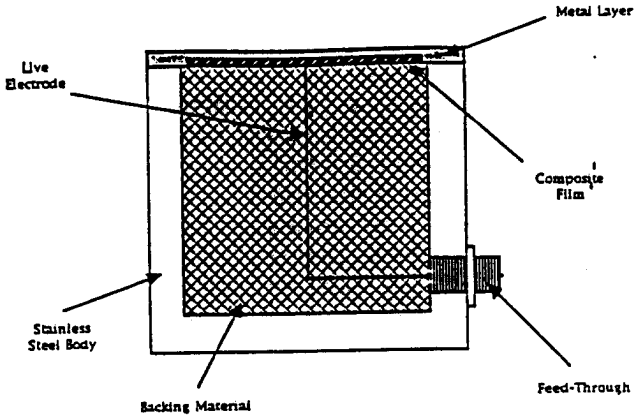

Fig. 1. Construction of a surface mounted AE transducer.

The frequency response of the surface mounted AE transducers were studied using a face to face method (6). The face of the transducer under test was acoustically coupled to the face of a driving transducer (Panametrics V109-RM) with known frequency response. The frequency response of the transducer under test was evaluated by deconvolution of the drive signal frequency spectrum, the driving transducer response and the detection electronics response.

One of the objectives of this work was to employ the ceramic/polymer films as multipurpose intelligent sensors for the nondestructive monitoring of acoustic emissions in fiber reinforced laminates. The ability of the composite transducers to detect plate waves in a glass/epoxy laminate plate was studied. The plates used measured 381 × 507 × 2.5 mm and were constructed so the fibers were all along one direction from layer to layer. Such a lay-up is known as a 0_{16} lay-up, i.e., the fiber direction was along the 0° direction with 16 layers. The source of the simulated acoustic emissions was produced by breaking a pencil lead on the surface of the plate. This method of generating acoustic emission sources is known as the Hsu-Nielsen method and requires the lead to be from a mechanical pencil (0.5 mm diameter lead, 2H) held within a Nielsen shoe [ASTM: E 976-84]. The plate was simply supported at its edges and the source to detector distance was 10 cm. The plate waves were detected in directions along the fiber axis (0°) and perpendicular to the fiber axis (90°). The output signals from the surface mounted transducers were recorded directly, or after preamplification by 40 or 60 dB, on a digital storage oscilloscope (Gould 4050) with a sampling rate of 5 MHz. Each mode of propagation was independently analyzed using fast Fourier transform (FFT) techniques to determine the frequencies present.

The nondestructive monitoring of fiber reinforced laminates will be enhanced when the sensors are incorporated within the laminates structures. In such a case the resulting structure becomes an integrated smart system which can perform both AE detection and health monitoring of the laminate structure. The poled composite sensors i.e., PTCa/P(VDF-TrFE) and PTCa/epoxy were embedded in between 0°–0° plies of glass-epoxy laminates with 0_{16} structure (*Fig. 2*). Embedded transducers, constructed from the piezoelectric composite films and of approximately the same dimensions as the surface mounted transducers, were used to detect plate waves within a laminate glass epoxy plate. Measurements were completed in the same way as for the surface mounted AE sensors. The dimensions of the plate were 304.8 × 304.8 mm with an average thickness of 1.9 mm. Two transducers have been embedded in the plate following the method described in previous work (14). These transducers were situated at positions of 152.4 mm along the length of the plate and 127 mm in from each side. One transducer was constructed from a PTCa/P(VDF-TrFE) 65/35 vol% composite, while the other was fabricated from a PTCa/epoxy 60/40 vol% composite material.

RESULTS AND DISCUSSION

The ceramic/polymer composites are a mixture of two components i.e. phases and the concept of connectivity (5) classifies different types of mixtures. In two phase composite each phase may be spatially self-connected in zero, one, two or three dimensions. The diphasic composite films, produced by dispersing randomly fine ceramic grains, as in the present case, are expected to have a 0-3 connectivity in which the ceramic grains are isolated from each other (0-dimensions) with the polymer phase, self-connected in 3-dimensions, around them. If the ceramics are well connected with each other in one direction, in the polymer matrix, the composite material will have 1-connectivity. The scanning electron microscopy of the composite films used in the present work, showed presence of both 0-3 and 1-3 pattern of mixed connectivity (14) which possibly originates from a wide distribution of the ceramic particle size, a high ceramic volume fraction and an agglomeration of the ceramic grains. It may be argued that the observed presence of mixed phase connectivity in our composite sensors is not detrimental as the piezo- and pyroelectric properties are enhanced (1). The mixed connectivity model is a two parameter model described by Dias and Das Gupta (1). The experimentally observed dielectric dat

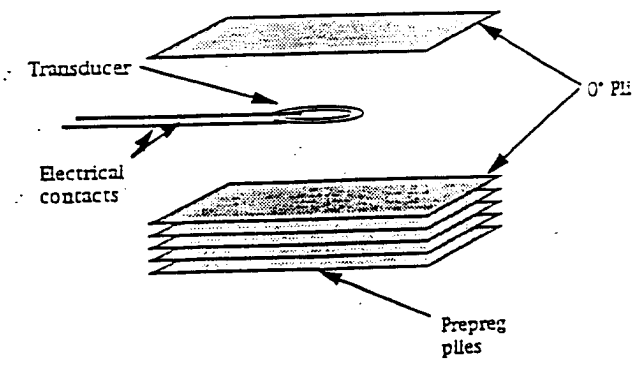

Fig. 2. Exploded view of a laminate structure containing composite transducer.

were fitted with this model to determine the magnitudes of the volume fractions of 1-3 and 0-3 connectivity. Within these composites films the typical amount of 1-3 connectivity is between 10 and 20 vol%.

Table 1 gives the measured values of permittivity, tanδ and the d_{33}- coefficient of the two compdsites PTCa/P(VDF-TrFE) and PTCa/epoxy (14) and of the ceramic PTCa. The values of the piezoelectric figure of merit, $(FOM)_{piezo}$, were calculated using the measured values of d_{33} and ϵ_r from

$$(FOM)_{piezo}\ (m^2N^{-1}) \equiv d_{33}g_{33} = \frac{d_{33}}{\epsilon_o\epsilon_r} = g_{33}^2\epsilon_o\epsilon_r \quad (1)$$

where ϵ_o is the permittivity of free space, g_{33} the piezoelectric voltage coefficient and ϵ_r the relative dielectric constant. These values are given in *Table 1* from which it may be observed that the ceramic/polymer composites can be superior to PTCa for piezoelectric transducers in the receiver mode of operation. The ceramics with high ϵ_r- values, on the other hand, are desirable for piezoelectric transducers for application in the transmitter mode of operation. In general, a piezoelectric material with a high value of d- coefficient, tends to have a low g- coefficient so that the dg product is of a compensating nature.

The values of k_t, the electromechanical coupling in the thickness mode, for these composite films were determined from measurements of the complex electrical impedance of a sample vibrating as a free resonator around the first resonance peak f_o (14). The k_t values and those of Q_m, the mechanical quality factor, of the composites and PTCa are also given in *Table 1*. The values of v_s and Z_o, the acoustic velocity and impedance respectively, were found from knowledge of the sample thickness and the resonant frequency f_o. It should be noted that the overall synergy effects of ϵ_r, d- and g- coefficients, k_t- and v_s values are complex because of their frequency dependence in an active piezoelectric material and care should be exercised in the choice of intelligent materials in order to obtain an optimum performance (18).

The pyroelectric coefficients p of the composites have been measured using a direct method (15). The values of p and $(FOM)_{pyro}$ for the two composites and PTCa are given in *Table 1*. The piezo- and pyroelectric coefficients, ϵ_r values and values of other parameters of PTCa, shown in *Table 1*, are from Dias (10). It may be observed from *Table 1* that the PTCa/P(VDF-TrFE) composite has the highest $(FOM)_{pyro}$ value and hence the best responsivity amongst these three materials. It may also be observed that the $(FOM)_{piezo}$ value of PTCa/epoxy is superior to those of the other two materials which would make it attractive for piezoelectric receiver applications. It may also be noted that a piezoelectric receiver should have low mechanical quality factor Q, which provides a wide bandwidth and reduced dielectric heating. In this respect PTCa/P(VDF-TrFE) appears to have an advantage over the other two materials. However, an ideal piezoelectric receiver should have a high k_t- value and the two composites appear to be significantly inferior to PTCa in this respect. The measured values of the relative permittivity ϵ_r, the piezoelectric d_{33}- and k_t- coefficients and the pyroelectric coefficient p agree with the respective theoretically calculated values using the mixed connectivity Cube model (1), which is a modification of a model by Banno (19). Using the mixed connectivity model (1), it has been shown that the $(FOM)_{pyro}$ is quite significantly dependent on the degree of poling of the series connectivity branch whilst the electromechanical coupling factor k_t is mostly dependent on the ceramics connected in parallel.

There are review papers published on the piezo- and pyroelectric properties of several ceramic/polymer composites with 0-3 connectivity and their applications ((20–24), and the references contained therein). Among these composites it appears that PTCa/P(VDF-TrFE) enjoy the highest k_t- value and the most reliable pyroelectric response. The $(FOM)_{piezo}$ for the PTCa/epoxy composite is also the highest for such composites and the observed magnitudes of its electroactive responses are in agreement with those of other workers (25–28). However, it should be stressed that ceramic/polymer composites with 1-3 connectivity will have superior piezo- and pyroelectric responses.

To evaluate the frequency response of the surface mounted AE sensors, constructed from the composite materials, the electrical signal produced from the out-

Table 1. Typical Piezoelectric, Pyroelectric and Other Relevant Properties of PTCa and Its Composites PTCa/P(VDF-TrFE) and PTCa/Epoxy.

Property	PTCa	PTCa/P(VDF-TrFE) 65/35 vol%	PTCa/Epoxy 60/40 vol%
Density (g/cm^3)	6.89	5.13	4.60
Relative Permittivity ϵ_r @ 1 kHz	230	67	23
tanδ @ 1 kHz, RT	0.006	0.013	0.010
d_{33} coefficient (pC/N)	68	33	26
d_{31} coefficient (pC/N)	−3.1	4.6	0.4
Electromechanical Coupling Factor, k_t	0.47	0.21	0.19
$(FOM)_{piezo}$:$d_{33} \times g_{33}$ ($\times 10^{-12}$ Pa^{-1})	2.24	1.84	3.32
Mechanical Quality Factor, Q_m	80	4.3	21.7
Acoustic Impedance, Z_o ($\times 10^6$ Rayls)	29.6	16.5	11.0
Acoustic Velocity, v_s (m/s)	4300	3200	2418
Pyroelectric Coefficient, p ($\times 10^{-6}$ C/m^{2}K) @ 30°C	380	130	30.1
$(FOM)_{pyro}$ ($\times 10^{-6}$/m^{2}K)	1.65	1.94	1.30

put of the transducer (TO) under evaluation can be considered to be a convolution of the electrical drive signal (EI), the output response of the driving transducer (DR), the input response of the sensing transducer (TR) and the response of the input and output electronics (DE). Assuming the coupling layer and impedance mismatch between the two transducers produce negligible losses of acoustic energy and the transducers behave in a reversible manner, then the output from the transducer is

$$TO = EI \otimes DR \otimes TR \otimes DE \quad (2)$$

Further assumptions are made that the detection electronics and the transducers behave in a linear fashion, with the response of the detection electronics being flat and equal to unity throughout the frequency range of interest. Then in the frequency domain the convolution becomes a straightforward product

$$TO(f) = EI(f) \times DR(f) \times TR(f) \quad (3)$$

To determine the frequency response of the driving transducer DR(f) two nominally identical transducers were used, one for the driving transducer and the other for the receiving transducer. Thus *Eq 3* becomes

$$TO(f) = EI(f) \times [DR(f)]^2 \quad (4)$$

giving the driving response from

$$DR(f) = \sqrt{\frac{TO(f)}{EI(f)}} \quad (5)$$

With knowledge of the output of the driving transducer then, the response of the transducer under test can be evaluated from

$$TR(f) = \frac{TO(f)}{EI(f) \times DR(f)} \quad (6)$$

and if the logarithmic responses are considered, the response in decibels is given by

$$\log(TR(f)) = \log(TO(f)) - \log(EI(f)) - \log(DR(f)) \quad (7)$$

The electrical driving signal was derived from the output of a network analyser [HP8702A] set at 18 dBm. The input to the driving transducer was essentially a constant power signal over the frequency range from 300 to 50 MHz. The frequency was increased in a stepwise manner with 400 points within the frequency range. The output from the transducer under test was fed into the input of channel two of the network analyzer and the logarithmic amplitude was recorded. The output of a V109-RM transducer was recorded after being driven by another similar V109-RM transducer. The driving response of these transducers were then found using *Eq 5*. The outputs and subsequently the deconvolved frequency responses of the composite transducers were then recorded and calculated.

Plate waves generated by AE sources propagate in two distinct modes, extensional and flexural. The extensional mode is a nondispersive mode of propagation with higher velocities and frequencies than the dispersive flexural mode. Because of this mismatch in mode velocities the signal produced, when a sensor detects an elastic plate wave originating from an acoustic emission, will comprise of two distinct components. The extensional mode, which has a higher velocity, will arrive at the sensor a time, depending on the distance from the source, before the flexural mode.

A broad bandwidth sensor should be able to detect the arrival of the extensional mode comprising of higher frequencies before the arrival of the flexural mode with its correspondingly lower frequencies. There are a number of factors affecting the form of the acoustic signals produced by lead breaks. The relative amplitudes of the two modes depend greatly on the orientation of the lead break. Gorman (29) has shown that a lead broken on the surface of the plate will result in an acoustic signal with a high amplitude flexural mode and smaller amplitude extensional mode. While lead breaks conducted on surfaces at varying angles to the plate surface will produce greater extensional mode amplitudes and lesser flexural mode amplitudes, the highest extensional/flexural amplitude ratio being when the lead is broken on the edge of the plate. Also within a 0_x laminate the anisotropy resulting from the unidirectional nature of the fibers has an effect on the overall form of the acoustic signal. The acoustic velocities of both modes are proportional to the direction of propagation within the laminate plate. This results in a separation in time of arrival between the two modes, which is dependent on the angle, with respect to the fiber axis, of the direction of propagation. Owing to the absorbent nature of the epoxy matrix of the laminate the acoustic waves are attenuated rapidly with distance, the higher frequency extensional modes being attenuated more rapidly than the flexural modes.

The frequencies encountered within plate waves are predominantly <1 MHz. The commercially available transducer used as a comparative standard in this work has a peak frequency of approximately 5 MHz whilst the composite transducers have peak frequencies in the range 5–12 MHz. It is believed that in the frequency range 0–1 MHz, which is far away from the peak frequency, the transducers will have a relatively flat frequency response. Typical frequency responses of the composite transducers compared to the comparative standard are shown in *Figs. 3* and *4*, their respective peak frequencies and bandwidths are shown in *Table 2*. The amplitude scales of *Figs. 3* and *4* refer to 1 mW into a 50 Ω load. The responses show the characteristic broad bandwidth nature of these transducers. The peak of the frequency response being centered on their respective resonant frequencies. A peak corresponding to the third harmonic resonance can also be seen in these figures. A good example of this can be seen in *Fig. 3* corresponding to the frequency response of a PTCa/P(VDF-TrFE) transducer. The peak frequency is ~8 MHz with the third harmonic occurring at ~24 MHz.

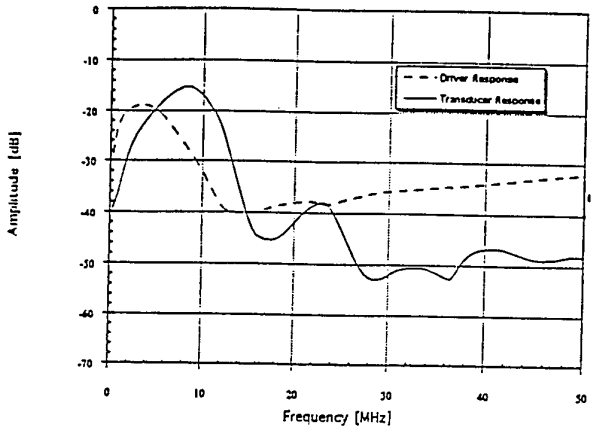

Fig. 3. Deconvoluted and smoothed frequency response of a PTCa/P(VDF-TrFE) 65/35 vol% surface mounted AE transducer.

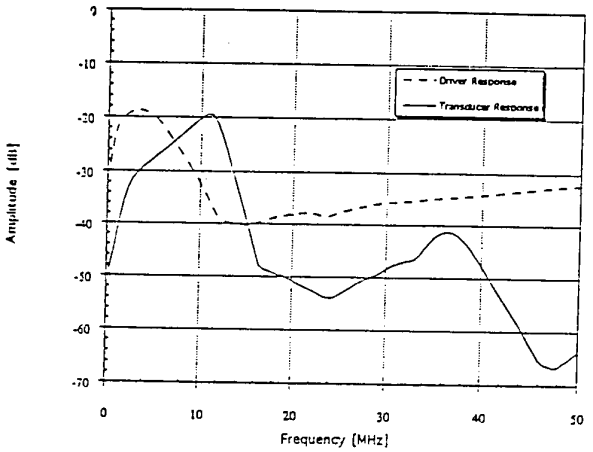

Fig. 4. Deconvoluted and smoothed frequency response of a PTCa/epoxy 60/40 vol% surface mounted AE transducer.

Table 2. Measured Peak Frequencies and Bandwidths of the Surface Mounted Transducers: f_o—Peak of Free Resonance, FF—Face to Face Method Peak Frequency, FFBW—Face to Face Bandwidth.

Transducer	f_o [MHz]	FF [MHz]	FFBW [MHz]
Panametrics V109-RM	—	3.29	4.98
PTCa/P(VDF-TrFE) 65/35 vol%	7.53	8.24	4.96
PTCa/epoxy 60/40 vol%	12.06	10.85	3.62

As can be seen from *Figs. 3* and *4* and from *Table 2*, the composite transducers performances are comparable with the performance of the commercially available AE transducer with respect to sensitivity and bandwidth. It is noted that the sensitivity of the PTCa/P(VDF-TrFE) composite transducer, at its peak is actually higher than the commercial transducer at its own respective peak. Both of the composite transducers, shown in the *Figures*, show enhanced sensitivity over the commercial transducer at their respective peak frequencies.

The detected signals from the surface mounted transducers, used to detect simulated AE in laminate plates, were recorded on a digital storage oscilloscope at a sampling rate of 5 MHz and analyzed using Fourier techniques to determine the frequencies present within the two modes of propagation. The results of these measurements can be seen in *Figs. 5–7*. The signals from the Panametrics transducer and the transducer made from PTCa/P(VDF-TrFE) composite materials have been recorded directly from the transducer without amplification. Preamplification of the signals from the PTCa/epoxy transducer was necessary for efficient observation of the signal. The preamplifier used [Physical Acoustics part no. 1220A] acted as a bandpass filter with bandpass between 20 and 1200 kHz with a gain of 40 or 60 dB.

From the signals it was seen that the composite transducers were able to detect lead breaks 10 cm away, in directions of 0° and 90° to the fibers, on the surface of the plate. Only the signals from the 0° di-

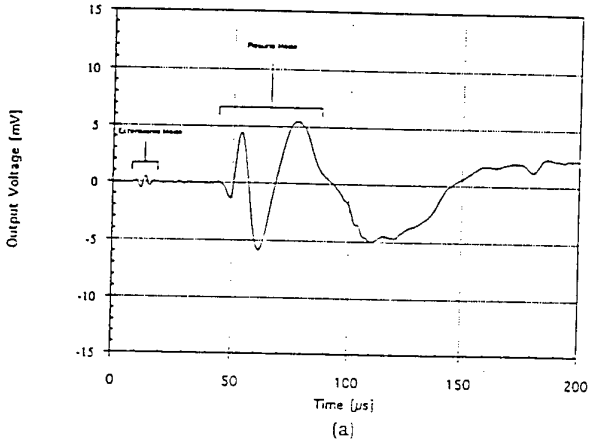

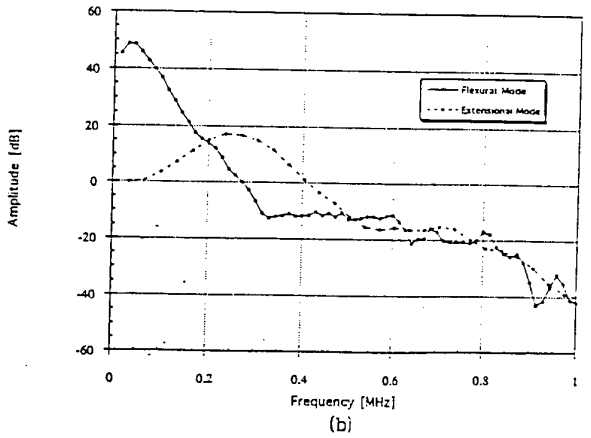

Fig. 5(a). V109 response to a lead break on the surface of a glass/epoxy laminate plate. Source to detector distance 10 cm @ 0° to the fiber axis.
Fig. 5(b). Flexural and extensional plate wave modes, detected by a Panametrics V109 transducer, in a 0_{16} glass/epoxy laminate plate.

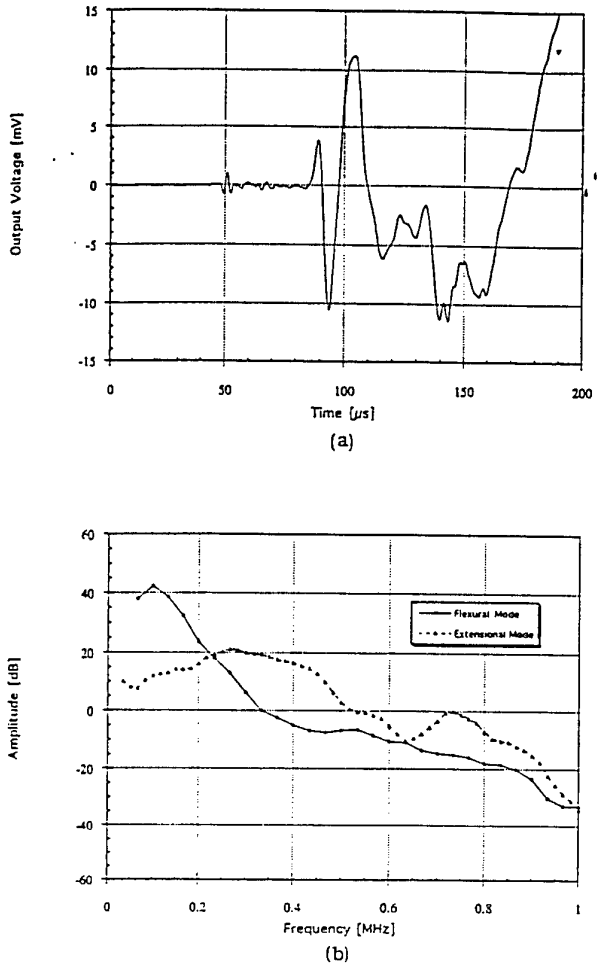

Fig. 6(a). PTCa/P(VDF-TrFE) transducer response to a lead break on the surface of a glass/epoxy laminate plate. Source to detector distance 10 cm @ 0° to the fiber axis.
Fig. 6(b). Flexural and extensional plate wave modes, detected by a PTCa/P(VDF-TrFE) transducer, in a 0_{16} glass/epoxy laminate plate.

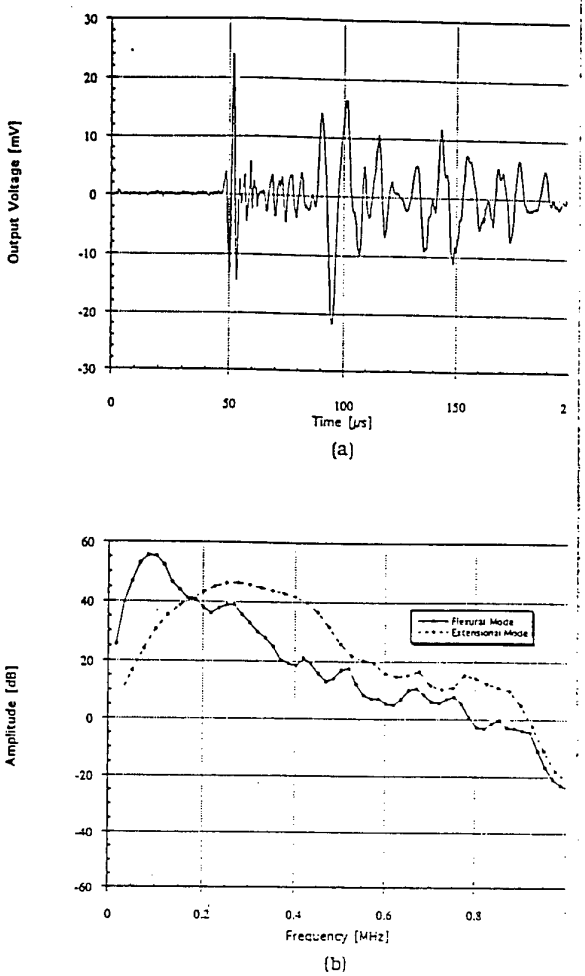

Fig. 7(a). PTCa/epoxy transducer response to a lead break o the surface of a glass/epoxy laminate plate. Source to detect distance 10 cm @ 0° to the fiber axis. Preamplification of 4 dB.
Fig. 7(b). Flexural and extensional plate wave modes. d tected by a PTCa/epoxy transducer, in a 0_{16} glass/epo laminate plate.

rection have been shown. The PTCa/P(VDF-TrFE) transducer shows signals similar to the Panametrics transducer but with higher amplitudes for the two modes. It should be noted here that the later part of the signal contains detected reflections from the edges of the plate and this information is ignored. The polarity of the signals is also noted to be reversed which only depends on the construction of the transducer, i.e. the direction of polarization of the piezoelectric material.

Figure 7 shows the output from a PTCa/epoxy transducer that has been amplified by 40 dB before detection. It is noted here that the extensional/flexural amplitude ratio for this transducer, which has been preamplified, is higher than those of the transducers that have not been amplified. This is believed to be due to the amplifier involved, and not a characteristic of the transducers, because the gain of the amplifier is greater at higher frequencies in comparison with that at lower frequencies.

For each of the signals recorded, the modes of prop agation were separated and analyzed using Fourie techniques to determine the frequency component present. For propagation along the fiber axis, the fre quencies present in the flexural and extensiona modes centered around 74 kHz and 288 kHz respec tively for the transducers used in the test. All th transducers could be seen to determine the respectiv frequencies of the two modes as can be seen fror *Table 3*. For the flexural mode, the Panametrics trans ducer produces the lowest value of 32 kHz whereа the composite transducers produce consistentl higher values. For propagation along a direction 90° t the fiber direction it was found that the signals pro duced by all the transducers were less clearly define in terms of the mode frequencies. The frequencie present in the extensional mode appeared to cente around 142 kHz, while the frequencies within the flex

Table 3. Peak Frequencies of the Propagation Modes of Plate Waves, Within a Laminate Plate, Detected by Surface Mounted AE Sensors.

	Extensional	Mode	Flexural	Mode
	0° direction	90° direction	0° direction	90° direction
Panametrics V109-RM	251 kHz	159 kHz	32 kHz	61 kHz
PTCa/P(VDF-TrFE) 65/35 vol%	269 kHz	146 kHz	63 kHz	67 kHz
PTCa/epoxy 60/40 vol%	263 kHz	203 kHz	90 kHz	72 kHz

ural mode appeared to be the same as when the wave propagates along the fiber axis.

The change in frequencies seen in the extensional mode when monitored along different directions within the plate, is a reflection of the anisotropy of the plate. The anisotropy is evident from measurements taken on the velocities of propagation of the two modes along different directions within the plane of the plate.

As can be seen from *Figs. 8* and *9* both of the embedded sensors have been able to detect the plate waves without a need for amplification. There was a need, however, to ensure enough electrical screening of the circuit, because of the placement of the leads. Once this was done the signal/noise ratio was adequately increased. As can be seen from *Fig. 8(a)*, the PTCa/PVDF-TrFE) transducer produces a very small, although observable, signal from the extensional mode traveling along the fiber axis. The signal produced from the flexural mode can be seen to have completely adequate amplitude for detection. In the 90° direction with the wave detected as it travels in a direction perpendicular to the fiber axis, the signal

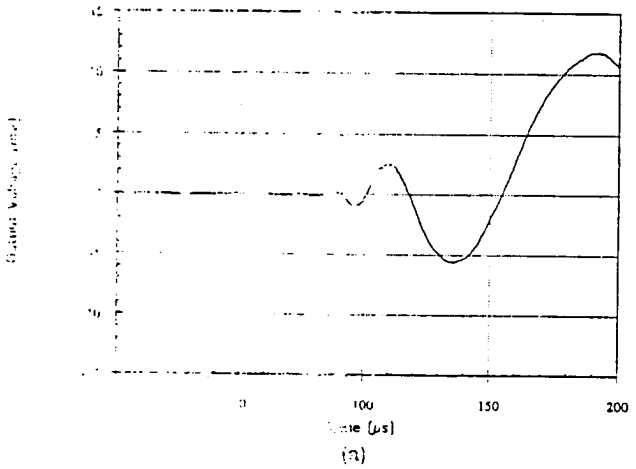

Fig. 8(a). Embedded PTCa/P(VDF-TrFE) sensor response to a lead break on the surface of a glass/epoxy laminate plate. Source to detector distance 10 cm @ 0° to the fiber axis.
Fig. 8(b). Flexural and extensional plate wave modes, detected by a PTCa/PVDF-TrFE) embedded sensor, in a 0_{16} glass/epoxy laminate plate.

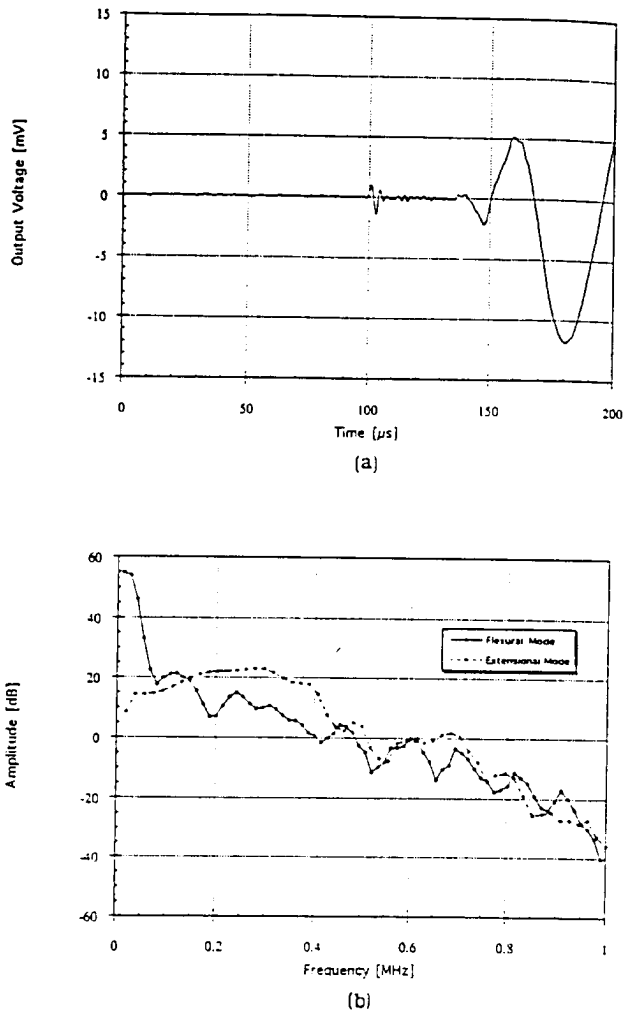

Fig. 9(a). Embedded PTCa/epoxy sensor response to a lead break on the surface of a glass/epoxy laminate plate. Source to detector distance 10 cm @ 0° to the fiber axis.
Fig. 9(b). Flexural and extensional plate wave modes, detected by a PTCa/epoxy embedded sensor, in a 0_{16} glass/epoxy laminate plate.

produced by this transducer failed to distinguish the extensional mode but again produced an adequate signal for the flexural mode.

The signal produced by the PTCa/P(VDF-TrFE) transducer shows that this transducer has been able to detect and distinguish both the extensional and flexural modes of a plate wave traveling in the 0° direction. In the 90° direction again the extensional mode appeared less discernible than in the 0° direction. From the frequency analysis of the signals from the embedded sensors it can be seen that in the 0° direction, for both the sensors the extensional mode is centered on 200 kHz for the PTCa/P(VDF-TrFE) sensor and 260 kHz for the PTCa/epoxy sensor. The flexural mode has produced signals with frequencies predominantly <30 kHz for both the sensors.

The obvious difference between the two sensors is that of the signals produced by the extensional mode. When using a surface mounted AE sensor, which has been acoustically coupled to the plate by means of a thin liquid film, to detect AE on the surface of the plate, only compressional stresses are transmitted into the sensing material. Because the liquid film cannot support shear stresses any shear stresses existing in the surface of the plate will not be transmitted into the transducer. Therefore the signals produced by the surface mounted AE sensors are a direct response of the d_{33} coefficient. When a piezoelectric film is embedded in a glass/epoxy laminate plate the signals produced, upon detection of an AE or lead break, will not be due solely to the d_{33} coefficient but also the d_{31} and d_{32} coefficients.

The typical measured values for the d_{31} coefficients of the two composites can be seen in *Table 1*. It was observed that the composite of PTCa/P(VDF-TrFE), having a d_{31} coefficient of 4.6 pC/N, showed the lower response to the extensional mode of the plate wave. Owing to the nature of the extensional mode, there will be appreciable stress in the 1-direction, therefore, when detecting the extensional mode the value of the d_{31} coefficient will have an effect on the response of the transducer. Depending on the characteristics of the wave the effect of the d_{31} coefficient will be to reduce the amplitude of the signal. Since the value of the d_{31} coefficient for the PTCa/epoxy composite is much lower than that of the PTCa/P(VDF-TrFE) composite then the contribution to the signal due to the stresses in the 1-direction will be less. The result is that the embedded transducer produces a signal comparable to that which would be produced by a surface mounted transducer, where the stresses normal to the film are dominant.

CONCLUSION

Through this work it has been possible to fabricate good quality films of PTCa/P(VDF-TrFE) of maximum size 8 cm × 6 cm having high electroactivity. The maximum electroactivity was found with a ceramic volume fraction of 65% with values of d_{33} and d_{31} being 33 and 4 pC/N respectively and a k_t value of 0.21. The pyroelectric coefficient of these films was found to b 130 $\mu C/m^2K$. Films of PTCa/epoxy have shown then selves to produce good electroactive properties wit the highest values being given by a ceramic volum fraction of 60%. Piezoelectric coefficients d_{33} and d_{31} 26 and 0.4 pC/N respectively with a k_t value of 0.1 and a pyroelectric coefficient of 30 $\mu C/m^2K$. The ma imum attainable size at present is ~5 cm × 5 cm.

For the application of AE detection within lamina plates, surface mounted transducers fabricated fro composite films of PTCa/P(VDF-TrFE) have prove themselves to be the most suited. The sensitivity these transducers is highest at the resonance fr quencies, which in turn is governed by the thickne of the piezoelectric material. While these composite show the higher piezoelectric d_{33} coefficient the would also benefit from the transducers being fabr cated from thicker films in an attempt to match th peak sensitivities to the frequencies of interest. In th case of the embedded transducers the PTCa/epo films seem to be the better choice of transducing m terial, producing signals comparable in amplitude those of an embedded PTCa/P(VDF-TrFE) film b more clearly defined.

REFERENCES

1. C. J. Dias and D. K. Das-Gupta. *Piezo- and Pyroelectr ity in Ferroelectric Ceramic-Polymer Composites*. in K *Engineering Materials*, p. 217. D. K. Das-Gupta, ed Trans. Tech. Publications, Switzerland (1994).
2. J. F. Campbell, E. G. Vanderheiden, L. A. Martinez, D. Cairns, and M. G. Abdallah. *J. Compos. Mater.*, **26**, 3 (1992).
3. S. Egusa and N. Iwasawa. *Proc. 2nd Int. Conf. on Intel gent Materials*, 486 (1994).
4. H. Lamb. *Proc. Roy. Soc. London*, Series A. **93**, 1 (1917).
5. R. E. Newnham, D. P. Skinner, and L. E. Cross. *Mate Res. Bull.*, **13**, 525 (1978).
6. W. H. Prosser. The Propagation Characteristics of t Plate Modes of Acoustic Emission Waves in Thin Alum nium Plates and Thin Graphite/Epoxy Composite Plat and Tubes. NASA. Technical Memorandum-1041 (1991).
7. W. Wersing, K. Lubitz, and J. Mohaupt. *IEEE Ultraso Ferroelec. Freq. Contr.*, **36**, 424 (1989).
8. H. Jaffe. *IEEE Trans. Electron Devices*. **ED-16**, 5 (1969).
9. Y. Yamashita, K. Yokoyama, H. Honda, and T. Tak hashi. *Jpn. J. Appl. Phys.*, **20**, 183 (1981).
10. C. J. M. M. Dias. PhD dissertation. University of Wale Bangor, U.K. (1994).
11. T. Furukawa, K. Ishida, and E. Fukada. *J. Appl. Phy* **50**, 4904 (1979).
12. H. Yamazaki and T. Kitayama. *Ferroelectrics*. **33**, 1 (1981).
13. M. P. Wenger, P. Blanas, R. J. Shuford, and D. K. Da Gupta. *2nd Euro. Conf. on Smart Struct. & Mat.*, 3 Glasgow, Scotland (1994).
14. M. P. Wenger, P. Blanas, C. J. Dias, R. J. Shuford, and K. Das-Gupta. *Ferroelectrics*. **187**, 75 (1996).
15. R. L. Byer and C. B. Roundy. *Ferroelectrics*. **3**, 3 (1972).
16. C. Dias, D. K. Das-Gupta, Y. Hinton, and R. J. Shufor *Sensors and Actuators A*. **37–38**, 343 (1993).
17. M. G. Grewe, T. R. Gururaja, R. E. Newnham, and T. Shrout. *IEEE Ultrasonics Symposium*. **2**, 713 (1989).

18. C. Dias, M. P. Wenger, P. Blanas, R. J. Shuford, Y. Hinton, and D. K. Das-Gupta, *Proc. 2nd Int. Conf. on Intelligent Materials*, p. 437, Williamsburg, Va. (1994).
19. H. Banno, *Jpn. J. Appl. Phys.*, **24**, 445 (1985).
20. T. R. Gururaja, W. A. Schulze, L. E. Cross, R. E. Newham, B. A. Auld, and Y. J. Wang, *IEEE Trans. Sonic. Ultrason.*, **SU-32**, 481 (1985).
21. W. A. Smith, *IEEE Ultrasonics Symposium*, **2**, 755 (1989).
22. R. Y. Ting, *Ferroelectrics*, **102**, 215 (1990).
23. D. K. Das-Gupta, *Ferroelectrics*, **118**, 165 (1991).
24. S. Bauer, *Trends Polym. Sci.*, **3**, 288 (1995).
25. J. A. Chilton, G. M. Garner, R. W. Whatmore, and F. W. Ainger, *Ferroelectrics*, **109**, 217 (1990).
26. L. Pardo, J. Mendiola, and C. Alemany, *Ferroelectrics*, **93**, 183 (1989).
27. G. M. Garner, N. M. Shorrocks, R. W. Whatmore, M. T. Goosey, P. Seth, and F. W. Ainger, *Ferroelectrics*, **93**, 169 (1989).
28. A. A. Shaulov, W. A. Smith, and R. Y. Ting, *Ferroelectrics*, **93**, 177 (1989).
29. M. R. Gorman and W. H. Prosser, *J. Acoustic Emission*, **9**, 283 (1990).

The Ferroelectric Properties of Piezoelectric Ceramic/Polymer Composites for Acoustic Emission Sensors

M.P. WENGER, P.L. ALMEIDA, P. BLANAS*, R.J. SHUFORD* and D.K. DAS-GUPTA

School of Electronic Engineering & Computer Systems,

University of Wales, Bangor,

Bangor, Gwynedd, LL57 1UT, U.K.

*U.S. Army Research Laboratory, Materials Directorate, Aberdeen Proving Ground,

MD 21005-5069, U.S.A.

Two different mixed connectivity composites, consisting of a ferroelectric ceramic powder of calcium modified lead titanate (PTCa) dispersed in a polymer matrix, have been fabricated and their ferroelectric properties have been investigated. Hysteresis measurements have been conducted on composites of PTCa with a polar polymer of polyvinylidene trifluoroethylene (P(VDF-TrFE)) and PTCa with a thermosetting epoxy resin to determine the coercive fields and remanent polarisation of the two different composites. The composites show noticeable differences in their behaviour during poling along with the values of their piezoelectric coefficients, with the composite of PTCa/P(VDF-TrFE) showing enhanced piezoelectric activity over that of PTCa/epoxy. This paper reports on the polarisation properties and the microstructural nature of the composites.

INTRODUCTION

The health monitoring of some of today's structures through nondestructive evaluation (NDE) techniques has become an integral part of their working lives. The faithful monitoring of the dynamic stresses produced by damage mechanisms can be used to determine the state of health of a structure via techniques such as acoustic emission (AE) detection and acousto-ultrasonics. These techniques rely heavily on sensor technology for detecting damage, fatigue or corrosion of the structures. Piezoelectric and ferroelectric materials have long been used as electromechanical transducers in a variety of applications for the production and detection of ultrasound.

Typically ferroelectric ceramics, such as lead zirconate titanate (PZT), lead titanate (PT) and barium titanate have been used as the transducer material in such sensors. Ceramics due to their inherent nature are invariably stiff brittle materials whose response is of a resonant nature due to the high quality factors associated with these materials. On the other hand, electroceramics usually posses high piezoelectric and electromechanical coupling coefficients making them attractive as electromechanical transducing materials. A composite material, fabricated by the dispersion of a ceramic powder into a compliant polymer matrix, although displaying a reduction in the piezoelectric properties will however show improved mechanical properties. The compliance of the composite materials will be lowered from that of the ceramic alone whilst the frequency dependent mechanical losses will increase, producing a sensor with a broad bandwidth response. The coupling of the piezoelectric coefficients, d_{33} and d_{31}, will also be lowered thus providing a high hydrostatic d_h coefficient. Within this study composites of a ferroelectric ceramic, calcium modified lead titanate, and two different polymer hosts, a thermoset epoxy resin and a thermoplastic polar polymer were prepared and investigated.

A composite material where a ceramic powder has been randomly dispersed in a polymer matrix, can be made to be ferroelectric through a process known as poling. An application of a large electric field to the material will cause the spontaneous electric polarisation of the ferroelectric phases to orientate so as to oppose the direction of the electric field lines. A reversal of the applied electric field will cause the aligned electric dipoles to switch their direction of orientation to that opposing the new field. Observation of the spontaneous polarisation reversal can be made by the application of a sinusoidally varying field whilst continuously monitoring the polarisation reversal current and/or charge. From these measurements a determination of the remanent polarisation, when the applied field is zero, of the material can be made along with the magnitude of the field needed to cause dipole switching, i.e. the coercive field. At very low fields and very high fields the ferroelectric material acts essentially as an ordinary dielectric although with a high value of the dielectric permittivity. As the applied field is increased and approaches the value of the coercive field polarisation reversal occurs giving rise to a large dielectric non-linearity and hysteresis loss. At large fields the value of the spontaneous polarisation tends to saturate. Experimental results from an investigation into the hysteresis measurements on composites of PTCa/P(VDF-TrFE) have previously been reported in a paper by Dias et al (1). This

paper reports on the results from a study on the hysteresis measurements on composites of PTCa/Epoxy and discusses the comparison between these composites and composites of PTCa/P(VDF-TrFE).

TECHNIQUES OF HYSTERESIS MEASUREMENT

Various techniques have been used to measure the ferroelectric hysteresis of low polarisation materials with high permittivity and/or conductivity such as is the case with composites. A widely used method for measurement of the electric displacement, D, versus field, E, hysteresis curves of ferroelectric polymers has been the Sawyer-Tower (2) method and its modifications (3, 4). Here, the sample, with capacitance C, is connected in series with a much larger capacitance C_o. The conductance G of the sample is compensated for by a conductance G_o in parallel with C_o, (figure 1). Another technique (5) uses the values of the current at maximum field to make estimates on the resistance of the sample, the capacitance of the sample is then estimated from the values of the current, with the resistive component removed and in the absence of ferroelectric switching. Other methods which have produced good results without the need to make estimates on the resistive and capacitive components of the current, have been to measure the bipolar and unipolar currents either sequentially (5) or simultaneously (1). The current measured is a combination of the currents due to the polarisation reversal and the resistive and capacitive components which is given by

$$I = A\frac{dP}{dt} + \frac{V}{R} + C\frac{dV}{dt} \qquad (1)$$

Polarisation reversal only occurs when the polarity of the poling field is reversed, therefore, the component of the current due to this mechanism only occurs during a bipolar cycle of the applied field. During a unipolar or rectified cycle of the applied field the expression for the current, (equation 1), will only contain the terms due the resistive and capacitive components, which are possibly non-linear at high fields, thus allowing the removal of these terms by a subtraction of both the positive, I_+, and negative, I_-, unipolar currents from the bipolar current.

EXPERIMENTAL

The composite materials were obtained through two different processes depending on which of the two polymers were to be used as the host matrix for the ceramic powder. The ceramic used here was calcium modified lead titanate (PTCa) with the following composition

$$Pb_{0.76}Ca_{0.24}\left[\left(Co_{0.5}W_{0.5}\right)_{0.04}Ti_{0.96}\right]O_3 + MnO_2$$

supplied by GEC -Marconi Materials Research Laboratory. The two polymers were a thermosetting epoxy resin (Epikote 828, Shell Resins) with a curing agent (K61B, Anchor Chemical) and the thermoplastic polar copolymer of vinylidene fluoride and trifluoroethylene, P(VDF-TrFE) (Solvay). The composites of the ceramic with the epoxy, PTCa/Epoxy, were prepared by gradually adding the ceramic powder to the resin whilst stirring continuously to ensure an even mixture. Thin films (~100μm) of the composite material were cast between two polished metal plates in a thermally controlled mechanical press at a temperature of 60°C. A full description of the preparation method has been described in a previous paper by Wenger et al (6). The composites containing the ceramic with the copolymer host of P(VDF-TrFE) were prepared by a solvent casting technique. Here the copolymer, which was supplied in fine powder form, was mixed thoroughly with the dry ceramic to produce a even mixture of the two powders. A sufficient amount of acetone was then added to the dry powders to dissolve the polymer and produce a thick slurry of ceramic with dissolved polymer. The mixture was then stirred continuously until all the acetone had evaporated leaving behind the solidified composite material. This was allowed to dry completely within a vacuum environment for approximately 24 hours to remove completely the solvent. Thin films (<100 μm) were produced by hot pressing the material between two polished stainless steel plates at the softening temperature of the copolymer (~170°C). Once thin films of the composite materials had been fabricated circular aluminium electrodes of 1 cm diameter and approximately 1000 Å thickness were deposited by vacuum ($<10^{-6}$ mbarr) evaporation onto the surfaces.

Hysteresis measurements, similar to the method used by Dickens (5), were performed on the composites by applying a sinusoidal varying electric field whilst measuring the current flowing through the sample. This method is analogous to the method used by Dias and Das-Gupta (1) where they simultaneously measured the current through three similar samples whilst applying a bipolar field to one sample and unipolar fields to the other two. The advantage of the method used here is that errors arising due to dissimilarities in the thickness and/or electrode areas of the samples do not have to be compensated for within the apparatus. The measurements were conducted by immersing the sample in silicone oil, which was used for prevention of electrical arcing and whose temperature was controlled by a hot plate, whilst an electric field was applied across the thickness of the sample.

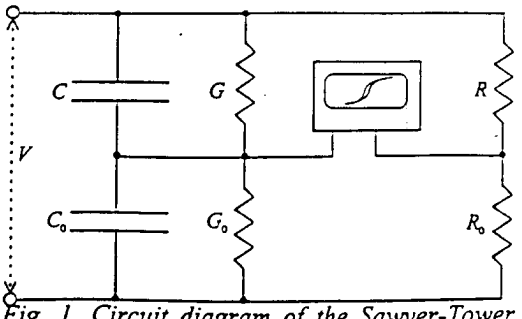

Fig. 1. Circuit diagram of the Sawyer-Tower method for measuring ferroelectric hysteresis (3).

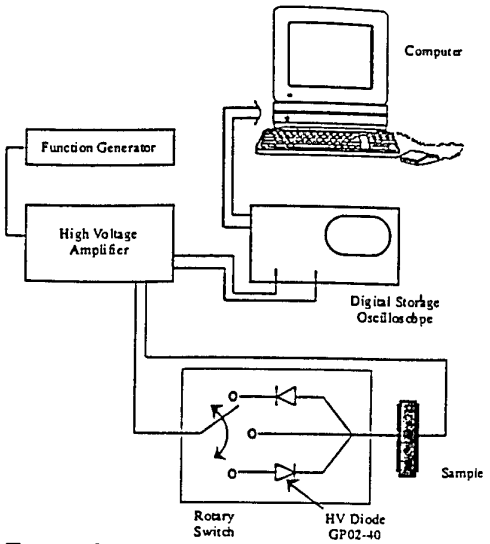

Fig. 2. Hysteresis measurements by monitoring the bipolar and unipolar currents.

Electrical connections were made to the sample electrodes from a high voltage amplifier (TREK 610C) which amplified the electrical input, from a sinusoidal signal generator, in a ratio of 1000:1. The HV amplifier was capable of monitoring the current through the high tension side of the circuit and producing a proportional voltage output which could be monitored on a suitable storage oscilloscope. Another proportional voltage output was available to monitor the high voltage applied to the sample. The proportional values of the current and the voltage were monitored on a digital storage oscilloscope (DSO) (GOULD 4050) and downloaded to a computer for further analyses. A mechanical switch was mounted into the HT side of the circuit to enable the introduction of high voltage diodes (GP02-40, Radio Supplies), as shown in figure 2.

The current through the sample consists of three components; the capacitive and resistive components, which are possibly non-linear at high fields and a component due to the switching of the spontaneous polarisation orientation, equation 1. It is the polarisation current which is of interest in this study in order to observe the ferroelectric hysteresis. With the composites the resistive component of the current can be quite large compared to the polarisation component, the capacitive component is usually small due to the low frequencies involved, therefore, there is a need to eliminate the unwanted resistive and capacitive components of the current as they can obscure the true value of the polarisation current. This was accomplished by measuring the total current, I_T, as a full wave sinusoidal field was applied to the sample, with further measurements of I_+ and I_- as positive and negative half-wave rectified fields, respectively, were applied. The polarisation current, I_{pol}, will then be given by

$$I_{pol} = I_T - (I_+ + I_-) \qquad (2)$$

The three current measurements and the voltage measurements were recorded on the DSO and downloaded to a computer. The polarisation current density was calculated from knowledge of the electrode area and through integration the polarisation charge was found. This enabled a ferroelectric hysteresis loop to be drawn, from which the remanent polarisation and coercive field could be determined.

RESULTS AND DISCUSSION

Within composite systems the manner in which the phases are coupled together is known as their connectivity (7). For diphasic composites consisting of a ceramic phase and a polymer phase there are ten possible combinations of phase connectivity which are usually described by using two digits, the first denoting the connectivity of the ceramic and the second, that of the polymer with itself in each case. Relevant examples of these connectivity patterns are 0-3 and 1-3 where the ceramic is connected to itself in zero directions and one direction, respectively, throughout the composite and the polymer is connected to itself in three directions for both patterns. The connectivity of the constituent phases of the composite materials has a large effect on their electroactive properties compared to those of the phases. Pardo et al (8) reported on the hysteresis properties of mixed connectivity composites formed by the dispersion of ceramic particles into a polymer matrix, where 0-3 composites having grain sizes comparable to their thicknesses possessed a certain amount of 1-3 connectivity. It was noted by these workers that the ceramic with 1-3 connectivity will acquire a polarisation value close to that of the ceramic alone under the same field, whereas, the ceramic within the 0-3 connectivity portion of the composite will experience a lower local field, due to the shielding of the polymer, and will therefore acquire a lower polarisation. The amount of 1-3 connectivity will depend greatly on the ratio of ceramic grain size to composite thickness and also the ceramic volume fraction of the composite.

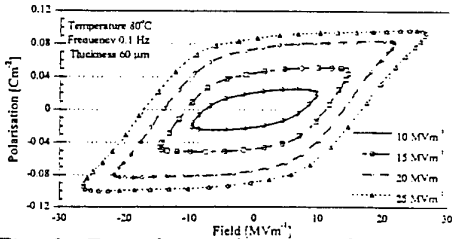

Fig. 3. Ferroelectric hysteresis loops for a composite of PTCa/P(VDF-TrFE) 65/35vol%.

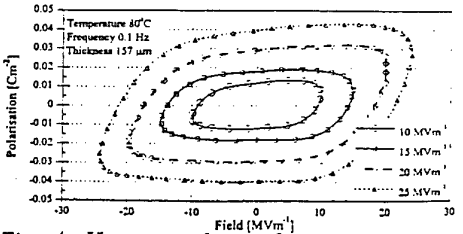

Fig. 4. Hysteresis loops for a composite of PTCa/Epoxy 60/40vol%.

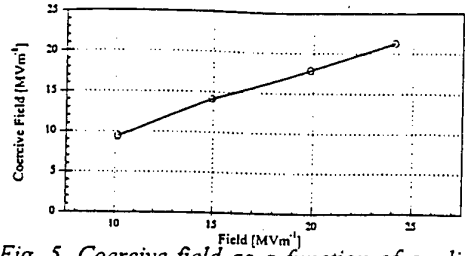

Fig. 5. Coercive field as a function of applied field for a composite of PTCa/Epoxy 60/40vol%.

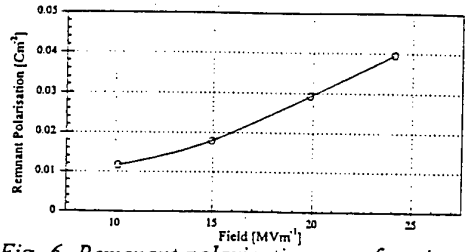

Fig. 6. Remenant polarisation as a function of field for a composite of PTCa/Epoxy 60/40vol%.

Figures 3 and 4 show hysteresis loops for varying applied electric fields of 10, 15, 20 and 25 MVm^{-1} for composites of PTCa/P(VDF-TrFE) and PTCa/Epoxy respectively containing 60 and 65 volume percentage of ceramic respectively. These loops were obtained by measurements at 80°C, the softening temperature of the epoxy, and at a frequency of 0.1 Hz. The sample thicknesses were 60 μm for the copolymer composite and 157 μm for the epoxy composite, the grain sizes of the ceramic being predominantly in the range 10 - 20 μm. The two main differences between the two sets of hysteresis curves are their relative magnitudes and apparent shapes. For the same poling conditions the saturation polarisations at 25 MVm^{-1} are 0.10 and 0.05 Cm^{-2} for the composites of PTCa/P(VDF-TrFE) 65/35vol% and PTCa/Epoxy 60/40vol% respectively. The apparent shapes of the two sets of hysteresis loops are indicative of a difference in the amount of 1-3 connectivity present in each composite, if we assume that the main electroactive component is the ceramic phase and the copolymer contributes a relatively small amount to the ferroelectric properties of it's composite. The permittivities of the ferroelectric copolymer and the non-polar epoxy are 12 and 4 respectively. It would thus be anticipated that the copolymer matrix will wet the electroactive ceramic more effectively than the epoxy which was evidenced from scanning electron microscopy (SEM) studies. As a result the volume fraction of the interfaces between the ceramic and polymer for the former case would be considerably lower than for the epoxy composite. It is well established that at such interfaces charges will accumulate and provide a space-charge conduction through the bulk (9). The roundness of the hysteresis loops, which indicates conduction through the sample, for the composite of PTCa/Epoxy 60/40vol% is typical for 0-3 connectivity composites. The effect of the decreased local field can also be noticed in the values for the coercive fields, which for the epoxy composite

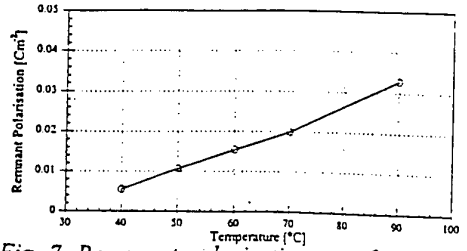

Fig. 7. Remenant polarisation as a function of temperature of a sample of PTCa/Epoxy 52/48vol%.

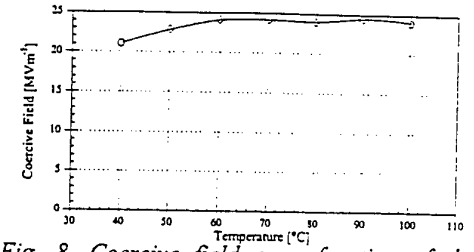

Fig. 8. Coercive field as a function of the temperature of a sample of PTCa/Epoxy 52/48vol%.

are relatively higher than those for the copolymer composite with the same applied field. A reduction in the local field experienced by the ceramic not only arises from the polymer shielding but also from the greater dielectric mismatch of the permittivities of the constituent phases (10).

The slopes of the hysteresis curves in figures 3 and 4, as the field decreases from the maximum to zero, can be seen to be relatively flat indicating that the resistive current does not contribute to the polarisation current. An enhancement of the polarisation is seen for both composites as the field decreases from the maximum to approximately 22 MVm^{-1} and 18 MVm^{-1} for the composite of PTCa/P(VDF-TrFE) and PTCa/Epoxy respectively, with no further enhancement seen for lower fields. The variation of the coercive field and the remanent polarisation with applied field for the composite of PTCa/Epoxy 60/40vol% are shown in figures 5 and 6. It can be seen that both these properties increase approximately linearly with increased applied field in the range 10 - 25 MVm^{-1}, the higher field being close to the breakdown strength of the composite. The behaviour of the remanent polarisation and coercive field of a similar composite with 52% ceramic volume loading with temperature is seen in figures 7 and 8 respectively. It can be seen here that for low temperatures the value of the coercive field is lower than that at respectively higher temperatures where the value is relatively independent of temperature. The lower coercive field is believed to be due to inefficient poling, as hindrance of domain wall movement at lower temperatures prohibits dipole alignment which results in the lower remanent polarisation. The remanent polarisation appears to vary linearly with temperature over the range 30 - 90°C above which the value would be expected to decrease as the temperature of the polymer exceeds that of the phase transition of the polymer.

The ferroelectric behaviour of 0-3 composites as a function of frequency is of

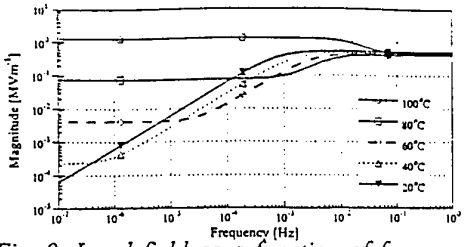

Fig. 9. Local field as a function of frequency experienced by series connected ceramic in a mixed connectivity composite.

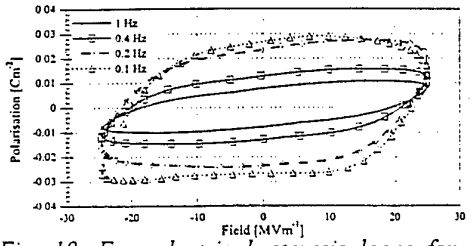

Fig. 10. Ferroelectric hysteresis loops for a composite of PTCa/Epoxy 50/50vol% at various frequencies.

interest when optimisation of poling efficiency is being sought (10). The local field experienced by the series connected ceramic in a 0-3 or mixed connectivity composite will depend on the resistivities and the permittivities of the constituent phases. At low frequencies the magnitude of the local field. E_{local}, will be dictated by the resistivities, ρ, of the ceramic and the polymer as in equation 3

$$E_{local} = \frac{\rho_c E_{applied}}{m\rho_c + (1-m)\rho_p} \qquad (3)$$

where the subscripts c and p refer to the ceramic and polymer respectively and the parameter m represents the volume fraction of the series connected ceramic (11). At higher frequencies the magnitude of the local field will be governed by the value of the permittivities, ε, as in equation 4

$$E_{local} = \frac{\varepsilon_p E_{applied}}{m\varepsilon_{applied} + (1-m)\varepsilon_c} \qquad (4).$$

Figure 9 shows theoretically derived local field magnitudes experienced by the series connected ceramics in a composite of PTCa/Epoxy as a function of frequency for varying temperatures. The values were derived from measurements on the electrical properties of the constituent phases over the temperature range 20 - 100°C. Figure 10 shows the hysteresis loops for a composite of PTCa/Epoxy 50/50vol% measured at various frequencies in the range 0.1 Hz to 1 Hz. For frequencies below 0.1 Hz the low value of the polarisation current compared to the total current made it difficult to observe a clearly defined hysteresis loop. In figures 11 and 12 the remanent polarisation and coercive field are shown as functions of frequency. From figure 11 it can be seen that the remanent polarisation falls off as the frequency increases, from 0.1 to 1 Hz. With higher frequencies an alignment of the domains is reduced, hence the remanent polarisation is reduced, as the time allowed for

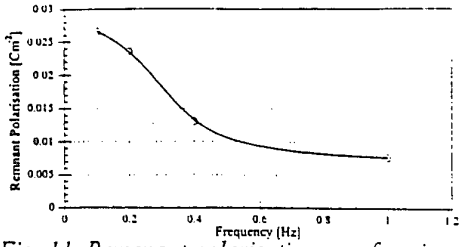

Fig. 11. Remenant polarisation as a function of frequency for a composite of PTCa/Epoxy 50/50vol%.

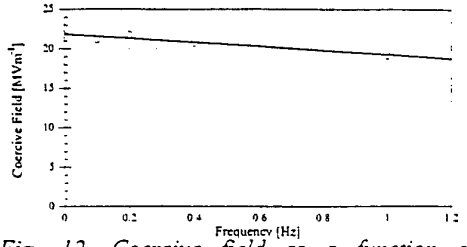

Fig. 12. Coercive field as a function of frequency for a composite of PTCa/Epoxy 50/50vol%.

the polarisation to switch becomes shorter than the time required by the dipoles to reorientate themselves. From figure 9 it can be seen that the series connected ceramic, at 80°C, would experience a lower local field with frequencies lower than approximately 0.1 Hz, thus it is assumed that the remanent polarisation would begin to decrease again as the frequency is lowered below this value although measurements of the hysteresis loops at low frequency with this method are difficult. The coercive field is seen to decrease approximately linearly with increasing frequency due to the inefficient poling at the higher frequencies, (figure 12).

A simple relaxation model proposed by Landauer et al (12) for the polarisation reversal is given by

$$I_{pol} = \frac{dP}{dt} = \nu(P_s - P) = \nu_0 e^{-E_i/E}(P_s - P) \qquad (5)$$

where the polarisation P changes towards it's saturation value P_s at a rate ν dependent on the applied field E. ν_0 is a rate constant independent of the applied field and E_i is known as the activation field. As the polarisation switches there is an instant where its value is zero, therefore, at this instant

$$I_0 = \nu_0 P_s e^{-E_i/E_c} \qquad (6)$$

where E_c is the coercive field and I_0 the current at zero polarisation. By plotting the relationship between $\ln(I_0)$ and $1/E_c$ the value of the activation field E_i may be obtained from the slope and the value of $\nu_0 P_s$ from the ordinate on the vertical axis. From the data presented in figures 3 and 4, values of I_0 and E_c for different applied fields were found for both the composite samples. (figure 13). Table 1 lists the calculated values for the

Table 1. Activation fields and rate constants for PTCa/P(VDF-TrFE) 65/35vol% and PTCa/Epoxy 60/40vol% composites.

Composite	E_A (MVm^{-1})	$\nu_0 P_S$	ν_0 (Hz)
PTCa/P(VDF-TrFE)	25.1	0.67	7.2
PTCa/Epoxy	32.9	0.05	1.1

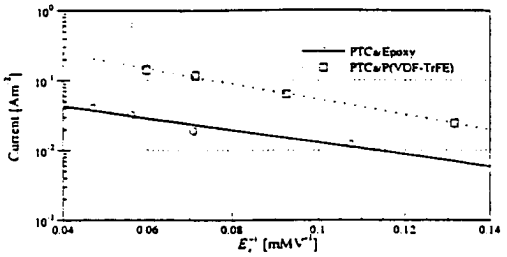

Fig. 13. Plot of $\ln(I_0)$ versus the inverse of the coercive field for composites of PTCa/P(VDF-TrFE) 65/35vol% and PTCa/Epoxy 60/40vol%.

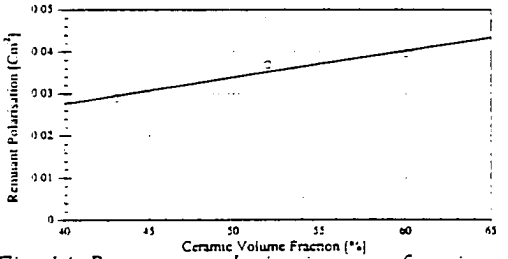

Fig. 14. Remanent polarisation as a function of ceramic volume for composites of PTCa/Epoxy.

activation field and the product $\nu_0 P_S$ for an applied field of 25 MVm^{-1} along with the values for ν_0 where the estimated values of the saturation polarisations have been taken from figures 3 and 4. From the values given in table 1, the rate constants ν for the composites of PTCa/P(VDF-TrFE) 65/35vol% and PTCa/Epoxy 60/40vol% are found to be 2.64 and 0.30 for a step input applied field of 25 MVm^{-1} respectively, indicating an approximate increase by a factor of 8 in the switching times between the two samples respectively.

The variations of remanent polarisation and coercive field with ceramic volume fraction are shown in figures 14 and 15 respectively. It can be seen that the coercive field is relatively independent of volume fraction of the ceramic between 40 and 60% while the remanent polarisation increases steadily as the ceramic

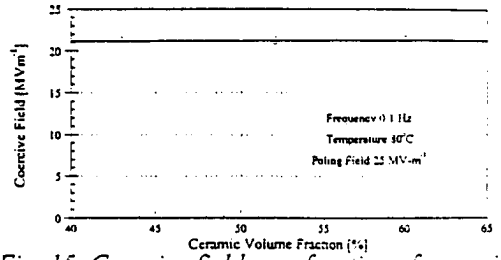

Fig. 15. Coercive field as a function of ceramic volume for composites of PTCa/Epoxy.

volume fraction increases. The limiting value of the ceramic volume fraction was 60%. With ceramic volume fractions higher than 60% the composite films fabricated were of low quality and not suitable for poling. For films with thickness approaching the grain size of the ceramic it is believed that the remanent polarisation would increase due to an increased amount of 1-3 connectivity although these are difficult to fabricate. The results found from this study are summarised in table 2. The electrical, mechanical and electroactive properties of these composites and their suitability as NDE sensors have been reported in a previous paper by Wenger et. al. (13).

CONCLUSION

It has been presented here the results of a study on the poling properties of mixed connectivity composites of calcium modified lead titanate with two different polymer matrices, polyvinylidene trifluoroethylene and an epoxy. The paper has concentrated on the results found for the composites of PTCa/Epoxy and have shown that for efficient poling of the electroactive ceramic a high applied field is needed as the polymer produces a large amount of electrical shielding. A field close to the electrical breakdown strength is the most suitable. Poling at an elevated temperature enhances the remanent polarisation although care must be taken when approaching the epoxy glass transition temperature as distortion of the sample will occur. The optimum poling

Table 2. Summary of the poling properties of the composite systems PTCa/P(VDF-TrFE) 65/35vol% and PTCa/Epoxy 60/40vol% at 80°C.

	PTCa/P(VDF-TrFE) 65/35vol%	PTCa/Epoxy 60/40vol%
Remanent Polarisation ($E_{applied}$ =25 MVm^{-1}) [Cm^{-2}]	0.10	0.05
ε'	54	36
ρ [MΩm]	600	300
$\tan\delta$	0.019	0.009
E_C [MVm^{-1}]	17	21
d_{33} [pCN^{-1}]	33	30

frequency at 80°C appears to be approximately 0.1 Hz to efficiently pole the series connected ceramic.

REFERENCES

1. C.J. Dias and D.K. Das-Gupta, J. Appl. Phys, 74, 6137 (1993).
2. C.B. Sawyer and C.H. Tower, Phys. Rev., 35, 269 (1930).
3. J.C. Hicks and T.E. Jones, Ferroelectrics, 32, 119 (1981).
4. S. Ikeda, S. Kobayashi, and Y. Wada, J. Polym. Sci.: Polym. Phys., 23, 1513 (1985).
5. B. Dickens, E. Balizer, A.S. DeReggi, and S.C. Roth, J. Appl. Phys., 72, 4258 (1992).
6. M.P. Wenger, P. Blanas, R.J. Shuford, and D.K. Das-Gupta, *2nd Euro. Conf. on Smart Struct. & Mat.*, Glasgow, Scotland, 358 (1994).
7. R.E. Newnham, D.P. Skinner, and L.E. Cross, Mater. Res. Bull., 13, 525 (1978).
8. L. Pardo, J. Mendiola, and C. Alemany, J. Appl. Phys., 64, 5092 (1988).
9. D.K. Das-Gupta, K. Doughty, and R.S. Brockley, J. Appl. Phys., 13, 2101 (1980).
10. C.J. Dias and D.K. Das-Gupta, Ferroelectrics, 157, 405 (1994).
11. C.J. Dias and D.K. Das-Gupta, IEEE Trans. Dielectr. & Electr. Insul., 3, 706 (1996).
12. R. Landauer, D.R. Young, and M.E. Drougard, J. Appl. Phys., 27, 752 (1956).
13. M.P. Wenger, P. Blanas, R.J. Shuford, and D.K. Das-Gupta, Polym. Eng. Sci., (1996).

Characterisation and Evaluation of Piezoelectric Composite Bimorphs for *in-situ* acoustic emission sensors

M.P. WENGER, P. BLANAS*, R.J. SHUFORD* and D.K. DAS-GUPTA

School of Electronic Engineering & Computer Systems
University of Wales, Bangor
Bangor, Gwynedd, LL57 1UT, U.K.

*U.S. Army Research Laboratory
Materials Directorate
Aberdeen Proving Ground, Maryland 21005-5069

Mixed connectivity composites consisting of a ferroelectric ceramic powder of calcium modified lead titanate dispersed in a polymer matrix have been fabricated into piezoelectric bimorph sensors. The piezoelectric, dielectric and electromechanical coupling coefficients of these sensors have been measured and a full characterisation of the electromechanical properties are reported. The suitability of these bimorph transducers as *in-situ* acoustic emission sensors, embedded into glass-epoxy laminate plate like structures, has been investigated. A comparison of the performance of these sensors to those of previously investigated monomorph sensors fabricated from the same material has been made.

INTRODUCTION

An acoustic emission (AE) transducer senses the dynamic stress waves propagating through a structure, which have been generated by the release of energy due to a failure mechanism. Within a fibre reinforced epoxy composite structure acoustic emissions can be generated by processes such as fibre breakage, delaminations, fibre-matrix debonding and matrix cracking, all of which will or are expected to produce distinct waveforms (1, 2). The inherent anisotropy of composite structures also means that the direction of propagation of the waves will also have an effect on the received signal. To effectively determine the position and nature of the damage mechanism through a non-destructive evaluation method such as AE detection the technique needs to gain as much knowledge as possible of the source of AE. Often an AE sensor will be situated on the surface of the structure some distance away from a possible AE source. The structure on many occasions may need to be removed from its working environment or continuous testing may not be practical, therefore, monitoring of the health of the structure may only be done after the damage has occurred or a decision must be made to replace or repair the structure prior to potential failure. All the above points make it an expensive and uncertain process to monitor the health of the structure. An *in-situ* AE sensor, where the sensor has become an integral part of the structure would facilitate it's continuous monitoring without any lapse of time. The continuous monitoring of the dynamic degradation of the structure would thus enable an informed decision to be made whether or not to replace or repair, all or part, of the structure.

With fibre reinforced epoxy composites the structures are predominantly plate like, i.e. two dimensions are large compared to the third. The elastic waves propagating away from an AE source will, therefore, propagate in distinct modes known as plate modes or lamb waves (3). The two prominent modes of propagation are referred to as the extensional and the flexural modes, (figure 1). The extensional mode of propagation is essentially a longitudinal wave which travels faster than the flexural mode which is essentially a transverse wave. The speed of propagation of the flexural mode is dependent on it's frequency and, therefore, is a dispersive mode. Due to the mismatching of propagation velocities there is a dispersion between the two sets of modes depending on the sensor location with respect to that of the source. The extensional modes will be sensed prior to the flexural modes at a time which will depend on the distance, from the source, that the plate waves have propagated.

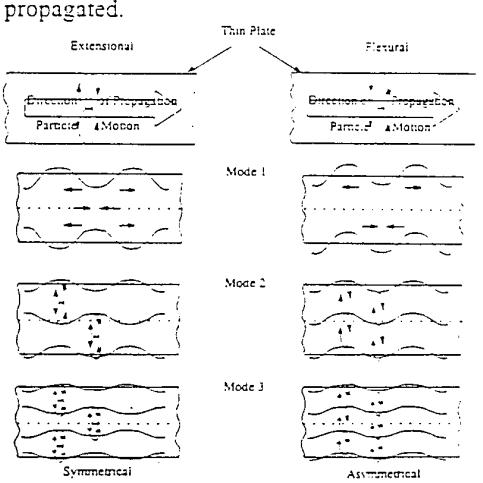

Fig. 1. Schematic representation of extensional and flexural plate waves showing their first three modes.

Piezoelectric composite transducers consisting of a ferroelectric ceramic powder dispersed in a polymer matrix can be fabricated to take advantage of the desired properties of the constituent materials. The strong piezoelectric and electromechanical properties of the ceramic phase are combined with the mechanical strength and low dielectric permittivity of the polymer to enhance the

overall properties of the composite (4). Along with the tailoring of the properties by the judicial choice of materials and their construction, composites can be formed into a variety of sizes and shapes to take advantages of the nature of the application at hand. A single film of composite material, referred to here as a monomorph, can be used as an acoustic emission sensor. It can be incorporated into a surface mounted AE sensor (5), where the electroactive composite is adhered to a backing material of the same acoustic impedance and electrical contacts are made to both faces, or be embedded into a fibre reinforced epoxy laminate structure (6). Two or more monomorphs can be incorporated into one sensor to form a bimorph or multimorph respectively. Previous work on bimorphs and multimorphs has concentrated on their actuation properties (7) either configured as cantilevers (8, 9) or as stacks (10). The present work is concerned with the sensing properties of piezoelectric bimorphs constructed from 0-3 connectivity (11) ceramic/polymer composites embedded into laminate structures. Simple bimorph sensors differ from monomorphs in their ability to work in either of two modes of operation, i.e. a thickness mode of operation or a bending mode of operation. A study on the ability of embedded monomorphs to detect simulated acoustic emissions has previously been completed and reported in a paper by Wenger et. al. (12). This paper will report the results obtained from a study on the ability of the embedded bimorph sensors to detect and distinguish simulated AE sources and a comparison will be made between the sensing properties of the monomorphs and the bimorphs.

FABRICATION

Two different compositions of piezoelectric composites have been used in this work. The ceramic used was calcium modified lead titanate (PTCa), which was supplied by GEC-Marconi Materials Technology (Caswell) in fine powder form with average grain size approximately 10-20μm. The two different polymer matrices were a polar copolymer, polyvinylidene trifluoroethylene (P(VDF-TrFE)) 75/25 molar percentage supplied by Solvay in fine powder form, and a non-polar epoxy resin, Epikote 828 (Shell Resins), with hardener, K61B (Anchor Chemical). Fabrication of the PTCa/P(VDF-TrFE) composite material consisted of dry mixing the ceramic and polymer powders until an even distribution was formed where upon enough acetone was added to the powder mix to fully dissolve the polymer. Continuous stirring of the mixture within a fume cabinet enabled the solvent to evaporate leaving behind the 0-3 composite material. Further drying of the material to ensure total evaporation of the acetone was completed in a vacuum chamber. Thin films (~100μm thickness) of the material were then formed by pressing the material, at the softening temperature (~170°C) of the polymer, in a mechanical press. The composites of PTCa/Epoxy were fabricated (13) by gradually mixing the ceramic powder into the epoxy resin and hardener mix whilst continuously stirring by hand. Once the correct amount of ceramic had been mixed with the resin, trapped gasses were removed by placing the mixture within a vacuum chamber and reducing the pressure. Further out-gassing was performed at the epoxy cure temperature (~60°C) prior to casting the composite materials into thin films (~100-150μm thickness) by pressing the material in a temperature controlled mechanical press.

The connectivity (11) description of the composites indicates the manner in which the constituent phases connect to themselves throughout the bulk of the material. The connectivity patterns for two phase composites are represented by two digits, the first representing the ceramic while the second the polymer. A composite where the ceramic particles are dispersed randomly in a polymer matrix possesses 0-3 connectivity, where the ceramic is connected to itself in zero directions and the polymer in 3 directions. For high ceramic volume fractions or where the thickness of the film approaches the dimensions of the ceramic grains the connectivity of the ceramic, in the thickness direction, increases, thus producing a proportion of 1-3 connectivity where the ceramic is connected to itself through the thickness of the sample. The 0-3 composites fabricated in this study are believed to possess a certain amount of 1-3 connectivity and are known as mixed connectivity composites (14).

Circular aluminium electrodes of 1cm diameter were deposited onto the surfaces of the films by evaporation of aluminium wire at a low pressure ($\leq 10^{-6}$ mbar). The electrodes consisted of a circular portion, which would define the electroactive area, and a small side lobe for electrical contact. The electrodes on both sides of the composite film coincided through the thickness of the film except for the side lobes which were offset from one another. Poling of the films was performed by applying an electric field of up to 25 MVm^{-1} across the thickness of each sample whilst holding it's temperature at 100°C, for the composites of PTCa/P(VDF-TrFE), and 80°C, the epoxy softening temperature, for the composites of PTCa/Epoxy. Poling time was approximately 30 minutes and the sample was allowed to cool in the presence of the field. Sample temperature was maintained and electrical breakdown across the surface avoided by submerging the sample in silicone oil.

Bimorphs were constructed by adhering two monomorphs together using an epoxy glue (*Araldite Rapid). Two different physical configurations of bimorph can be accomplished by using two monomorphs. Series connected bimorphs were constructed by adhering two monomorphs together such that their directions of polarisation are opposing one another, (figure 2). Parallel connected bimorphs were constructed in a similar manner except the directions of polarisation were the same for the two individual monomorphs. The adhesive layer between the monomorphs was made to be as thin as possible. This was accomplished by coating one surface of one monomorph with the epoxy resin whilst the corresponding surface of the second monomorph was coated with the hardener. Sufficient time was left for both the liquids to

wet their respective surfaces prior to being all but totally removed by a blade. The mating surfaces were then placed face to face and the epoxy was allowed to cure whilst light pressure (~1Pa) was applied by placing the bimorph between two polished metal plates. The bimorphs were constructed in such a way so that electrical contacts could be made to all three electrodes, the centre two electrodes, in contact with each other, acting as one.

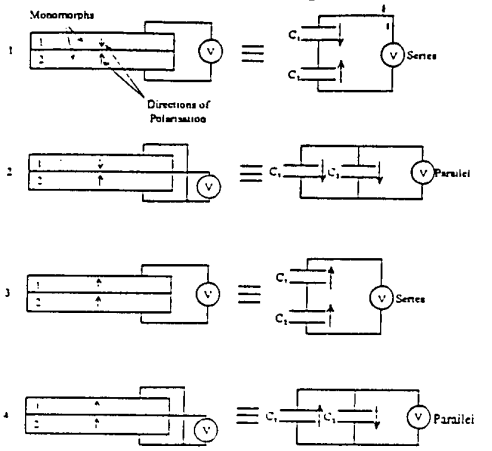

Fig. 2. Schematic representation of bimorph configurations.

Acoustic wave detection results reported in this paper were obtained from two composite plate specimens with embedded sensors. The plates were fabricated from prepreg material of S-Glass continuous reinforcing fibres in an epoxy (NCT-301) matrix supplied by Newport Adhesives and Composites, Inc. (U.S.A.). Two laminate plates were fabricated, both containing four embedded sensors and consisted of 25 plies with a stacking sequence of $[0]_{25}$ and a nominal thickness of approximately 0.3 cm. The in plane dimensions of the unidirectional laminates were 56 x 56cm and 70 x 70cm respectively. The sensors were embedded using different configurations for each plate and away from the edges to avoid signal reflection problems. Two monomorphs and two bimorphs were embedded in each plate for a total of eight sensors. In the smaller plate the sensors were embedded in a 10cm square array at the centre of the plate and two layers down from the surface, (figure 3(a)), consisting of two bimorphs constructed from composites of PTCa/P(VDF-TrFE) 65/35vol% and PTCa/P(VDF-TrFE) 60/40vol% respectively with their respective monomorph polarities opposing and two monomorphs fabricated from the two composite systems. The sensors in the larger plate, (figure 3(b)), were embedded in line, 10cm apart from each other, along the fibre direction, 0°-axis, at the plate centreline and 5 layers down from the surface. The bimorphs and monomorphs were constructed as those in the smaller plate except that the polarities of the monomorphs comprising the bimorphs were in the same direction. After the sensors had been embedded, the plates were cured in an autoclave at 80°C and 0.55 MPa for 6hrs according to the manufacturers specifications. A low temperature cure cycle was used in this case because it was desired to stay below the poling temperature of the composite films, thus avoiding depoling problems. The composite plates so obtained had 60% fibre volume and a tensile modulus of 56.5 GPa (NCT-301 Product Data Sheet).

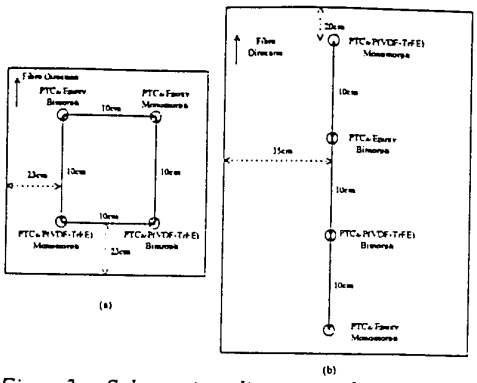

Fig. 3. Schematic diagram showing the embedded bimorph sensor locations within the composite plates.

CHARACTERISATION

The composite films were characterised with respect to their piezoelectric and electrical properties. The piezoelectric d_{33} coefficients were measured using a Pennebaker Model 8000 Piezo d_{33} Tester which gave the values directly in pCN^{-1}. The dielectric permittivities and dielectric loss tangents were found from measurements on the sample capacitances and conductances using a General Radio Bridge (Model 1621) at a frequency of 1kHz. The d_{31} coefficients for the composites were measured (15) by suspending a weight from the lower end of a sample, measuring 1cm x 4cm , which was rigidly clamped at it's upper end. The weight was almost instantaneously removed by means of a solenoid lift and the charge developed across the sample electrodes was recorded on a storage oscilloscope. The d_{31} coefficient is then given by

$$d_{31} = \frac{CVt}{lmg} \qquad (1)$$

where C in the sample capacitance, V the developed voltage, t the sample thickness, l the length of the electrode and mg the force applied by the weight. The electromechanical coupling coefficient, k_t, of the composites was found from an analysis of the impedance spectrum measured by a network analyser (HP 8702A). The composite samples were suspended freely in air and their electrical impedances measured over the frequency range 300 kHz to 50 MHz where the total impedance at resonance is given by the sum of the electrical impedance and the acoustic impedances (14, 16-18). The piezoelectric, electrical and electromechanical coupling coefficients for these composites have been reported in previous papers (6, 12), typical values seen in the composite materials are given here in table 1.

The embedded bimorph sensors were characterised by their response to a simulated AE source. Simulation of an AE source can be accomplished by the breakage of a pencil lead

on the surface of the test structure (19). The method, known as the Hsu-Nielson method, requires the pencil lead (0.5 mm diameter) to be held within a Nielson-Shoe, fixed on the end of a mechanical pencil, with approximately 2 to 3 mm of lead protruding from the shoe. When the lead breaks, there is a sudden release of stress on the surface of the plate where the lead was touching. The release of the stress produces an acoustic wave which can be efficiently reproduced by always ensuring the lead is broken at the same point on the plate with the same angle and orientation of the pencil. The output of the sensors were recorded directly on a digital storage oscilloscope for analyses.

RESULTS AND DISCUSSION

A bimorph transducer can be configured from two monomorphs in four different ways depending on the monomorph polarisations and the electrode configurations, (figure 2). The first two configurations, shown in figure 2, are for a bimorph constructed from two monomorphs with their directions of polarisation opposing one another, their equivalent capacitor circuits are shown to the right of the figure. Configurations three and four are for a bimorph constructed from monomorphs whose directions of polarisations are the same.

When a bimorph acts as a sensor there are essentially two modes in which it can sense. These modes are termed here as the thickness mode and the bending mode respectively. In configuration one of figure 2 an application of a stress normal to the film, i.e. on the thickness of the bimorph, will result in a cancellation of the signals from the two monomorphs arising from the piezoelectric g_{33} coefficients as the signals will be of opposite signs due to the opposite polarisations. The piezoelectric g_{ij} coefficient relates the electric field developed on the electroactive material to the applied stress, the subscript indices, i and j, indicating the direction of the response and the applied stimulus respectively. Application of a bending moment will result in the signals from the two monomorphs, arising from the piezoelectric g_{31} coefficients, complimenting each other. When the bimorph is bent the monomorph making up the top half of the bimorph will be under extension (or compression) while the other monomorph making up the lower half of the bimorph will be under compression (or extension), thus, the signals will be of the same polarity due to the applied stresses being of opposite sign. It can be seen that in this configuration the bimorph will only be sensing in the bending mode as the thickness mode will produce a null response. With configuration two, where the outer two electrodes of the bimorph are connected together and the signal is sensed between the inner electrode to the outer electrodes, it can be seen that the opposite will be true. With this configuration the bimorph will be working in the thickness mode as here the bending mode will produce the null result. Therefore, for one configuration of monomorph polarisations the sensing mode can be defined by the electrode arrangement, i.e. the bimorph has a dual mode of operation. Further examination of figure 2 will reveal that there is a certain equivalence between the various configurations. The properties of configuration 1 can be seen to be equivalent to the properties of configuration 4 while configurations 2 and 3 are equivalent in their own right. The preceding discussion has assumed that the properties of the individual monomorphs are the same and the thickness of the glue layer is negligible. Furthermore, it needs to be stated that the sensors themselves must not be too thick to jeopardise signal cancellation in the bending mode. However, the thickness of the sensors must not be too thin either in relation to the thickness of the plate to maintain appropriate signal strength in the bending mode.

If we consider configuration 2, for example, it may be assumed that there will be an amplification of the signal due to the fact that we are using a bimorph instead of a monomorph. This is of course incorrect as an application of a normal stress will produce a charge displacement in both monomorphs. resulting in double the charge on the central electrode, but the voltage will be the same as the capacitance of the system has also doubled. There will, however, be an amplification of current in the external part of the circuit as the total resistance will have been halved. For an actuator it is possible to produce twice the displacement or force, in a bimorph as opposed to a monomorph, with the same amount of voltage, although with a corresponding cost in current.

For an acoustic wave to propagate as a Lamb wave (3), the material in which it propagates must be plate-like, i.e. it must possess two dimensions which are large compared to it's thickness. If this criterion is met Lamb waves with wavelengths in excess of the thickness of the material will propagate. There are two general types of Lamb (or plate) waves depending on the particle motion within the material as the wave propagates through the plate. Figure 1 shows a representation of the first modes of the symmetrical (extensional) and asymmetrical (flexural) plate waves along with the second and third modes. The symmetrical or extensional plate wave velocities are independent of frequency, i.e. non-dispersive, whereas the asymmetrical or flexural plate wave velocities are dispersive in nature with a square root dependence on the frequency of the wave. The extensional plate waves propagate faster and with higher frequencies than the slower and lower frequency flexural waves. Elastic waves generated by acoustic emission sources in a plate-like structure will propagate as plate waves. Therefore, if the wave is sensed some distance from the AE source, the extensional modes will be sensed some time before the slower flexural modes.

The plate wave velocities within the composite plates were found by measuring the time taken for the waves to propagate along a 10cm distance through the plate. Two surface mounted sensors were situated 10cm apart and a lead break was made on the surface of the plates 10cm away from the first sensor. The arrival times of the plate waves were recorded

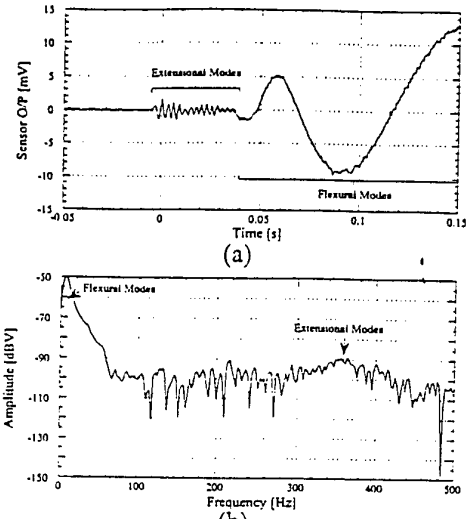

Fig. 4(a). Output response of an embedded PTCa/Epoxy bimorph sensor with electrode configuration 2 to a simulated AE source 10cm away, 0° to the fibre axis in an unidirectional S-glass reinforced epoxy composite plate.
Fig. 4(b). FFT frequency analysis, using a Hanning window, on the signal shown in figure 4(a).

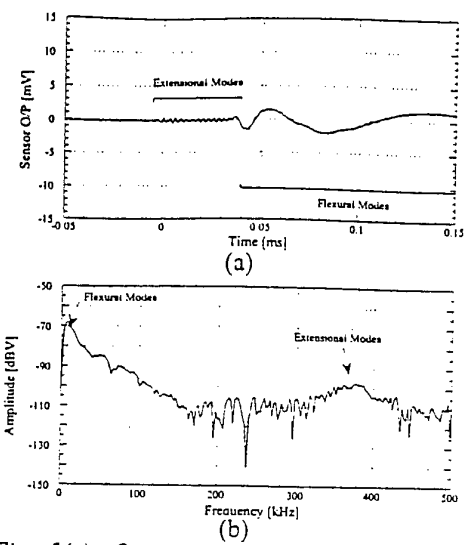

Fig. 5(a). Output response of an embedded PTCa/Epoxy bimorph sensor with electrode configuration 1 to a simulated AE source 10cm away, 0° to the fibre axis in an unidirectional S-glass reinforced epoxy composite plate.
Fig. 5(b). FFT frequency analysis, using a Hanning window, on the signal shown in figure 5(a).

from which the plate wave velocities were deduced. Table 2 outlines the wave velocities of the extensional and flexural modes of propagation for E- and S-glass reinforced epoxy composite plates. Their corresponding approximate wavelengths are also shown which were found from the peak frequencies of the modes. Surface mounted sensors were only used to characterise the plates with respect to their plate wave velocities.

Responses of embedded bimorph sensors to simulated AE sources a distance 10cm away can be seen in figures 4 and 5. Figure 4(a) shows the response of an embedded PTCa/Epoxy bimorph with configuration 2, (figure 2). It can be clearly seen from this figure the two plate wave modes of propagation. The oscilloscope was triggered on the arrival of the extensional mode which is seen as the higher frequency component to the signal arriving before the lower frequency component from the flexural modes. Fast Fourier transform (FFT) analyses performed on the signal with a Hanning window gives the spectrum shown in figure 4(b). From this figure the two distinct frequency components, associated with the two types of wave propagation, are clearly distinguished. Although not shown here, this signal is equivalent to a signal given by a single monomorph in response to the same input (12). In figure 5(a) the response of the same bimorph, but with electrode configuration 1, is shown along with its FFT frequency spectrum shown in figure 5(b). The immediate noticeable difference between the two responses is that of attenuation. The latter response showing a greatly attenuated signal to that of the former. Upon examination of the corresponding frequency spectra it can be seen that the flexural modes have been attenuated more than the extensional modes, by a factor of 18dBV as opposed to 8dBV. A slight shift in peak frequencies was also observed between the two responses, but this is believed to be due to the resolution of the FFT and not an artefact of the response.

Similar responses are shown in figures 6 and 7 for an embedded bimorph constructed from PTCa/P(VDF-TrFE) composites. Again the two modes of propagation can clearly be defined from the signal observed with configuration 2 of the bimorph electrodes (figure 6(a)), the higher frequency extensional modes arriving before the lower frequency flexural modes. Figure 6(b) shows the corresponding frequency spectrum for this signal. Figure 7(a) shows a signal from the same bimorph but with electrode configuration 1. Again it can be seen that the signal has been greatly attenuated as with the PTCa/Epoxy bimorph but from examination of the frequency spectrum of figure 7(b) it can be seen that the flexural modes have been attenuated by 27dBV whereas the extensional modes have only been attenuated by 6dBV. The difference in signal attenuations between the two types of bimorphs can be understood when considering their respective coupling coefficients. The measured piezoelectric d_{31} coefficients are 4.5 and 0.4 pCN^{-1} and their dielectric permittivities are 45 and 26 for the composites of PTCa/P(VDF-TrFE) and PTCa/Epoxy respectively. These figures would indicate an approximate 20dBV difference in a signal arising from the g_{31} coefficients as would be the case for a bimorph sensing in it's bending mode.
From table 2 it can be seen that the approximate wavelengths found for the extensional and the flexural modes are 1.4 and 11.0 cm respectively for a plate wave travelling along the direction of the fibres in a unidirectional composite plate. It is noted here that the dimensions of the bimorph transducers are close to those of the wavelengths of the

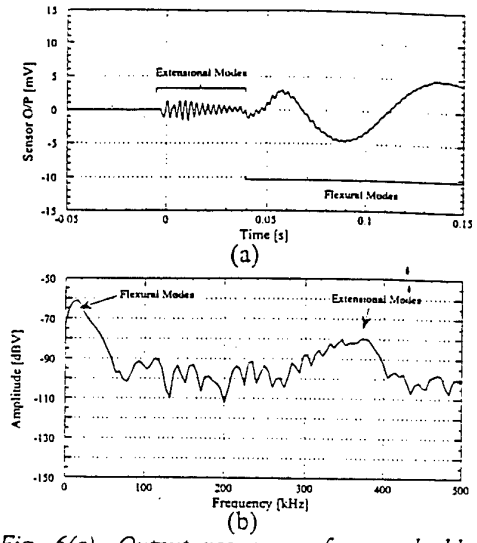

Fig. 6(a). Output response of an embedded PTCa/P(VDF-TrFE) bimorph sensor with electrode configuration 2 to a simulated AE source 10cm away, 0° to the fibre axis in an unidirectional S-glass reinforced epoxy composite plate.
Fig. 6(b). FFT frequency analysis, using a Hanning window, on the signal shown in figure 6(a).

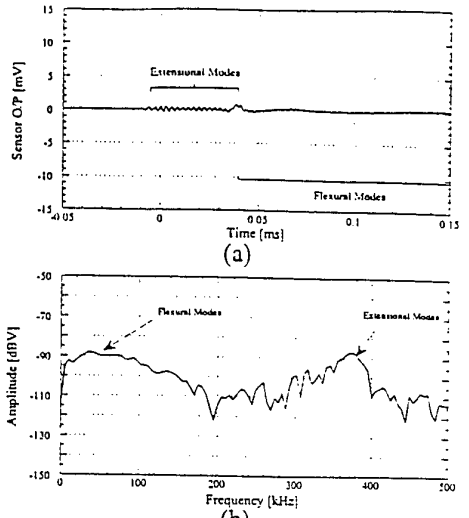

Fig. 7(a). Output response of an embedded PTCa/P(VDF-TrFE) bimorph sensor with electrode configuration 1 to a simulated AE source 10cm away, 0° to the fibre axis in an unidirectional S-glass reinforced epoxy composite plate.
Fig. 7(b). FFT frequency analysis, using a Hanning window, on the signal shown in figure 7(a).

extensional modes. With configuration 1 (figure 2) of the bimorph electrodes the bimorph will be sensing in it's bending mode as stresses experienced on the thickness of the bimorph will cancel. It is suggested that as the extensional modes of the plate wave are sensed by the bimorph a sufficient bending moment is applied to it giving rise to the signal, whereas the bending moment applied to the bimorph by the flexural mode is somewhat reduced, due to the greater wavelengths involved, therefore, the signal being produced is greatly attenuated.

Further work is being made on the acousto-ultrasonic properties of the embedded sensors, where an embedded bimorph is excited electrically to produce an acoustic wave for detection by another embedded sensor at a distance or by the same sensor upon reflection and on the positioning of the sensors to optimise their response to plate waves.

CONCLUSION

From the above results the dual mode of operation of bimorph sensors has been illustrated. The signals have shown that the embedded bimorphs have detected plate waves generated by a simulated AE source in a S-glass reinforced epoxy plate. The bimorphs have essentially differentiated between the two types of plate wave propagation, although the differentiation has been determined by the wavelength of the acoustic wave compared to the sensor dimensions. Comparison of monomorphs signals to bimorph signals, where the monomorph is essentially operating in a hydrostatic mode and differentiation between the plate wave propagation modes could be made by signal processing, the bimorphs would appear to be the more cost effective way of detection due to their inherent nature of operation which reduces the need for post processing of the signals.

REFERENCES

1. M.R. Gorman, J. Acoust. Soc. Am., 90, 358 (1991).
2. F.R. Breckenridge, C.E. Tschiegg, and M. Greenspan, J. Acoust. Soc. Am., 57, 626 (1975).
3. H. Lamb, Proc. Roy. Soc. London, Series A, 93, 114 (1917).
4. J.A. Chilton, GEC Review, 6, 156 (1991).
5. C. Dias, D.K. Das-Gupta, Y. Hinton, and R.J. Shuford, Sensors and Actuators A, 37 - 38, 343 (1993).
6. M.P. Wenger, P. Blanas, C.J. Dias, R.J. Shuford, and D.K. Das-Gupta, Ferroelectrics, 187, 75 (1996).
7. M. Toda, Ferroelectrics, 32, 127 (1981).
8. J.G. Smits and A. Ballato, J. Microelectromechanical Sys., 3, 105 (1994).
9. J.G. Smits and W.S. Choi, Ferroelectrics, 145 (1993).
10. M. Toda and S. Osaka, IECE Japan, E61, 507 (1978).
11. R.E. Newnham, D.P. Skinner, and L.E. Cross, Mater. Res. Bull., 13, 525 (1978).
12. M.P. Wenger, P. Blanas, R.J. Shuford, and D.K. Das-Gupta, Polym. Eng. Sci., (1996).
13. M.P. Wenger, P. Blanas, R.J. Shuford, and D.K. Das-Gupta, *2nd Euro. Conf. on Smart Struct. & Mat.*, Glasgow, Scotland, 358 (1994).
14. C.J. Dias and D.K. Das-Gupta, IEEE Trans. Dielectr. & Electr. Insul., 3, 706 (1996).
15. R.S. Brockley, *Nature and Origins of Absorbtion Currents and Piezoelectricity in Polyvinylidene Flouride*, Ph.D. Thesis, University College of North Wales, (1979).
16. H. Ohigashi, Ultrasonic transducers in the megahertz range, in The Applications of Ferroelectric Polymers T.T. Wang, J.M. Herbert and A.M. Glass, eds., Blackie & Son Ltd: Glasgow. p. 237 (1988).

17. L.N. Bui, H.J. Shaw, and L.T. Zitelli, IEEE Trans. Sonics Ultrasonics, SU-24, 331 (1977).
18. M. Platte, Ferroelectrics, 115, 229 (1991).
19. *Standard Guide for Determining the Reproducibility of Acoustic Emission Sensor Reponse*, ASTM, E 976-84-(1988).

Section D: Metrology and Applications
Paper presented at Sensors and their Applications VIII, 7–10 September 1997

Embedded Piezoelectric Composite Bimorphs as Non-Destructive Testing Sensors

M.P. Wenger, P. Blanas*, R.J. Shuford* & D.K. Das-Gupta

School of Electronic Engineering & Computer Systems, University of Wales, Bangor, Dean Street, Bangor, Gwynedd, LL57 1UT, UK.

*US. Army Research Laboratory, Materials Directorate, Aberdeen Proving Ground, MD 21005-5069, U.S.A.

Abstract. Acoustic emission detection is gathering favour among the non-destructive testing techniques available nowadays, especially for structures fabricated from fibre reinforced composites. Composite piezoelectric materials have come about from a need to tailor the electrical, mechanical and acoustical properties of sensing materials to enhance their overall performance. Normal piezoelectric monomorphs, fabricated from ferroelectric composite materials, have shown themselves to be adequate for detecting simulated acoustic emission sources within fibre reinforced composite plates, both as surface mounted and embedded sensors. Piezoelectric bimorphs, however, not only can be used in a thickness or hydrostatic mode but can also be used in a bending mode by suitable configurations of their electrodes. This paper reports on the results of a study to determine the suitability of embedded piezoelectric bimorph sensors for the detection of acoustic emissions within fibre reinforced composite plate structures.

1. Introduction

An acoustic emission (AE) transducer senses the dynamic stress waves propagating through a structure, which have been generated by the release of energy due to a failure mechanism. Within a fibre reinforced epoxy composite structure acoustic emissions can be generated by processes such as fibre breakage, delaminations, fibre-matrix debonding and matrix cracking, all of which are expected to produce distinct waveforms [1]. To effectively determine the position and nature of the damage mechanism through a non-destructive evaluation method, such as AE detection, the technique needs to gain as much knowledge as possible of the source. Often an AE sensor will be situated on the surface of the structure some distance away from a possible AE source. The structure on many occasions may need to be removed from its working environment or continuous testing may not be practical, therefore, monitoring of the health of the structure may only be done after the damage has occurred or a decision must be made to replace or repair the structure prior to potential failure. An *in-situ* AE sensor, where the sensor has become an integral part of the structure would facilitate its continuous monitoring without any lapse of time. The continuous

monitoring of the dynamic degradation of the structure would thus enable an informed decision to be made whether or not to replace or repair, all or part, of the structure.

Piezoelectric composite transducers consisting of a ferroelectric ceramic powder dispersed in a polymer matrix can be fabricated to take advantage of the desired properties of the constituent materials. The strong piezoelectric and electromechanical properties of the ceramic phase are combined with the mechanical strength and low dielectric permittivity of the polymer to enhance the overall properties of the composite [2]. Along with the tailoring of the properties by the judicial choice of materials and their construction, composites can be formed into a variety of sizes and shapes to take advantages of the nature of the application at hand. A single film of composite material, referred to here as a monomorph, can be used as an acoustic emission sensor. It can be incorporated into a surface mounted AE sensor [3] or be embedded into a fibre reinforced epoxy laminate structure [4]. Two or more monomorphs can be incorporated into one sensor to form a bimorph or multimorph respectively. Previous work on bimorphs and multimorphs has concentrated on their actuation properties. The present work is concerned with the sensing properties of piezoelectric bimorphs constructed from 0-3 connectivity [5] ceramic/polymer composites embedded into laminate structures. Simple bimorph sensors differ from monomorphs in their ability to work in either of two modes of operation, i.e. a thickness mode of operation or a bending mode of operation. A study on the ability of embedded monomorphs to detect simulated acoustic emissions has previously been completed and reported in a paper by Wenger et. al. [6]. The piezoelectric, electrical and electromechanical coupling coefficients for these composites have been reported in previous papers [4, 6]. This paper will report the results obtained from a study on the ability of the embedded bimorph sensors to detect and distinguish simulated AE sources and a comparison will be made between the sensing properties of the monomorphs and the bimorphs.

2. Experimental

Two different piezoelectric composites have been used in this work. The ceramic, calcium modified lead titanate (PTCa), was supplied by GEC-Marconi Materials Technology (Caswell) in fine powder form with average grain size approximately 10 - 20 μm. The two different polymer matrices were a polar copolymer, polyvinylidene fluoride trifluoroethylene (P(VDF-TrFE)) 75/25 molar percentage supplied by Solvay in fine powder form, and a non-polar epoxy resin, Epikote 828 (Shell Resins), with hardener, K61B (Anchor Chemical). Fabrication of the PTCa/P(VDF-TrFE) composites consisted of dry mixing the powders prior to the addition of acetone to dissolve the polymer. Continuous stirring of the mixture within a fume cabinet enabled the solvent to evaporate leaving behind the 0-3 composite material. Thin films (~100 μm thickness) of the material were formed by pressing the material, at the softening temperature (~170°C) of the polymer. The composites of PTCa/Epoxy were fabricatedby gradually mixing the ceramic powder into the epoxy resin and hardener mix whilst continuously stirring. Trapped gasses were removed by placing the mixture in a vacuum at the epoxy cure temperature (~60°C) prior to casting the composite material into thin films (~100 - 150 μm thickness) in a temperature controlled press.

The connectivity [5] description of the composites indicates the manner in which the constituent phases connect to themselves throughout the bulk of the material. The connectivity patterns for two phase composites are represented by two digits, the first representing the ceramic, the second the polymer. A composite where the ceramic particles

are dispersed randomly in a polymer matrix possesses 0-3 connectivity, where the ceramic is connected to itself in zero directions and the polymer in 3 directions. For high ceramic volume fractions or where the thickness of the film approaches the dimensions of the ceramic grains, the connectivity of the ceramic, in the thickness direction, increases, thus producing a proportion of 1-3 connectivity where the ceramic is connected to itself through the thickness of the sample. The 0-3 composites fabricated in this study are believed to possess a certain amount of 1-3 connectivity and are known as mixed connectivity composites [7].

Circular aluminium electrodes of 1cm diameter were deposited onto the surfaces of the films by evaporation of aluminium wire at low pressure (10^{-6} mbar). Poling of the films was performed by applying an electric field of 25 MVm^{-1} across the thickness of each sample whilst holding its temperature at 100°C, for the composites of PTCa/P(VDF-TrFE), and 80°C, the epoxy softening temperature, for the composites of PTCa/Epoxy. Poling time was approximately 30 minutes and the sample was allowed to cool in the presence of the field.

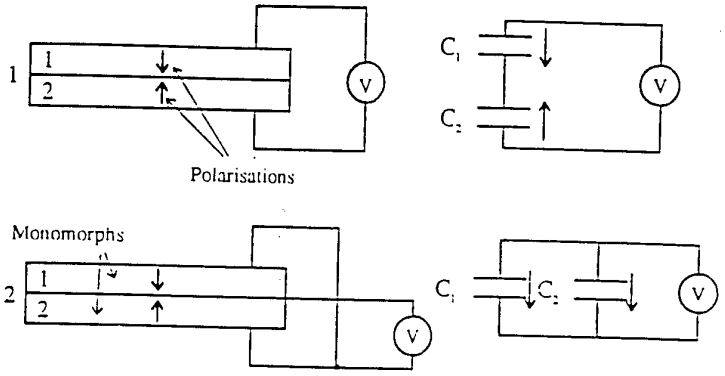

Fig. 1 Schematic representation of bimorph configurations.

Bimorphs were constructed by adhering two monomorphs together using an epoxy glue (® Araldite Rapid) with their respective directions of polarisations opposing one another, (fig. 1). The adhesive layer between the monomorphs was made to be as thin as possible. This was accomplished by coating one surface of one monomorph with the epoxy resin whilst the corresponding surface of the second monomorph was coated with the hardener. The liquids were all but totally removed by a blade prior to the mating surfaces being placed face to face. Electrical contacts were made to all three electrodes, the centre two electrodes, in contact with each other, acting as one.

A composite plate with four embedded sensors, two monomorphs and two bimorphs was fabricated from prepreg material of S-Glass continuous reinforcing fibres in an epoxy (NCT-301) matrix supplied by Newport Adhesives and Composites, Inc. (U.S.A.) consisting of 25 plies with a stacking sequence of $[0]_{25}$ and a nominal thickness of approximately 0.3 cm. The in plane dimensions of the unidirectional laminate were 56 x 56 cm. The sensors were embedded in a 10 cm square array at the centre of the plate, away from the edges to avoid signal reflection problems and two layers down from the surface. The sensor array consisted of two bimorphs constructed from composites of PTCa/P(VDF-TrFE) 65/35vol% and PTCa/P(VDF-TrFE) 60/40vol% respectively with their respective monomorph polarities

opposing and two monomorphs fabricated from the two composite systems. After the sensors had been embedded, the plate was cured in an autoclave at 80°C and 0.55 MPa for 6 hrs. A low temperature cure cycle was used to stay below the poling temperature of the composite films, thus avoiding depoling problems. The composite plate obtained had 60% fibre volume and a tensile modulus of 56.5 GPa (NCT-301 Product Data Sheet).

The embedded bimorph sensors were characterised by their response to a simulated AE source. Simulation of an AE source was accomplished by breaking a pencil lead on the surface of the plate [8]. The method, known as the Hsu-Nielson method, requires the pencil lead (0.5 mm diameter) to be held within a Nielson-Shoe, fixed on the end of a mechanical pencil, with approximately 2 to 3 mm of lead protruding from the shoe. When the lead breaks, there is a sudden release of stress on the surface of the plate where the lead was touching. The release of the stress produces an acoustic wave which can be efficiently reproduced. The output of the sensors were recorded directly on a digital storage oscilloscope for analyses.

3. Results and Discussion

A bimorph transducer can be configured from two monomorphs in four different ways depending on the monomorph polarisations and the electrode configurations. Figure 1 shows two electrode configurations for a bimorph with opposing monomorph polarities with equivalent capacitor circuits. Similar configurations can be constructed from bimorphs with monomorph polarities in the same direction.

When a bimorph acts as a sensor there are essentially two modes in which it can sense. These modes are termed here the thickness and bending modes respectively. In configuration 1 of figure 1 an application of a stress normal to the film will result in a cancellation of the signals from the two monomorphs arising from the piezoelectric g_{33} coefficients as the signals will be of opposite signs due to the opposite polarisations. The piezoelectric g_{ij} coefficient relates the electric field developed to the applied stress, the subscript indices, i and j, indicating the direction of the response and the applied stimulus respectively. Application of a bending moment will result in the signals from the two monomorphs, arising from the piezoelectric g_{31} coefficients, complimenting each other. When the bimorph is bent the monomorph making up the top half of the bimorph will be under extension (or compression) while the other monomorph making up the lower half of the bimorph will be under compression (or extension), thus, the signals will be of the same polarity due to the applied stresses being of opposite sign. It can be seen that in this configuration the bimorph will only be sensing in the bending mode as the thickness mode will produce a null response. With configuration two, where the outer two electrodes of the bimorph are connected together and the signal is sensed between the inner electrode and the outer electrodes, it can be seen that the opposite will be true. With this configuration the bimorph will be working in the thickness mode as here the bending mode will produce the null result. Therefore, for one configuration of monomorph polarisations the sensing mode can be defined by the electrode arrangement, i.e. the bimorph has a dual mode of operation. The preceding discussion has assumed that the properties of the individual monomorphs are the same and the thickness of the glue layer is negligible. Furthermore, it needs to be stated that the sensors themselves must not be too thick to jeopardise signal cancellation in the bending mode. However, the thickness of the sensors must not be too thin either in relation to the thickness of the plate to maintain appropriate signal strength in the bending mode.

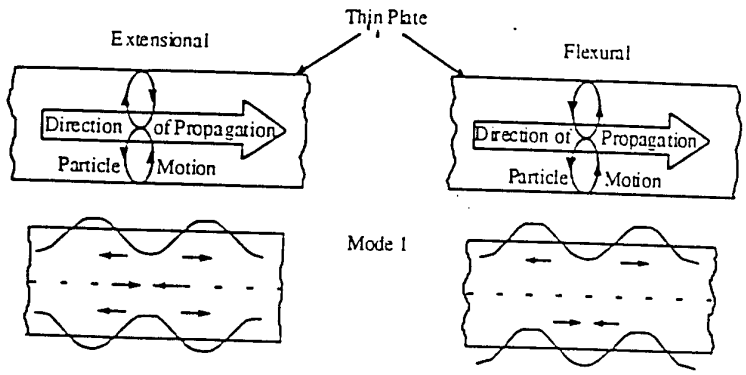

Fig. 2 Schematic representation of extensional and flexural plate waves.

For an acoustic wave to propagate as a Lamb wave [9], the material in which it propagates must be plate-like, i.e. it must possess two dimensions which are large compared to it's thickness. If this criterion is met, Lamb waves with wavelengths in excess of the thickness of the material will propagate. There are two general types of Lamb (or plate) waves depending on the particle motion within the material as the wave propagates through the plate. Figure 2 shows a representation of the first modes of the symmetrical (extensional) and asymmetrical (flexural) plate waves. The symmetrical or extensional plate wave velocities are independent of frequency, i.e. non-dispersive, whereas the asymmetrical or flexural plate wave velocities are dispersive in nature with a square root dependence on the frequency of the wave. The extensional plate waves propagate faster and with higher frequencies than the slower and lower frequency flexural waves. Elastic waves generated by acoustic emission sources in a plate-like structure will propagate as plate waves. Therefore, if the wave is sensed some distance from the AE source, the extensional modes will be sensed some time before the slower flexural modes.

Responses of embedded bimorph sensors to simulated AE sources a distance 10cm away can be seen in figures 3(a) and 4(a). Figure 3(a) shows the response of an embedded PTCa/P(VDF-TrFE) bimorph with configuration 2, (fig. 1). It can be clearly seen from this figure the two plate wave modes of propagation. The oscilloscope was triggered on the arrival of the extensional mode which is seen as the higher frequency component to the signal arriving before the lower frequency component from the flexural modes. Fast Fourier transform (FFT) analyses performed on the signal with a Hanning window gives the spectrum shown in figure 3(b). From this figure the two distinct frequency components, associated with the two types of wave propagation, are clearly distinguished. Although not shown here, this signal is equivalent to a signal given by a single monomorph in response to the same input [6]. In figure 4(a) the response of the same bimorph, but with electrode configuration 1, is shown along with it's FFT frequency spectrum shown in figure 4(b). The immediate noticeable difference between the two responses is that of attenuation. The latter response showing a greatly attenuated signal to that of the former. Upon examination of the corresponding frequency spectra it can be seen that the flexural modes have been attenuated more than the extensional modes, by a factor of 27 dBV as opposed to 6 dBV. A slight shift in peak frequencies was also observed between the two responses, but this is believed to be due to the resolution of the FFT and not an artefact of the response.

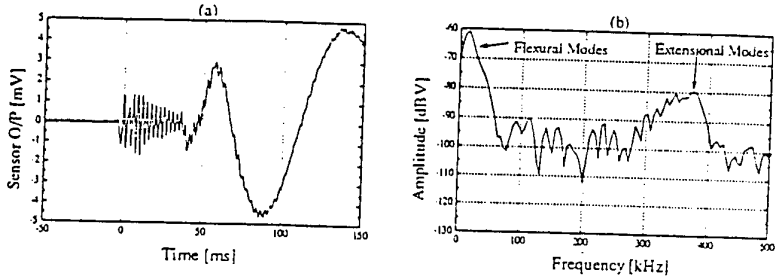

Fig. 3 (a) Output response of an embedded PTCa/P(VDF-TrFE) bimorph sensor with electrode configuration 2 to a simulated AE source 10 cm away, 0° to the fibre axis in an unidirectional S-glass reinforced epoxy composite plate. (b) FFT frequency analysis, using a Hanning window, on the signal shown in figure 3(a).

Similar results were seen for bimorphs constructed from PTCa/Epoxy, but the relative attenuations were 18 and 8 dBV for the flexural and extensional modes respectively for a change in the electrode configurations from 1 to 2. The difference in signal attenuations between the two types of bimorphs can be understood when considering their respective coupling coefficients. The measured piezoelectric d_{31} coefficients are 4.5 and 0.4 pCN^{-1} and their dielectric permittivities are 45 and 26 for the composites of PTCa/P(VDF-TrFE) and PTCa/Epoxy respectively. These figures would indicate an approximate 20 dBV difference in a signal arising from the g_{31} coefficients as would be the case for a bimorph sensing in its bending mode.

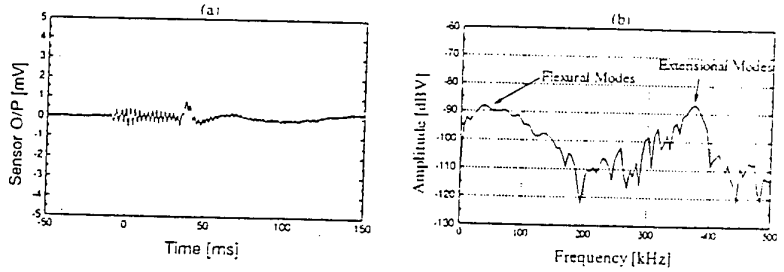

Fig. 4 (a) Output response of an embedded PTCa/P(VDF-TrFE) bimorph sensor with electrode configuration 2 to a simulated AE source 10 cm away, 0° to the fibre axis in an unidirectional S-glass reinforced epoxy composite plate. (b) FFT frequency analysis, using a Hanning window, on the signal shown in figure 4(a).

From measurements on the wave velocities of the two modes, approximate wavelengths found for the extensional and the flexural modes were 1.4 and 11.0 cm respectively for a plate wave travelling along the direction of the fibres in a unidirectional composite plate. It is noted here that the dimensions of the bimorph transducers were close to those of the wavelengths of the extensional modes. With configuration 1 (fig. 1) of the bimorph electrodes the bimorph senses in it's bending mode as stresses experienced on the thickness of the bimorph will cancel. It is suggested that as the extensional modes of the plate wave are sensed by the bimorph a sufficient bending moment is applied to it giving

rise to the signal, whereas the bending moment applied to the bimorph by the flexural mode is somewhat reduced, due to the greater wavelengths involved, therefore, the signal being produced is greatly attenuated.

Further work is being made on the acousto-ultrasonic properties of the embedded sensors, where an embedded bimorph is excited electrically to produce an acoustic wave for detection by another embedded sensor at a distance or by the same sensor upon reflection.

4. Conclusion

From the above results the dual mode of operation of bimorph sensors has been illustrated. The signals have shown that the embedded bimorphs have detected plate waves generated by a simulated AE source in a S-glass reinforced epoxy plate. The bimorphs have essentially differentiated between the two types of plate wave propagation, although the differentiation has been determined by the wavelength of the acoustic wave compared to the sensor dimensions. Comparison of monomorph signals to bimorph signals, where the monomorph is essentially operating in a hydrostatic mode and differentiation between the plate wave propagation modes could be made by signal processing, the bimorphs would appear to be the more cost effective way of detection, due to their inherent nature of operation which reduces the need for post processing of the signals.

5. References

[1] Gorman M R, Prosser W H 1990 *J. Acoustic Emission* 9(4) 283 - 288

[2] Chilton J A 1991 *GEC Review* 6(3) 156-164

[3] Dias C, Das-Gupta D K, Hinton Y, Shuford R J 1993 *Sensors and Actuators A* 37-38 343 - 347

[4] Wenger M P, Blanas P, Dias C J, Shuford R J, Das-Gupta D K 1996 *Ferroelectrics* 187 75-86

[5] Newnham R E, Skinner D P, Cross L E 1978 *Mat. Res. Bull.* 13 525-536

[6] Wenger M P, Blanas P, Shuford R J, Das-Gupta D K 1996 *Poly. Eng. Sci.* 36(24) 2945-2954

[7] Wenger M P, Blanas P, Shuford R J, Das-Gupta D K 1994 2nd Euro. Conf. on Smart Struct. & Mat. (Glasgow, Scotland: SPIE - The Int. Soc. for Optical Engineering) 358 - 361

[8] Standard Guide for Mounting Piezoelectric Acoustic Emission Sensors ASTM E 650-85

[9] Lamb H 1917 *Proc. Royal Soc. London* 93 114-128